

UNIVERSITY OF BELGRADE

FACULTY OF CIVIL ENGINEERING

Marko D. Radišić

**ITM-BASED DYNAMIC ANALYSIS OF
FOUNDATIONS RESTING ON A
LAYERED HALFSPACE**

Doctoral Dissertation

Belgrade, 2018

UNIVERZITET U BEOGRADU

GRAĐEVINSKI FAKULTET

Marko D. Radišić

**DINAMIČKA ANALIZA TEMELJA NA
SLOJEVITOM POLUPROSTORU
PRIMJENOM METODE INTEGRALNE
TRANSFORMACIJE**

doktorska disertacija

Beograd, 2018

Advisors:

Prof. Dr. Mira Petronijević

University of Belgrade, Faculty of Civil Engineering

Univ.-Prof. Dr.-Ing. Gerhard Müller

Technical University of Munich, Civil, Geo and Environmental Engineering

Committee:

Prof. Dr. Mira Petronijević

University of Belgrade, Faculty of Civil Engineering

Univ.-Prof. Dr.-Ing. Gerhard Müller

Technical University of Munich, Dpt. of Civil, Geo and Environmental Engineering

Prof. Dr. Đorđe Lađinović

University of Novi Sad, Faculty of Technical Sciences

Assoc. Prof. Dr. Marija Nefovska-Danilović

University of Belgrade, Faculty of Civil Engineering

Assoc. Prof. Dr. Mirjana Vukićević

University of Belgrade, Faculty of Civil Engineering

Defense date: _____

Acknowledgments

First of all I want to express my deep gratitude to my mentor Prof. Mira Petronijević for her selfless support, encouragement, patience, and for giving me scientific freedom during this work. She introduced me to the world of science and guided me through it for years for which I am immensely grateful.

I would like to express my sincere gratitude to my mentor Prof. Gerhard Müller for giving me the opportunity to stay at the Lehrstuhl für Baumechanik at Technische Universität München and benefit from his wonderful research group for years. Meetings with Prof. Müller were always eye-opening, leading to creative solutions that were pushing me forward.

I owe my profound gratitude to Marija Nefovska-Danilović, Georg Frühe and Martin Buchschmid. Thank you for sharing your knowledge with me unreservedly, and for having a lot of patience and understanding during the discussions.

Thanks to my colleagues from Office 333 for inspiring discussions, support, and for covering my duties during my research stays in Germany and during the final stages of writing this thesis.

Thanks to all members of the Lehrstuhl für Baumechanik for accepting me as a part of their great team and helping me around TUM.

Thanks to my flatmates from Munich that made my life in Germany easy and enjoyable. I am grateful for having you as friends.

To my family I would like to thank for their patience, care, support and unselfish and true love.

Financial Support

The work on this thesis was supported by the Government of the Republic of Serbia Ministry of Education, Science and Technological Development, under the Project TR-36046 (project leader Prof. Dr. Mira Petronijević).

The financial support has been also provided through the SEEFORM (South Eastern European Graduate School for Master and Ph.D. Formation in Engineering) project financed by German Academic Exchange Service - DAAD (project leader Prof. Dr. Rüdiger Höffer). The full license of MATLAB® software was provided through this project. The author was granted a DAAD scholarship that gave him the opportunity to spend one year in frame of three years at the Technical University of Munich, at the chair of Structural Mechanics under management of Univ.-Prof. Dr.-Ing. Gerhard Müller.

ITM-Based Dynamic Analysis of Foundations Resting on a Layered Halfspace

Abstract:

In this dissertation, the solution of the soil-foundation interaction problems is solved using the substructuring approach. The modeling of the substructures is performed using transform methods. The governing system of equations of motion is transformed from the original space-time domain into space-frequency or wavenumber-frequency domain, where the effects of the input parameters on the results are more visible. The foundation is modeled using the Spectral Element Method, obtaining the exact solution of the differential equations of wave propagation in plate in space-frequency domain. The soil medium is modeled using the Integral Transform Method. The method is based on the analytical solution of Lamé's differential equations of motion in wavenumber-frequency domain. The differential equation of the soil-foundation system is solved in space-frequency domain using the modal superposition technique. The proposed method is used for obtaining the approximate analytical solution of soil-foundation interaction problems involving surface massless foundations. The solutions of following problems are presented: rigid square foundation on halfspace, group of rigid square foundations on a layer over the bedrock, flexible strip foundation on halfspace, and flexible square foundation on halfspace. The results are presented in terms of compliance functions, displacement fields and stress fields of the foundation. The main contribution of the proposed method is reflected in solving the soil-foundation interaction problems involving flexible foundations.

Keywords: Integral Transform Method, Spectral Element Method, Fourier Transformation, Wave Propagation

Scientific field: Civil Engineering

Scientific subfield: Engineering Mechanics and Theory of Structures

UDC: 624.04:624.151(043.3)

Dinamička analiza temelja na slojevitom poluprostoru primjenom Metode integralne transformacije

Sažetak:

U ovom radu prikazano je rešenje problema interakcije temelja i tla primjenom metode podstruktura. Podstrukture su modelirane metodama transformacije. Ove metode podrazumijevaju transformaciju diferencijalnih jednačina kretanja sistema iz originalnog domena definisanog u prostoru i vremenu, u domen prostornih koordinata i frekvencija, ili u domen talasnih brojeva i frekvencija. Prednost ovih metoda je transparentnost uticaja ulaznih podataka na rezultat analize. Temelj je modeliran korišćenjem Metode spektralnih elemenata, na osnovu koje je određeno tačno rešenje diferencijalnih jednačina kretanja talasa u ploči u domenu prostornih koordinata i frekvencija. Tlo je modelirano korišćenjem Metode integralne transformacije. Metoda je bazirana na analitičkom rešenju Laméovih diferencijalnih jednačina kretanja u domenu talasnih brojeva i frekvencija. Diferencijalna jednačina sistema tlo-temelj riješena je u domenu prostornih koordinata i frekvencija korišćenjem metode modalne superpozicije. Predstavljeni postupak je iskorišćen za sračunavanje aproksimativnog analitičkog rešenja problema površinskih temelja bez mase. Sračunati su odgovori sledećih sistema: kruti kvadratni temelj na poluprostoru, sistem krutih kvadratnih temelja na sloju iznad krute baze, fleksibilni trakasti temelj na poluprostoru i fleksibilni kvadratni temelj na poluprostoru. Glavni doprinos predloženog postupka ogleda se u rešavanju problema interakcije tla i fleksibilnih temelja.

Ključne riječi: Metoda integralne transformacije, Metoda spektralnih elemenata, Furijeove transformacije, propagacija talasa

Naučna oblast: Građevinarstvo

Uža naučna oblast: Tehnička mehanika i teorija konstrukcija

UDK: 624.04:624.151(043.3)

Contents

Acknowledgments	i
Financial Support	iii
List of symbols	viii
1 Introduction	1
1.1 Motivation	1
1.2 State of Research	3
1.3 Layout of the Thesis	8
2 Wave Propagation in Halfspace by ITM	10
2.1 Wave Propagation in Continuum	10
2.2 Wave Equations in Elastic Halfspace	14
2.3 Boundary Conditions	16
2.3.1 Layered Halfspace	20
2.4 Static load	23
2.5 Plane Strain	24
2.6 Damping	25
2.7 Surface Displacements	26
2.7.1 Numerical Examples	27

2.8	Moving load	34
2.8.1	Numerical example	35
3	Dynamic Stiffness and Flexibility of Surface Foundations	38
3.1	Introduction	38
3.2	Rigid Foundation	42
3.2.1	Numerical example: Square foundation on a homogeneous halfspace	51
3.2.2	Group of rigid foundations	53
3.2.3	Numerical example: Group of foundations on a layer over bedrock	54
3.3	Flexible Foundation	67
3.3.1	Flexible strip foundation	68
3.3.2	Flexible square foundation	78
3.3.3	Numerical examples	88
4	Summary	107
A	Appendix	112
A.1	Tensor Notation	112
A.2	Fourier transformation	115
A.2.1	Continuous Fourier transformation	115
A.2.2	Discrete Fourier transformation	116
	Biography	125

List of symbols

\mathbf{A}	Block diagonal kinematic matrix
\mathbf{a}	Kinematic matrix
a_0	Dimensionless frequency
A_1, A_2, B_{i1}, B_{i2}	Coefficients of integration, $i = x, y$
B, L	Foundation dimensions
B_x	Soil surface truncation length
c_p, c_s	Velocities of P- and S-waves
D	Bending stiffness of the Kirchhoff plate
δ_{ij}	Kronecker delta
Δ_i	Dimensionless vertical displacement of the flexible foundation at the point i
∇	Differential operator
Δk_x	Soil surface discretization unit in wavenumber domain
Δx	Soil surface discretization unit
e_{ijk}	Permutation symbol

E	Young's modulus of elasticity
ϵ	Small strain tensor
$F(t), F(\bar{\omega})$	Compliance function
f, \hat{f}	Arbitrary functions
F_{kl}^{ij}	The compliance function of foundation i in direction k due to the force acting on foundation j in direction l
$\bar{\mathbf{F}}_r$	Dynamic flexibility matrix of the rigid foundation
$[\mathbf{F}_s]$	Modal compliance matrix of the soil
$\bar{\mathbf{F}}_s$	Dynamic flexibility matrix of the surface of the soil
$\circ\bullet$	Fourier transformation
$\bullet\circ$	Inverse Fourier transformation
G	Shear modulus
h_1, H	Depth of the soil layer
$[\mathbf{I}]$	Identity matrix
$\hat{\mathbf{K}}_\sigma$	Matrix relating stress components and unknown coefficients in halfspace
$\hat{\mathbf{K}}_u$	Matrix relating displacement components and unknown coefficients in halfspace
k	Pure bending wavenumber of a spectral beam element
$K(t), K(\bar{\omega})$	Impedance function
K, K^*	Foundation-soil stiffness ratios

k_p, k_s	P- and S-waves wavenumbers
k_x, k_y	Wavenumbers
$[\mathbf{k}^4]$	Pure bending wavenumber matrix of the spectral beam element
${}_{BC}\hat{\mathbf{K}}^\sigma$	Matrix relating boundary conditions and coefficients of integration
$\bar{\mathbf{K}}_r$	Dynamic stiffness matrix of the rigid foundation
k_r	Radial wavenumber
$[\mathbf{K}_s]$	Modal impedance matrix of the soil
$\bar{\mathbf{K}}_s$	Dynamic stiffness matrix of the surface of the soil
λ_1, λ_2	Roots of the characteristic equation
λ, μ	Lamé's material constants
ν	Poisson's ratio
N_x	Number of soil surface discretization points
ω	Radial frequency
$\boldsymbol{\omega}$	Rotation tensor
P	Unit force amplitude
$p(x), p(x, y)$	Foundation active load
p_i	External load components, $i = x, y, z$
$\phi(x)$	Spectral beam mode shape
φ, ψ	Helmholtz potentials
$\phi_n^*(x)$	Orthonormalized mode shape function of the spectral beam element

$\bar{\mathbf{P}}_r$	Force vector of the rigid foundation
$\bar{\mathbf{P}}_s$	Force vector of the surface of the soil
$q(x), q(x, y)$	Foundation reactive load
ρ	Material density
$\bar{\sigma}$	Dimensionless stress
$\boldsymbol{\sigma}$	Cauchy stress tensor
$\epsilon_{ii}, \gamma_{ij}$	Deformation field components, $i = x, y, z, j = x, y, z$
σ_{ii}, τ_{ij}	Stress field components, $i = x, y, z, j = x, y, z$
t	Time
$\widehat{\mathbf{TF}}$	Transfer function matrix relating displacement vector and load vector
\mathbf{u}	Displacement vector
u_i	Displacement field components, $i = x, y, z$
$\bar{\mathbf{u}}_r$	Displacement vector of the rigid foundation
$\bar{\mathbf{u}}_s$	Displacement vector of the surface of the soil
u_s	Displacement vector of the surface of the soil
v	Moving load velocity
$w(x), w(x, y)$	Transverse deflection of the foundation
w_{SS}	The displacement field of the plate for the double symmetry case
\mathbf{x}	Position vector

X	The distance between the centroids of the foundations in the system of two foundations
x, y, z	Cartesian coordinates
x_j	Coordinate axis
$\{\mathbf{Y}\}, \{\mathbf{P}\}, \{\mathbf{Q}\}$	Vectors of modal coefficients
Y_n, P_n, Q_n	Modal coefficients
ζ	Damping ratio

Acronyms

SSI	Soil Structure Interaction
SFI	Soil Foundation Interaction
FEM	Finite Element Method
FE	Finite Element
BEM	Boundary Element Method
ITM	Integral Transform Method
SEM	Spectral Element Method
TLM	Thin Layer Method
PML	Perfectly Matched Layer
ABC	Absorbing Boundary Conditions
PIM	Precise Integration Method

FSFI Foundation Soil Foundation Interaction

FT Fourier Transformation

CFT Continuous Fourier Transform

DFT Discrete Fourier Transform

FFT Fast Fourier Transform

1 Introduction

1.1 Motivation

In the dynamic analysis of structures, the effect of Soil Structure Interaction (SSI) is usually neglected for the sake of the simplicity. It is often assumed that the structure is rigidly fixed on its base. This assumption is not always justified. Critical and monumental facilities, as well as facilities equipped with sensitive instruments are demanding detailed analysis of their interaction with the environment.

The SSI analysis involves the soil and the structure model. The modeling of structures is usually done using the Finite Element Method (FEM) considering its ability to handle detailed and complex geometry. On the other hand, the application of the FEM in the soil modeling is very resource demanding, especially in the field of dynamics. It requires a special boundary at the sufficient distance from the structure that is able to let the waves pass through and propagate toward infinity. Therefore, the soil modeling calls for a different modeling technique. This is the reason the classical approach of solving SSI problems is based on substructuring techniques. The domain is decomposed in two subdomains: the unbounded domain - soil, and the bounded domain - structure. The subdomains are modeled separately. The interaction is realized through the compatibility of the boundaries that reside in the

interface between the subdomains. The boundaries outside the interface zone assume free surface boundary conditions.

The SSI analysis could be reduced to the Soil Foundation Interaction (SFI) analysis. The aim is to find the dynamic stiffness of the foundation-soil system that could be assembled into the dynamic stiffness of the structure. The SFI problem is commonly solved by assuming the foundation as a rigid plate. That simplifies the formulation of the problem, but it reduces the scope of applicability of the solution. In reality, foundations are always flexible to a certain degree.

The response of the flexible foundation on a halfspace is solved using substructuring technique. Different methods have been used for subdomains modeling, regarding their distinct nature. The solution of the problem is usually obtained by using the Boundary Element Method (BEM) for soil modeling and the FEM for the model of the foundation.

In this work, analytical methods based on transform techniques are used. The original problem formulated in the space-time domain is transformed into the space-frequency or wavenumber-frequency domain. The system of partial differential equations in space-time domain becomes the system of uncoupled ordinary differential equations in the transformed domain. The solution of the system is obtained by taking into account boundary conditions. The new domain is more convenient for the calculation and the effects of the input parameters on the results are more visible than in the original domain. That gives a clear insight into the physics of the problem. The Integral Transform Method (ITM) is used for soil modeling. Using ITM, it is possible to obtain the analytical solution of the wave propagation in soil medium. The solution is exact, but applicable on simple geometries and linear elastic materials. The Spectral Element Method (SEM) is used for the foundation modeling. The modeling technique is similar to the FEM, but it provides the exact solution of the wave propagation in plates.

The aim of this dissertation is to develop a coupling approach of the ITM and the SEM in order to solve the problem of a strip and rectangular flexible foundation on a halfspace.

1.2 State of Research

According to Kausel [1], the roots of SSI lead to the early part of the 19th century when Lamé and Clapeyron were studying the fundamental solution of an infinite or semi infinite elastic body: an analytical expression for the response anywhere in a body excited by a static or dynamic point source at an arbitrary location. They have failed to obtain useful results, but they were the first to address the problem. The first significant contribution in the scope of dynamics was published by Lamb [2] 1904. He presented the fundamental solution for a homogeneous halfspace subjected to a dynamic load on its surface in terms of integral transforms. Lamb analyzed in detail only the response at a remote distance from the source (far field).

The theory of dynamic SSI begins in 1936 with Reissner's publication concerning the response of cylindrical disk on an elastic halfspace subjected to a time harmonic vertical load. He was the first to address the radiation damping phenomena: an energy loss occurring due to the wave propagation from the zone of the structure towards infinity. Later researches were directed toward the generalization of Reissner's model. According to [3], Sung and Quinlan analyzed vertically excited rectangular foundations. Vertical, horizontal and rocking oscillations of circular foundations were analyzed by Bycroft [4]. A true mixed boundary problem was not solved. It was assumed that the contact stress and the displacement field at the interface between the footing and the soil is uniform or linear - similar to static stress. Therefore, the solution was only applicable to low frequency problems.

The first mixed boundary problem solutions appear in the third quarter of the XX century. A specific displacement distribution under the rigid footing and vanishing stresses over the remaining portion of the surface of the soil are assumed. The problem is also simplified by assuming that there are no secondary contact stresses. For example, vertical vibrations are not induced by horizontal stresses. Oscillations of rigid circular and strip foundations are analyzed by Awojobi [5] using integral techniques. According to [3], Lysmer obtained the solution for vertical vibrations discretizing the contact surface into concentric rings of uniform frequency depended vertical stresses. He also considered the approximation of the soil-foundation system with a single degree of freedom oscillator, suggesting the frequency dependent stiffness and damping coefficients. This idea was well accepted among other researches and extended on the solution for horizontal, rocking and torsional vibrations. The solution was applicable to low and medium frequency range problems.

Contemporary era starts with Luco and Westmann [6] who analyzed rigid circular footings on halfspace using Fredholm integral equations. They extended the existing halfspace solution to the high frequency range, also introducing a viscoelastic material with linear hysteretic damping. Luco [7] also presented analytical solutions for rigid strip and rectangular foundations on the surface of layered halfspace or a layered stratum.

The development of powerful digital computers led to the expansion of numerical methods. Various FEM formulations with energy absorbing lateral boundaries were developed, such as viscous [8] and consistent boundary [9]. Consistent boundaries could be placed in the vicinity of the foundation, saving computational effort and time, but they could be applied only for plane strain and axisymmetrical problems. The Thin Layer Method (TLM) was built on the basis of the FEM formulation and it was used for the analysis of horizontally layered soils. The discretization of the soil is performed using unbounded thin horizontal layers over the bedrock.

The equations of the system describes the exact solution of wave propagation in horizontal directions, while a linear variation of the displacements in the vertical direction is assumed. Lysmer et al. developed a software package SASSI [10] using a substructure approach where the structure is modeled using the FEM and the soil is modeled using the TLM. These FEM formulations could not take into account the infinite soil medium in vertical direction. An infinite halfspace was simulated with a finite number of deep layers resting on the bedrock.

The modeling of the unbounded domain in the scope of the FEM could be also performed using infinite elements. They were derived by Peter Bettles and Jacqueline A. Bettles; first for static problems [11] and then for dynamic problems [12]. They are applied in elastodynamics in both time [13] and frequency domain [14].

Application of the FEM in 3D dynamic soil modeling is very cumbersome and therefore rarely used in practice. The main disadvantage is observed in the high frequency range. Lysmer [10] concluded that in order to be sure that the finite element transmits wave at a certain frequency, the dimension of the finite element should be at least eight times smaller than the corresponding wavelength. The resulting model must contain a fine FE mesh that leads to a large number of elements and unknowns. Finding a solution of such systems is time consuming, resource demanding and hard for practical implementation. On the other hand, the scope of applicability of pure analytical solutions is narrow. For example, analytical solutions of flexible foundations resting on the soil exist only for circular footings in cylindrical coordinates [15, 16]. That led to the development of approximate analytical or semi-analytical methods. These methods are using the fundamental solution of the governing equations of the problem but they involve discretization of the soil surface - boundary. Since only the soil surface has to be discretized, in comparison with the FEM, the dimension of the problem is reduced by one. In order to solve boundary integral equations, different techniques were developed over time using

different fundamental solutions. Whittaker and Christiano [17] used Lamb's solution for a point loaded halfspace. Wong [18] used the solution for a uniformly loaded rectangle. According to [1] and [3], Dominguez was one of the first to use the BEM for foundation mechanics problem. Fundamental solution of the BEM is the Green's function. The Green's function represent the solution of dynamic differential equation with point source defined on a soil domain with specified boundary conditions. The solution to the arbitrary force can be obtained by integrating the Green's function against the forcing term. The Green's function satisfies the radiation condition automatically, but it is limited to linear homogeneous medium problems. In general, its integration is not easy, since it relates to the problem involving a concentrated load - singularity. Although the BEM results in smaller system matrices than the FEM, the system matrices are fully populated. Therefore, the computational requirements grow to the square of the size of the problem, unlike in the FEM where the growth is linear.

The BEM is the most used soil modeling technique today. Together with the FEM it creates a coupling method for dynamic SSI analysis that is used by many authors. This coupling technique is used for the analysis of various problems: a group of rigid circular [19] and rectangular foundations [19, 20], flexible rectangular [21] and flexible strip foundations [22, 23] on halfspace. The technique is also applied on problems involving layered halfspace [24]. The problems could be formulated in time [22] or in frequency [23] domain.

Another soil modeling technique is ITM. The methodology of ITM is described by Wolf [25], 1985. The properties and the application of the ITM has been a subject of several doctoral dissertations at the Technical Univeristy of Munich [26, 27, 28, 29, 30, 31, 32, 33, 34, 35]. The method is based on an analytical solution of the equations of motion, obtained by transforming the system of equations from the time-space domain to the frequency-wavenumber domain using Fourier transforms.

The response of the system is transferred in the original domain using inverse Fourier transforms. The inverse transform procedure is not an easy task. It could be very time and resource demanding, especially if the response function involves singularities. Müller [28] expanded the applicability of ITM to problems of dynamic SSI using mixed boundary conditions for describing the layered halfspace surface. Although the ITM is limited to regular geometries, Rastandi [36] and Hackenberg [26] showed that the description of complex geometries is possible through coupling with the FEM. Radišić et al. [37] showed that the ITM is applicable on problems of rigid rectangular foundations resting on halfspace. The application of ITM for the calculation of the response of the system subjected to a moving load is shown by Grundmann [38] and Radišić et al. [39].

The analysis of SFI problems involving flexible rectangular foundations is possible using ITM-SEM coupling. The SEM is proved to be a good alternative to the FEM in structural dynamics [40]. The method is based on the spectral form of the displacement field and on the exact solution of the governing differential equations of motion in the frequency domain. SEM could be applied to a wide spectrum of structures: beams, bars, plates and cylindrical shells [41]. According to Banerjee and Williams [42], the roots of the SEM leads to Kolousek, who was the first to develop the dynamic stiffness matrix of an Euler-Bernoulli beam. In the last couple of decades, a lot of effort was put into developing a high precision continuous element for transverse vibration analysis of plates with arbitrary boundary conditions. Kulla [43] was the first one to do so. The dynamic stiffness matrix of 2D completely free Kirchhoff plate element is built by Casimir et al. [44] using Gorman's superposition method. Boscolo and Banerjee developed the dynamic stiffness matrix of plate using the first order shear deformation theory [45]. They have also formulated the dynamic stiffness of the composite Mindlin plate using spectral elements [46, 47]. The dynamic stiffness matrix of plate undergoing in-plane vibrations and the coupling of 1D and 2D spectral elements has been developed by Nefovska-Danilović [48]. The coupling

with the soil could be established using the substructure method. The application of SEM on 2D frames founded on the halfspace is shown by Petronijević et al. [49].

1.3 Layout of the Thesis

This thesis presents the derivation of a coupled ITM-SEM approach for analyzing the behavior of rigid and flexible foundations resting on the soil. The stiffness matrix of the soil-foundation system is obtained using the substructure technique. The ITM is used for obtaining the fundamental solution of wave propagation in soil. The SEM is used for obtaining the fundamental solution of wave propagation in the foundation. The coupling of the obtained fundamental solutions is performed using the modal superposition technique.

Chapter 2 presents the formulation of the ITM. The method is based on solving Lamé's differential equation by decoupling it using the Helmholtz decomposition and transforming it from partial to ordinary differential equation using a threefold Fourier Transform. The ordinary differential equation is solved by taking into account the boundary conditions of the system. The solutions of the homogeneous halfspace and the horizontally layered halfspace are presented. Since the solution in rectangular coordinates is semi-analytical, the numerical example is provided, explaining the influence of the discretization of the problem on the accuracy of the results. A brief presentation on obtaining the fundamental solution of the halfspace due to a moving load with the numerical example is given at the end of the chapter.

Chapter 3 deals with obtaining the dynamic stiffness and dynamic flexibility matrices of the foundation. First, the dynamic stiffness matrix of the rigid, surface and massless foundation is derived using the fundamental solution of the halfspace and the kinematic transform. It is shown that a similar procedure could be used to obtain

the response of the group of rigid foundations resting on the soil. The presented numerical examples analyze the compliance functions of the square rigid foundation resting on the halfspace and the foundation-soil-foundation interaction of the group of two rigid foundations resting on the layer over the bedrock.

The main contribution of this thesis, the formulation of a coupled ITM-SEM approach, is given in this chapter. First, the dynamic stiffness matrix of the foundation is obtained using SEM. The natural frequencies and the mode shapes of the foundation are calculated using its dynamic stiffness matrix. The differential equation of the soil-foundation system is transformed to the system of algebraic equations using the modal superposition method. The soil-foundation coupling is realized through the modal stiffness matrix of the soil obtained using the ITM. The ITM-SEM approach is applied on the flexible strip foundation and the flexible square foundation resting on the halfspace. The results of the analyses in terms of foundation compliance functions, displacement fields and contact stress fields are compared with the results from literature.

Chapter 4 gives the summary of the dissertation and the ideas for the future research.

2 Wave Propagation in Halfspace by ITM

This chapter describes the formulation of the wave propagation in the soil. The problem is formulated in 3D space, where an arbitrarily chosen point is defined by three Cartesian coordinates x, y and z . The soil is considered as a halfspace, bounded with the plane $xy0$ as surface of the soil. The halfspace is considered isotropic, homogeneous and elastic. The material properties of the halfspace may vary with depth, forming layers, but the properties within the layer must remain constant.

2.1 Wave Propagation in Continuum

For the following formulation it is convenient to use a tensor notation. Scalars are denoted with light italic symbols (u, σ), vectors and second order tensors with bold symbols ($\mathbf{u}, \boldsymbol{\sigma}$), matrices with upright bold letters ($\mathbf{u}, \boldsymbol{\sigma}, \mathbf{A}$). A tensor notation is explained in details in Appendix A.1.

The coordinate axes are denoted by x_j , where $j = 1, 2, 3$. The displacement vector at a point \mathbf{x} and time t is $\mathbf{u}(\mathbf{x}, t)$.

The stress and the deformation state of a continuum body of elemental volume is described by Cauchy stress tensor $\boldsymbol{\sigma}$ and small strain tensor (linearized strain tensor)

ϵ . The components of the small strain tensor ϵ are defined by

$$\epsilon_{ij} = \frac{1}{2} (u_{i,j} + u_{j,i}) \quad (2.1)$$

where $u_{i,j}$ is the first derivative of displacement component u_i with respect to x_j , $\partial u_i / \partial x_j$, and $u_{j,i}$ is the first derivative of displacement component u_j with respect to x_i , $\partial u_j / \partial x_i$.

The components of the rotation tensor ω are given by

$$\omega_{ij} = \frac{1}{2} (u_{i,j} - u_{j,i}) \quad (2.2)$$

The Cauchy's first law of motion could be obtained from the balance of linear momentum. In the absence of body forces, it is described as following

$$\sigma_{kl,k} = \rho \ddot{u}_l \quad (2.3)$$

where σ_{kl} are the components of the Cauchy stress tensor σ and ρ is the material density, and \ddot{u}_l is the second derivative of displacement component u_l with respect to time t , $\partial^2 u_l / \partial t^2$. . Since the material is homogeneous, elastic and isotropic, the stress strain relation is given by

$$\sigma_{ij} = \lambda \epsilon_{kk} \delta_{ij} + 2\mu \epsilon_{ij} \quad (2.4)$$

where λ and μ are Lamé's material constants, and δ_{ij} is Kronecker delta (A.4). Lamé's constants can be expressed in terms of Young's modulus of elasticity E and Poisson's ration ν :

$$\lambda = \frac{E\nu}{(1+\nu)(1-2\nu)} \quad (2.5)$$

$$\mu = G = \frac{E}{2(1+\nu)}$$

A complete system of equations of motion of homogeneous, isotropic and linear elastic bodies is formed by equations (2.1), (2.3) and (2.4). If we substitute Equation (2.1) in Equation (2.4) we obtain

$$\sigma_{ij} = \lambda u_{k,k} \delta_{ij} + \mu u_{i,j} + \mu u_{j,i} \quad (2.6)$$

Then

$$\begin{aligned} \sigma_{ij,j} &= (\lambda u_{k,k} \delta_{ij})_{,j} + \mu u_{i,jj} + \mu u_{j,ij} \\ &= \lambda u_{j,ij} + \mu u_{i,jj} + \mu u_{j,ij} \\ &= \mu u_{i,jj} + (\lambda + \mu) u_{j,ij} \end{aligned}$$

Substituting Equation (2.7) into Cauchy's law of motion (2.3) we obtain Navier's equations of motion:

$$\mu u_{i,jj} + (\lambda + \mu) u_{j,ij} = \rho \ddot{u}_i \quad (2.7)$$

These equations represent the system of partial differential equations. The system is transformed into the system of uncoupled differential equations using Helmholtz decomposition. Helmholtz decomposition states that any sufficiently smooth, rapidly decaying vector field in three dimensions can be resolved into the sum of an irrotational (curl-free) vector field (φ_i) and a solenoidal (divergence-free) vector field ($e_{ijk} \psi_{k,j}$):

$$u_i = \varphi_i + e_{ijk} \psi_{k,j} \quad (2.8)$$

where φ and ψ are Helmholtz potentials and e_{ijk} is permutation symbol (A.5).

Equations (2.7) and (2.8) could be written in vector form as follows:

$$\mu \nabla^2 \mathbf{u} + (\lambda + \mu) \nabla \nabla \cdot \mathbf{u} = \rho \ddot{\mathbf{u}} \quad (2.9)$$

$$\mathbf{u} = \nabla\varphi + \nabla \times \boldsymbol{\psi} \quad (2.10)$$

Substituting equation (2.10) into equation (2.9) we obtain

$$\mu \nabla^2 [\nabla\varphi + \nabla \times \boldsymbol{\psi}] + (\lambda + \mu) \nabla \nabla \cdot [\nabla\varphi + \nabla \times \boldsymbol{\psi}] = \rho \frac{\partial^2}{\partial t^2} [\nabla\varphi + \nabla \times \boldsymbol{\psi}] \quad (2.11)$$

Using identities $\nabla \cdot \nabla\varphi = \nabla^2\varphi$ and $\nabla \cdot \nabla \times \boldsymbol{\psi} = 0$ equation (2.11) could be written as following

$$\nabla [(\lambda + \mu) \nabla^2\varphi - \rho \ddot{\varphi}] + \nabla \times [\mu \nabla^2\boldsymbol{\psi} - \rho \ddot{\boldsymbol{\psi}}] = 0 \quad (2.12)$$

From equation (2.12) follows:

$$\nabla^2\varphi = \frac{1}{c_p^2} \ddot{\varphi} \quad (2.13)$$

and

$$\nabla^2\boldsymbol{\psi} = \frac{1}{c_s^2} \ddot{\boldsymbol{\psi}} \quad (2.14)$$

where c_p and c_s are velocities of the waves propagating through continuum:

$$c_p^2 = \frac{\lambda + 2\mu}{\rho} \quad (2.15)$$

$$c_s^2 = \frac{\mu}{\rho} \quad (2.16)$$

The velocity c_p is called the velocity of compressional, longitudinal or P-waves, since it has influence on the irrotational vector field only. The velocity c_s is called the velocity of shear, transverse or S-waves, since it has influence on the solenoidal vector field only.

2.2 Wave Equations in Elastic Halfspace

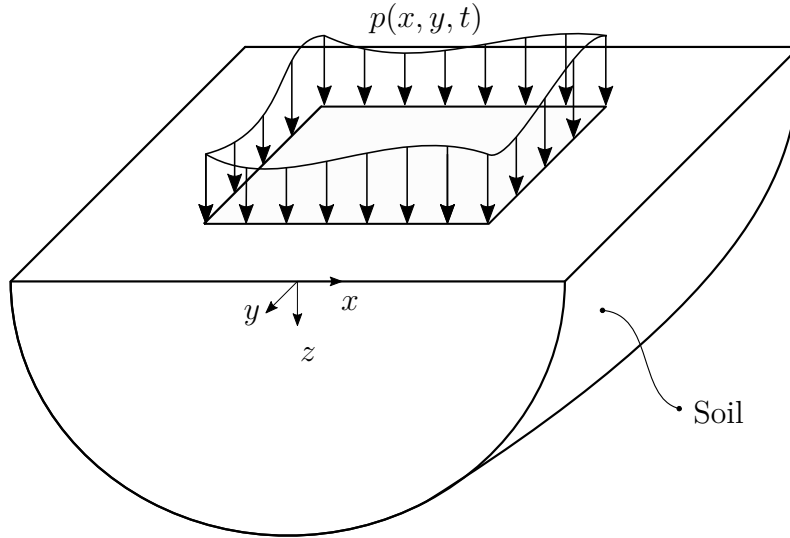


Figure 2.1: Halfspace model excited by a load acting on the surface

The system of the halfspace excited by a load acting on the surface is depicted in Figure 2.1. The solution is obtained in Cartesian coordinate system.

The four potentials φ , ψ_x , ψ_y and ψ_z from equation (2.8) are not uniquely determined with the three displacement vector components u_x , u_y and u_z . However, choosing $\psi_z = 0$ does not affect the accuracy of the solution [50].

Considering $\psi_z = 0$, equations (2.13) and (2.14) become

$$\begin{aligned} \left(\frac{\partial^2}{\partial x^2} + \frac{\partial^2}{\partial y^2} + \frac{\partial^2}{\partial z^2} - \frac{1}{c_p^2} \frac{\partial^2}{\partial t^2} \right) \varphi(x, y, z, t) &= 0 \\ \left(\frac{\partial^2}{\partial x^2} + \frac{\partial^2}{\partial y^2} + \frac{\partial^2}{\partial z^2} - \frac{1}{c_s^2} \frac{\partial^2}{\partial t^2} \right) \psi_x(x, y, z, t) &= 0 \\ \left(\frac{\partial^2}{\partial x^2} + \frac{\partial^2}{\partial y^2} + \frac{\partial^2}{\partial z^2} - \frac{1}{c_s^2} \frac{\partial^2}{\partial t^2} \right) \psi_y(x, y, z, t) &= 0 \end{aligned} \quad (2.17)$$

Also, Equation (2.8) in expanded form reads

$$\begin{aligned}
 u_x &= \varphi_x - \psi_{y,z} \\
 u_y &= \varphi_y + \psi_{x,z} \\
 u_z &= \varphi_z - \psi_{x,y} + \psi_{y,x}
 \end{aligned} \tag{2.18}$$

The solution of the system (2.17) is obtained using ITM. The system is transformed into the system of ordinary differential equations using a threefold Fourier transformation given as

$$\hat{f}(k_x, k_y, z, \omega) = \int_{x=-\infty}^{\infty} \int_{y=-\infty}^{\infty} \int_{t=-\infty}^{\infty} f(x, y, z, t) e^{-ik_x x} e^{-ik_y y} e^{-i\omega t} dx dy d\omega \tag{2.19}$$

where $\hat{f}(k_x, k_y, z, \omega)$ is a Fourier transform of an arbitrary function $f(x, y, z, t)$. The transformation is applied to the spatial coordinates $x \circ \bullet k_x$, $y \circ \bullet k_y$ and time $t \circ \bullet \omega$, while the spatial coordinate z remains untransformed. After the transformation the system (2.17) becomes:

$$\begin{aligned}
 \left(-k_x^2 - k_y^2 + k_p^2 + \frac{\partial^2}{\partial z^2} \right) \hat{\varphi}(k_x, k_y, z, \omega) &= 0 \\
 \left(-k_x^2 - k_y^2 + k_s^2 + \frac{\partial^2}{\partial z^2} \right) \hat{\psi}_x(k_x, k_y, z, \omega) &= 0 \\
 \left(-k_x^2 - k_y^2 + k_s^2 + \frac{\partial^2}{\partial z^2} \right) \hat{\psi}_y(k_x, k_y, z, \omega) &= 0
 \end{aligned} \tag{2.20}$$

where k_p and k_s are wavenumbers of P- and S-waves for a given frequency ω

$$\begin{aligned}
 k_p &= \frac{\omega}{c_p} \\
 k_s &= \frac{\omega}{c_s}
 \end{aligned} \tag{2.21}$$

while the symbol $\hat{}$ denotes quantities in the transformed domain (k_x, k_y, z, ω) .

The solution of differential equations (2.20) is given in exponential form

$$\begin{aligned}\hat{\varphi} &= A_1 e^{\lambda_1 z} + A_2 e^{-\lambda_1 z} \\ \hat{\psi}_i &= B_{i1} e^{\lambda_2 z} + B_{i2} e^{-\lambda_2 z}\end{aligned}\tag{2.22}$$

where λ_1 and λ_2 represents the roots of the characteristic equation

$$\begin{aligned}\lambda_1 &= \sqrt{k_x^2 + k_y^2 - k_p^2} \\ \lambda_2 &= \sqrt{k_x^2 + k_y^2 - k_s^2}\end{aligned}\tag{2.23}$$

while $i = x, y$. The unknown coefficients A_1, A_2, B_{i1} and B_{i2} are obtained using the boundary conditions of the system.

2.3 Boundary Conditions

The physical interpretation of the solution depends on the sign of λ_1 and λ_2 . If λ_1 takes imaginary values ($k_x^2 + k_y^2 < k_p^2$), the solution represents the spatially propagating P-waves. Depending on the sign of λ_1 the waves are propagating in positive ($\lambda_1 < 0$) or negative ($\lambda_1 > 0$) z direction. If λ_1 takes real values ($k_x^2 + k_y^2 > k_p^2$), the solution consists of surface waves. Depending on the sign of λ_1 the waves are exponentially increasing or decaying with depth. Analogously, depending on the λ_2 the solution represents the spatially propagating S-waves ($k_x^2 + k_y^2 < k_s^2$) or surface waves ($k_x^2 + k_y^2 > k_s^2$).

According to the Sommerfeld radiation condition [51] “the energy which is radiated from the sources must scatter to infinity; no energy may be radiated from infinity into the prescribed singularities of the field”. Since the load is applied only on the surface of the halfspace, some of the coefficients A_1, A_2, B_{i1}, B_{i2} could be set to zero. In the case of $\omega > 0$, for spatially propagating waves, coefficients A_2 and B_{i2} could

be set to zero, as well as coefficients A_1 and B_{i1} for surface waves. They are either describing the waves propagating from infinity toward the surface of the halfspace (A_2 and B_{i2}), or surface waves with amplitudes exponentially increasing with the depth (A_1 and B_{i1}). Müller [28] showed that for $\omega < 0$, coefficients that describe the waves that are impossible to occur are A_1 and B_{i1} for both spatially propagating and surface waves. Thus, using negative frequencies is more convenient.

The three remaining constants A_2 , B_{x2} and B_{y2} are obtained from the boundary conditions on the surface of the halfspace

$$\begin{aligned}\hat{\sigma}_{zz} &= -\hat{p}_z \\ \hat{\tau}_{zy} &= -\hat{p}_y \\ \hat{\tau}_{zx} &= -\hat{p}_x\end{aligned}\tag{2.24}$$

where $\hat{\mathbf{p}}(\hat{p}_x, \hat{p}_y, \hat{p}_z)$ is the active load vector. The relation between stress components and unknown coefficients is derived using material law (2.4), kinematic relations (2.1) and Helmholtz decomposition (2.10). The equations (2.4), (2.1) and (2.10) must be transformed into (k_x, k_y, z, ω) domain:

$$(2.4) \circ \bullet \begin{pmatrix} \hat{\sigma}_{xx} \\ \hat{\sigma}_{yy} \\ \hat{\sigma}_{zz} \\ \hat{\tau}_{xy} \\ \hat{\tau}_{yz} \\ \hat{\tau}_{zx} \end{pmatrix} = \begin{bmatrix} \lambda + 2\mu & \lambda & \lambda & 0 & 0 & 0 \\ \lambda & \lambda + 2\mu & \lambda & 0 & 0 & 0 \\ \lambda & \lambda & \lambda + 2\mu & 0 & 0 & 0 \\ 0 & 0 & 0 & 2\mu & 0 & 0 \\ 0 & 0 & 0 & 0 & 2\mu & 0 \\ 0 & 0 & 0 & 0 & 0 & 2\mu \end{bmatrix} \begin{pmatrix} \hat{\epsilon}_{xx} \\ \hat{\epsilon}_{yy} \\ \hat{\epsilon}_{zz} \\ \hat{\gamma}_{xy} \\ \hat{\gamma}_{yz} \\ \hat{\gamma}_{zx} \end{pmatrix}\tag{2.25}$$

$$(2.1) \circ \bullet \left\{ \begin{array}{c} \hat{\epsilon}_{xx} \\ \hat{\epsilon}_{yy} \\ \hat{\epsilon}_{zz} \\ \hat{\gamma}_{xy} \\ \hat{\gamma}_{yz} \\ \hat{\gamma}_{zx} \end{array} \right\} = \begin{bmatrix} ik_x & 0 & 0 \\ 0 & ik_y & 0 \\ 0 & 0 & \frac{\partial}{\partial z} \\ \frac{1}{2}ik_y & \frac{1}{2}ik_x & 0 \\ 0 & \frac{1}{2}\frac{\partial}{\partial z} & \frac{1}{2}ik_y \\ \frac{1}{2}\frac{\partial}{\partial z} & 0 & \frac{1}{2}ik_x \end{bmatrix} \left\{ \begin{array}{c} \hat{u}_x \\ \hat{u}_y \\ \hat{u}_z \end{array} \right\} \quad (2.26)$$

$$(2.10) \circ \bullet \left\{ \begin{array}{c} \hat{u}_x \\ \hat{u}_y \\ \hat{u}_z \end{array} \right\} = \begin{bmatrix} ik_x & 0 & -\frac{\partial}{\partial z} \\ ik_y & \frac{\partial}{\partial z} & 0 \\ \frac{\partial}{\partial z} & -ik_y & ik_x \end{bmatrix} \left\{ \begin{array}{c} \hat{\varphi} \\ \hat{\psi}_x \\ \hat{\psi}_y \end{array} \right\} \quad (2.27)$$

Equation (2.22) could be written in matrix form

$$\left\{ \begin{array}{c} \hat{\varphi} \\ \hat{\psi}_x \\ \hat{\psi}_y \end{array} \right\} = \begin{bmatrix} e^{\lambda_1 z} & e^{-\lambda_1 z} & 0 & 0 & 0 & 0 \\ 0 & 0 & e^{\lambda_2 z} & e^{-\lambda_2 z} & 0 & 0 \\ 0 & 0 & 0 & 0 & e^{\lambda_2 z} & e^{-\lambda_2 z} \end{bmatrix} \left\{ \begin{array}{c} A_1 \\ A_2 \\ B_{x1} \\ B_{x2} \\ B_{y1} \\ B_{y2} \end{array} \right\} \quad (2.28)$$

Substituting equation (2.28) into equation (2.27) gives the relation between the displacement components and the unknown coefficients

$$\begin{pmatrix} \hat{u}_x \\ \hat{u}_y \\ \hat{u}_z \end{pmatrix} = \underbrace{\begin{bmatrix} ik_x & ik_x & 0 & 0 & -\lambda_2 & \lambda_2 \\ ik_y & ik_y & \lambda_2 & -\lambda_2 & 0 & 0 \\ \lambda_1 & -\lambda_1 & -ik_y & -ik_y & ik_x & ik_x \end{bmatrix}}_{\hat{\mathbf{K}}_u} \begin{pmatrix} A_1 e^{\lambda_1 z} \\ A_2 e^{-\lambda_1 z} \\ B_{x1} e^{\lambda_2 z} \\ B_{x2} e^{-\lambda_2 z} \\ B_{y1} e^{\lambda_2 z} \\ B_{y2} e^{-\lambda_2 z} \end{pmatrix} \quad (2.29)$$

The relationship between the stress components and the unknown coefficients is obtained substituting equation (2.29) into equation (2.26) and then further into equation (2.25)

$$\begin{pmatrix} \hat{\sigma}_{xx} \\ \hat{\sigma}_{yy} \\ \hat{\sigma}_{zz} \\ \hat{\tau}_{xy} \\ \hat{\tau}_{yz} \\ \hat{\tau}_{zx} \end{pmatrix} = \mu \begin{bmatrix} -2k_x^2 - \frac{\lambda}{\mu} k_p^2 & -2k_x^2 - \frac{\lambda}{\mu} k_p^2 & 0 & 0 & -2ik_x \lambda_2 & 2ik_x \lambda_2 \\ -2k_y^2 - \frac{\lambda}{\mu} k_p^2 & -2k_y^2 - \frac{\lambda}{\mu} k_p^2 & 2ik_y \lambda_2 & -2ik_y \lambda_2 & 0 & 0 \\ 2k_r^2 - ks^2 & 2k_r^2 - ks^2 & -2ik_y \lambda_2 & 2ik_y \lambda_2 & 2ik_x \lambda_2 & -2ik_x \lambda_2 \\ -2k_x k_y & -2k_x k_y & ik_x \lambda_2 & -ik_x \lambda_2 & -ik_y \lambda_2 & ik_y \lambda_2 \\ 2ik_y \lambda_1 & -2ik_y \lambda_1 & \lambda_2^2 + k_y^2 & \lambda_2^2 + k_y^2 & -k_x k_y & -k_x k_y \\ 2ik_x \lambda_1 & -2ik_x \lambda_1 & k_x k_y & k_x k_y & -\lambda_2^2 - k_x^2 & -\lambda_2^2 - k_x^2 \end{bmatrix} \begin{pmatrix} A_1 e^{\lambda_1 z} \\ A_2 e^{-\lambda_1 z} \\ B_{x1} e^{\lambda_2 z} \\ B_{x2} e^{-\lambda_2 z} \\ B_{y1} e^{\lambda_2 z} \\ B_{y2} e^{-\lambda_2 z} \end{pmatrix} \quad (2.30)$$

where

$$k_r = \sqrt{k_x^2 + k_y^2} \quad (2.31)$$

Considering equation (2.30), the boundary conditions (2.24) at the surface of the halfspace ($z = 0$) can be expressed in terms of unknown coefficients

$$\begin{pmatrix} \hat{\sigma}_{zz} \\ \hat{\tau}_{zy} \\ \hat{\tau}_{zx} \end{pmatrix} = \mu \underbrace{\begin{bmatrix} 2k_r^2 - ks^2 & 2ik_y\lambda_2 & -2ik_x\lambda_2 \\ -2ik_y\lambda_1 & \lambda_2^2 + k_y^2 & -k_xk_y \\ -2ik_x\lambda_1 & k_xk_y & -\lambda_2^2 - k_x^2 \end{bmatrix}}_{\hat{\mathbf{K}}_\sigma} \begin{pmatrix} A_2 \\ B_{x2} \\ B_{y2} \end{pmatrix} = \begin{pmatrix} -\hat{p}_z \\ -\hat{p}_y \\ -\hat{p}_x \end{pmatrix} \quad (2.32)$$

The system of equations (2.32) gives a unique solution $\{A_2, B_{x2}, B_{y2}\}$. The displacement components could be derived using Eq. (2.29) and transformed into original domain (x, y, z, t) using a threefold inverse Fourier transformation defined as

$$f(x, y, z, t) = \int_{k_x=-\infty}^{\infty} \int_{k_y=-\infty}^{\infty} \int_{\omega=-\infty}^{\infty} \hat{f}(k_x, k_y, z, \omega) e^{ik_x x} e^{ik_y y} e^{i\omega t} dx dy d\omega \quad (2.33)$$

where $f(x, y, z, t)$ is an inverse Fourier transform of an arbitrary function $\hat{f}(k_x, k_y, z, \omega)$.

2.3.1 Layered Halfspace

The solution of layered halfspace is based on the solution of homogeneous halfspace. Since layers are of finite depth the Sommerfeld condition does not apply and all six coefficients contribute to the solution (2.22). The coefficients are obtained using boundary conditions at the top and at the bottom of the layer.

A simple example of a layered halfspace is shown in Figure 2.2. The system is consisted of one layer on top of the halfspace. The unknowns related to the halfspace are $A_{2,l_2}, B_{x2,l_2}, B_{y2,l_2}$, according to Section 2.3. The unknowns related to the layer are $A_{1,l_1}, A_{2,l_1}, B_{x1,l_1}, B_{x2,l_1}, B_{y1,l_1}, B_{y2,l_1}$. The unknown coefficients are obtained by

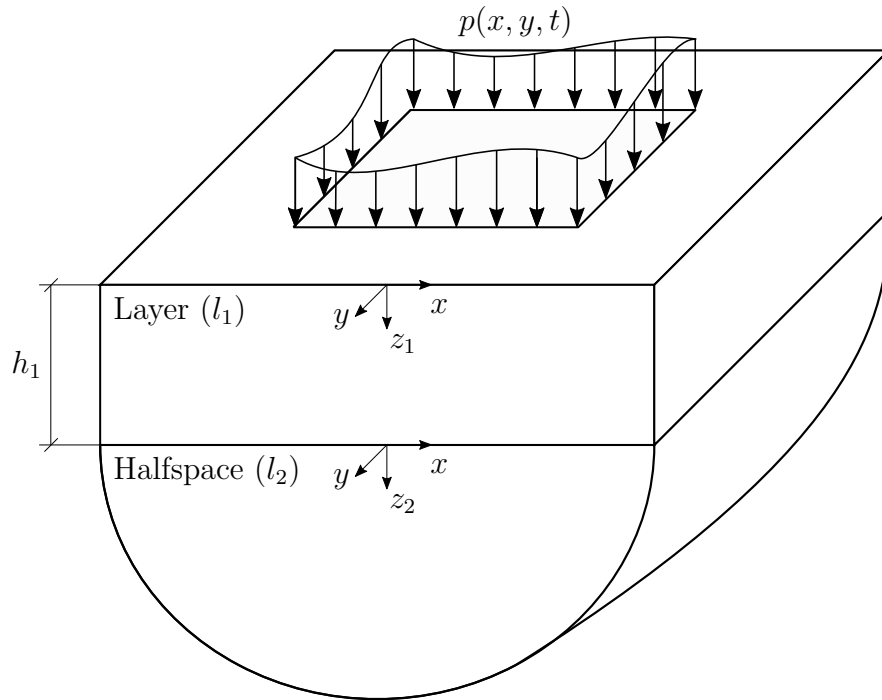


Figure 2.2: Layered halfspace

taking into account boundary conditions at the surface of the soil ($z_1 = 0$)

$$\begin{aligned}
 \hat{\sigma}_{zz,l_1}(k_x, k_y, z_1 = 0, \omega) &= -\hat{p}_z(k_x, k_y, \omega) \\
 \hat{\sigma}_{zy,l_1}(k_x, k_y, z_1 = 0, \omega) &= -\hat{p}_y(k_x, k_y, \omega) \\
 \hat{\sigma}_{zx,l_1}(k_x, k_y, z_1 = 0, \omega) &= -\hat{p}_x(k_x, k_y, \omega)
 \end{aligned}
 \tag{2.34}$$

and transition conditions at the contact between the layer and the halfspace ($z_1 = h_1, z_2 = 0$)

$$\begin{aligned}
\hat{\sigma}_{zz,l_1}(k_x, k_y, z_1 = h_1, \omega) &= \hat{\sigma}_{zz,l_2}(k_x, k_y, z_2 = 0, \omega) \\
\hat{\sigma}_{zy,l_1}(k_x, k_y, z_1 = h_1, \omega) &= \hat{\sigma}_{zy,l_2}(k_x, k_y, z_2 = 0, \omega) \\
\hat{\sigma}_{zx,l_1}(k_x, k_y, z_1 = h_1, \omega) &= \hat{\sigma}_{zx,l_2}(k_x, k_y, z_2 = 0, \omega) \\
\hat{u}_{x,l_1}(k_x, k_y, z_1 = h_1, \omega) &= \hat{u}_{x,l_2}(k_x, k_y, z_2 = 0, \omega) \\
\hat{u}_{y,l_1}(k_x, k_y, z_1 = h_1, \omega) &= \hat{u}_{y,l_2}(k_x, k_y, z_2 = 0, \omega) \\
\hat{u}_{z,l_1}(k_x, k_y, z_1 = h_1, \omega) &= \hat{u}_{z,l_2}(k_x, k_y, z_2 = 0, \omega)
\end{aligned} \tag{2.35}$$

In order to avoid numerical issues occurring for exponential functions with great arguments [36], the unknowns A_{1,l_1}, B_{x1,l_1} and B_{y1,l_1} should be replaced by $\bar{A}_{1,l_1}, \bar{B}_{x1,l_1}$ and \bar{B}_{y1,l_1}

$$\begin{aligned}
A_1 e^{\lambda_1 z} &= A_1 e^{\lambda_1 h_1} e^{-\lambda_1 h_1} e^{\lambda_1 z} = \bar{A} e^{\lambda_1(z-h_1)} \\
B_{i1} e^{\lambda_2 z} &= B_{i1} e^{\lambda_2 h_1} e^{-\lambda_2 h_1} e^{\lambda_2 z} = \bar{B}_{i1} e^{\lambda_2(z-h_1)}, \quad i = x, y
\end{aligned} \tag{2.36}$$

The relationship between unknown coefficients and stress components (2.30) and the relationship between unknown coefficients and displacement components (2.29) for one layer can be written as follows

$$\begin{pmatrix} \hat{\sigma}_{zz} \\ \hat{\tau}_{yz} \\ \hat{\tau}_{zx} \end{pmatrix} = \mu \begin{bmatrix} 2k_r^2 - ks^2 & 2k_r^2 - ks^2 & -2ik_y \lambda_2 & 2ik_y \lambda_2 & 2ik_x \lambda_2 & -2ik_x \lambda_2 \\ 2ik_y \lambda_1 & -2ik_y \lambda_1 & \lambda_2^2 + k_y^2 & \lambda_2^2 + k_y^2 & -k_x k_y & -k_x k_y \\ 2ik_x \lambda_1 & -2ik_x \lambda_1 & k_x k_y & k_x k_y & -\lambda_2^2 - k_x^2 & -\lambda_2^2 - k_x^2 \end{bmatrix} \begin{pmatrix} \bar{A}_{1,l_1} e^{\lambda_1 z} \\ A_{2,l_1} e^{-\lambda_1 z} \\ \bar{B}_{x1} e^{\lambda_2(z-h_1)} \\ B_{x2,l_1} e^{-\lambda_2 z} \\ \bar{B}_{y1,l_1} e^{\lambda_2(z-h_1)} \\ B_{y2,l_1} e^{-\lambda_2 z} \end{pmatrix} \tag{2.37}$$

$$\begin{pmatrix} \hat{u}_x \\ \hat{u}_y \\ \hat{u}_z \end{pmatrix} = \begin{bmatrix} ik_x & ik_x & 0 & 0 & -\lambda_2 & \lambda_2 \\ ik_y & ik_y & \lambda_2 & -\lambda_2 & 0 & 0 \\ \lambda_1 & -\lambda_1 & -ik_y & -ik_y & ik_x & ik_x \end{bmatrix} \begin{pmatrix} \bar{A}_{1,l_1} e^{\lambda_1(z-h_1)} \\ A_{2,l_1} e^{-\lambda_1(z-h_1)} \\ \bar{B}_{x1,l_1} e^{\lambda_2(z-h_1)} \\ B_{x2,l_1} e^{-\lambda_2(z-h_1)} \\ \bar{B}_{y1,l_1} e^{\lambda_2(z-h_1)} \\ B_{y2,l_1} e^{-\lambda_2(z-h_1)} \end{pmatrix} \quad (2.38)$$

In the case of a system with more than one layer, the number of unknowns is increased by six per layer, along with the number of boundary and transition conditions giving the system of equations with unique solution.

2.4 Static load

In the case of a static load ($\omega = 0$) the solution of the system (2.30) is not possible since the determinant of the system becomes zero. In order to obtain the solution, a different approach is used [26] giving the relationship between the stresses and the unknowns

$$\begin{pmatrix} \hat{\sigma}_{xx} \\ \hat{\sigma}_{yy} \\ \hat{\sigma}_{zz} \\ \hat{\tau}_{xy} \\ \hat{\tau}_{yz} \\ \hat{\tau}_{zx} \end{pmatrix} = \mu \begin{bmatrix} -2k_x^2 z - 2\frac{\lambda k_r}{\lambda + \mu} & -2k_x^2 z + 2\frac{\lambda k_r}{\lambda + \mu} & 0 & 0 & -2ik_x k_r & 2ik_x k_r \\ -2k_y^2 - 2\frac{\lambda k_r}{\lambda + \mu} & -2k_y^2 + 2\frac{\lambda k_r}{\lambda + \mu} & 2ik_y k_r & -2ik_y k_r & 0 & 0 \\ 2k_r^2 z - 2\frac{(\lambda + 2\mu)k_r}{\lambda + \mu} & 2k_r^2 z + 2\frac{(\lambda + 2\mu)k_r}{\lambda + \mu} & -2ik_y k_r & 2ik_y k_r & 2ik_x k_r & -2ik_x k_r \\ -2k_x k_y z & -2k_x k_y z & ik_x k_r & -ik_x k_r & -ik_y k_r & ik_y k_r \\ 2ik_y \left(k_r z - \frac{\mu}{\lambda + \mu} \right) & -2ik_y \left(k_r z + \frac{\mu}{\lambda + \mu} \right) & k_r^2 + k_y^2 & k_r^2 + k_y^2 & -k_x k_y & -k_x k_y \\ 2ik_x \left(k_r z - \frac{\mu}{\lambda + \mu} \right) & -2ik_x \left(k_r z + \frac{\mu}{\lambda + \mu} \right) & k_x k_y & k_x k_y & -k_r^2 - k_x^2 & -k_r^2 - k_x^2 \end{bmatrix} \begin{pmatrix} A_{01} e^{\lambda_1 z} \\ A_{02} e^{-\lambda_1 z} \\ B_{0x1} e^{\lambda_2 z} \\ B_{0x2} e^{-\lambda_2 z} \\ B_{0y1} e^{\lambda_2 z} \\ B_{0y2} e^{-\lambda_2 z} \end{pmatrix} \quad (2.39)$$

2.5 Plane Strain

The analysis of strip foundations is performed using plane strain analysis (see Section 2.5). The plane strain analysis is considered a special case of 3D analysis. If the plane of interest is xz plane, the relationship between displacement components, stress components and unknown coefficients is derived from equations (2.29), (2.30) and (2.39), by taking out the components containing index y and let $k_y = 0$. Accordingly, coefficients B_{x1} , B_{x2} , B_{0x1} and B_{0x2} vanish.

$$\begin{Bmatrix} \hat{u}_x \\ \hat{u}_y \\ \hat{u}_z \end{Bmatrix} = \begin{bmatrix} ik_x & ik_x & -\lambda_2 & \lambda_2 \\ \lambda_1 & -\lambda_1 & ik_x & ik_x \end{bmatrix} \begin{Bmatrix} A_1 e^{\lambda_1 z} \\ A_2 e^{-\lambda_1 z} \\ B_{y1} e^{\lambda_2 z} \\ B_{y2} e^{-\lambda_2 z} \end{Bmatrix} \quad (2.40)$$

$$\begin{Bmatrix} \hat{\sigma}_{xx} \\ \hat{\sigma}_{zz} \\ \hat{\tau}_{zx} \end{Bmatrix} = \mu \begin{bmatrix} -2k_x^2 - \frac{\lambda}{\mu} k_p^2 & -2k_x^2 - \frac{\lambda}{\mu} k_p^2 & -2ik_x \lambda_2 & 2ik_x \lambda_2 \\ 2k_r^2 - ks^2 & 2k_r^2 - ks^2 & 2ik_x \lambda_2 & -2ik_x \lambda_2 \\ 2ik_x \lambda_1 & -2ik_x \lambda_1 & -\lambda_2^2 - k_x^2 & -\lambda_2^2 - k_x^2 \end{bmatrix} \begin{Bmatrix} A_1 e^{\lambda_1 z} \\ A_2 e^{-\lambda_1 z} \\ B_{y1} e^{\lambda_2 z} \\ B_{y2} e^{-\lambda_2 z} \end{Bmatrix} \quad (2.41)$$

$$\begin{Bmatrix} \hat{\sigma}_{xx} \\ \hat{\sigma}_{zz} \\ \hat{\tau}_{zx} \end{Bmatrix} = \mu \begin{bmatrix} -2k_x^2 z - 2\frac{\lambda k_x}{\lambda + \mu} & -2k_x^2 z + 2\frac{\lambda k_x}{\lambda + \mu} & -2ik_x^2 & 2ik_x^2 \\ 2k_x^2 z - 2\frac{(\lambda + 2\mu)k_x}{\lambda + \mu} & 2k_x^2 z + 2\frac{(\lambda + 2\mu)k_x}{\lambda + \mu} & 2ik_x^2 & -2ik_x^2 \\ 2ik_x \left(k_x z - \frac{\mu}{\lambda + \mu} \right) & -2ik_x \left(k_x z + \frac{\mu}{\lambda + \mu} \right) & -2k_x^2 & -2k_x^2 \end{bmatrix} \begin{Bmatrix} A_{01} e^{\lambda_1 z} \\ A_{02} e^{-\lambda_1 z} \\ B_{0y1} e^{\lambda_2 z} \\ B_{0y2} e^{-\lambda_2 z} \end{Bmatrix} \quad (2.42)$$

In the case of halfspace, coefficients A_1 and B_{1y} also vanishes (see Section 2.3).

$$\begin{pmatrix} \hat{u}_x \\ \hat{u}_y \\ \hat{u}_z \end{pmatrix} = \underbrace{\begin{bmatrix} ik_x & \lambda_2 \\ -\lambda_1 & ik_x \end{bmatrix}}_{\hat{\mathbf{K}}_u} \begin{pmatrix} A_2 e^{-\lambda_1 z} \\ B_{y2} e^{-\lambda_2 z} \end{pmatrix} \quad (2.43)$$

$$\begin{pmatrix} \hat{\sigma}_{xx} \\ \hat{\sigma}_{zz} \\ \hat{\tau}_{zx} \end{pmatrix} = \mu \underbrace{\begin{bmatrix} -2k_x^2 - \frac{\lambda}{\mu} k_p^2 & 2ik_x \lambda_2 \\ 2k_r^2 - ks^2 & -2ik_x \lambda_2 \\ -2ik_x \lambda_1 & -\lambda_2^2 - k_x^2 \end{bmatrix}}_{\hat{\mathbf{K}}_\sigma} \begin{pmatrix} A_2 e^{-\lambda_1 z} \\ B_{y2} e^{-\lambda_2 z} \end{pmatrix} \quad (2.44)$$

$$\begin{pmatrix} \hat{\sigma}_{xx} \\ \hat{\sigma}_{zz} \\ \hat{\tau}_{zx} \end{pmatrix} = \mu \underbrace{\begin{bmatrix} -2k_x^2 z + 2\frac{\lambda k_x}{\lambda + \mu} & 2ik_x^2 \\ 2k_x^2 z + 2\frac{(\lambda + 2\mu)k_x}{\lambda + \mu} & -2ik_x^2 \\ -2ik_x \left(k_x z + \frac{\mu}{\lambda + \mu} \right) & -2k_x^2 \end{bmatrix}}_{\hat{\mathbf{K}}_\sigma} \begin{pmatrix} A_{02} e^{-\lambda_1 z} \\ B_{0y2} e^{-\lambda_2 z} \end{pmatrix} \quad (2.45)$$

In this dissertation, 2D analysis is referred to plane strain analysis.

2.6 Damping

The specific energy of the system decreases as the wave travels through the material. This behaviour is influenced by two different mechanisms: radiation damping and material damping. It is already mentioned that the radiation damping is successfully modeled using the ITM. Since the analysis is performed in the frequency domain, the material damping can be incorporated into the soil model by using a complex Young's modulus:

$$\bar{E} = E(1 + 2i\zeta) \quad (2.46)$$

where ζ is the damping ratio.

This formulation refers to the usage of hysteretic material damping. It is derived by assuming that the material acts as Kelvin-Voigt solid that describes viscoelastic wave propagation successfully [52].

2.7 Surface Displacements

The calculation of the displacement field of the surface of the halfspace is important step in obtaining the dynamic stiffness of the foundation. It completely relies on ITM. However, the solution of the system of ordinary differential equations could not be obtained analytically in rectangular coordinates. A numerical procedure is performed, requiring the usage of Discrete Fourier Transform (DFT). The surface is discretized and the solution is obtained at every point of discretization. The discretization is performed to satisfy the requirements imposed by DFT. In order to demonstrate those requirements and the procedure itself, two numerical examples with the most common load patterns are presented. The load patterns are

- uniformly distributed load and
- unit force

For the sake of simplicity, the examples assumes 2D analysis and load acting in z direction. The calculation is performed using a script written in MathWorks MATLAB [53].

2.7.1 Numerical Examples

2.7.1.1 Displacements of the surface of the halfspace due to a uniformly distributed load

In this example, plane strain analysis of the halfspace loaded with a uniformly distributed harmonic load is performed. The load is acting on the width of 1 m with the excitation frequency of 30 Hz. The amplitude of the load is such that the resultant of the load is 1 kN/m. The halfspace is modeled with the elasticity modulus $E = 5 \times 10^7 \text{ N/m}^2$, damping coefficient $\zeta = 2\%$, Poisson's coefficient $\nu = 0.3$ and density $\rho = 2 \times 10^3 \text{ kg/m}^3$. The disposition of the problem is given in Figure 2.3

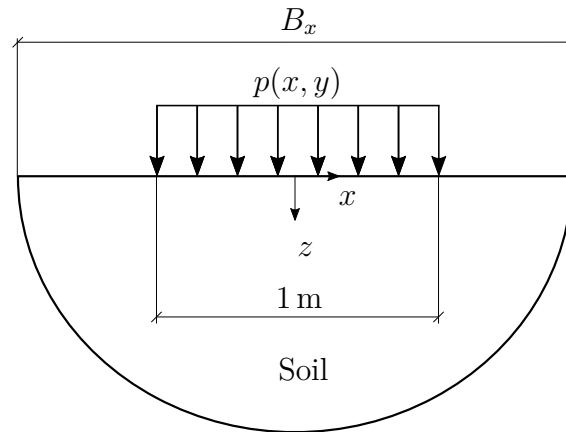


Figure 2.3: Halfspace excited by a uniformly distributed load

According to Equation (2.44), boundary conditions on the surface of the halfspace could be written as

$$\begin{Bmatrix} -\hat{p} \\ 0 \end{Bmatrix} = \mu \underbrace{\begin{bmatrix} 2k_r^2 - ks^2 & -2ik_x\lambda_2 \\ -2ik_x\lambda_1 & -\lambda_2^2 - k_x^2 \end{bmatrix}}_{BC \hat{\mathbf{K}}^\sigma} \begin{Bmatrix} A_2 e^{-\lambda_1 z} \\ B_{y2} e^{-\lambda_2 z} \end{Bmatrix} \quad (2.47)$$

The displacements of the surface of the halfspace are obtained using equations (2.43) and (2.47)

$$\hat{\mathbf{u}} = \underbrace{\hat{\mathbf{K}}^u}_{\widehat{\mathbf{TF}}} \left({}_{BC} \hat{\mathbf{K}}^\sigma \right)^{-1} \begin{Bmatrix} -\hat{\mathbf{p}} \\ 0 \end{Bmatrix} \quad (2.48)$$

where $\widehat{\mathbf{TF}}$ is the transfer function matrix, that gives the relation between displacements components $\hat{\mathbf{u}}$ and the load vector $\hat{\mathbf{p}}$.

Although the halfspace should exist for $x \in (-\infty, \infty)$, it has to be truncated to fit the requirements of the numerical simulation. The truncation length is denoted with B_x . Therefore, the domain of the halfspace is $x \in [-B_x/2, B_x/2]$, $z \in [0, \infty)$. The discretization is performed with discretization unit Δx . The number of discretization points is N_x

$$N_x = \frac{B_x}{\Delta x} \quad (2.49)$$

That leads to the discretization in k_x domain with discretization unit Δk_x

$$\Delta k_x = \frac{2\pi}{B_x} = \frac{2\pi}{N_x \Delta x} \quad \text{for } k_x \in \left[-\frac{N_x}{2} \Delta k_x, \frac{N_x}{2} \Delta k_x \right] \quad (2.50)$$

Since the truncation length is a repetition length of Fourier Transformation (FT), the choice of B_x must ensure that the aliasing effect does not occur. Therefore, the choice of B_x is related to the nature of the external load and to the characteristics of the soil, such as material damping and Rayleigh wavelength.

The truncation length for the given example is $B_x = 128$ m. The variable x takes discrete values between -64 m and 64 m equally spaced by $\Delta x = 0.1$ m. The variable k_x takes discrete values between -31.42 m and 31.42 m equally spaced by $dk_x = 0.0491$ m.

Figure 2.4 shows the procedure of calculating vertical displacements. Only real values of the functions are presented. First, the load pattern \bar{p} (Figure 2.4a) is transformed into wavenumber-frequency domain \hat{p} (Figure 2.4b) using Fast Fourier Transform (FFT). The transfer function of the halfspace $\widehat{\mathbf{TF}}$ is calculated for the given input parameters using equations (2.43), (2.47) and (2.48). The element (2, 1) of the transfer function $\widehat{\mathbf{TF}}$, $\widehat{\mathbf{TF}}_{21}$, required for the calculation of the vertical displacements is shown in Figure 2.4c. The multiplication of \hat{p} and $\widehat{\mathbf{TF}}_{21}$ gives the vertical displacements function in transformed domain \hat{u} (Figure 2.4d). The transformation of \hat{u} into original domain \bar{u} is performed with inverse FFT (Figure 2.4e).

The discretization parameters Δx and Δk_x must be chosen to describe the functions \hat{p} and $\widehat{\mathbf{TF}}_{21}$ well with minimal computational effort. That is a challenging task. It depends on many parameters and cannot be generalized. The domain of k_x must be wide enough to include the area of highest amplitudes of \hat{p} and $\widehat{\mathbf{TF}}$ and Δk_x must be small enough to describe the peaks at $\pm\omega/c_s$ and $\pm\omega/c_p$.

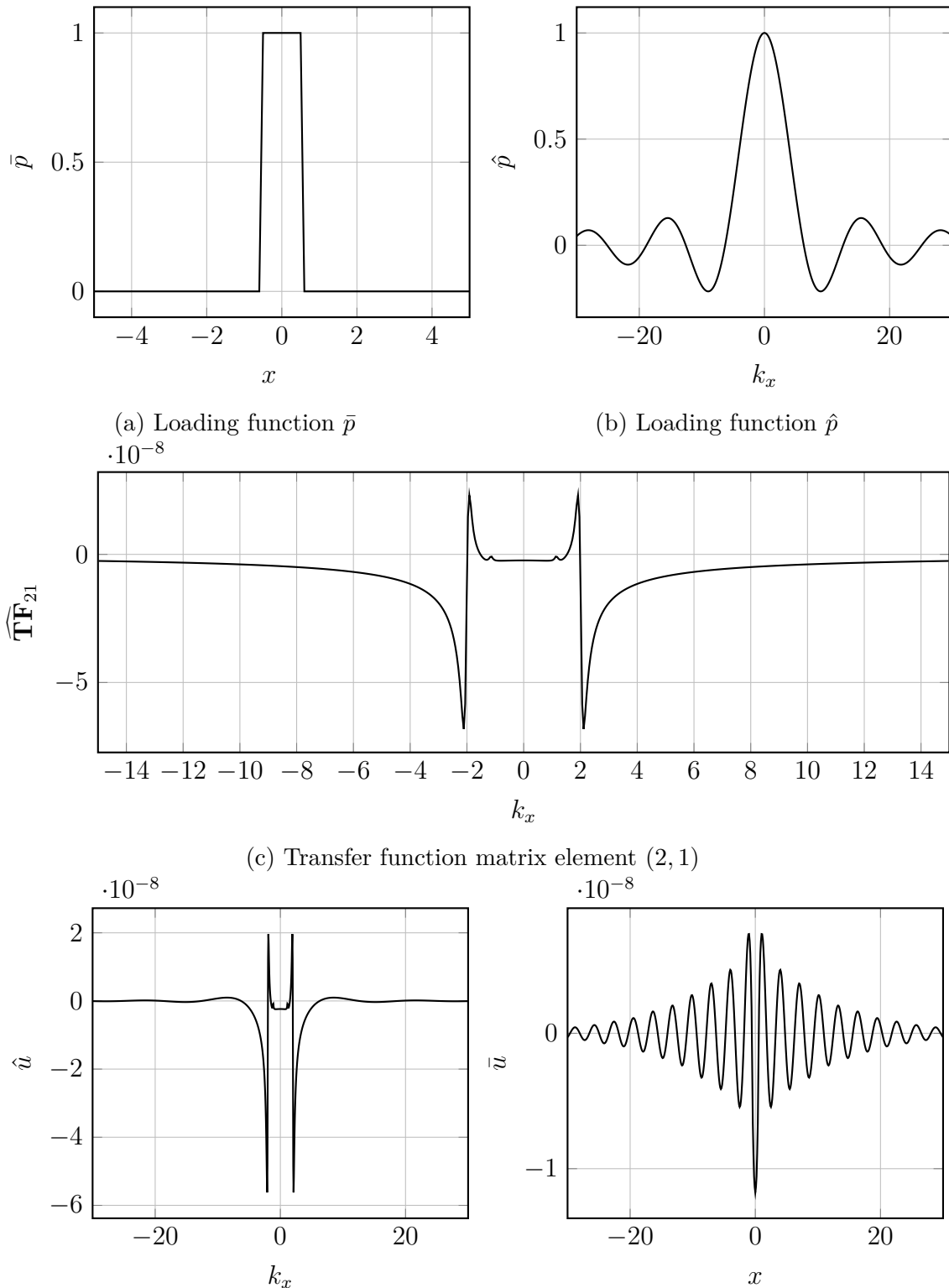


Figure 2.4: Halfspace excited by a uniformly distributed load

2.7.1.2 Displacements of the surface of the halfspace due to a unit force

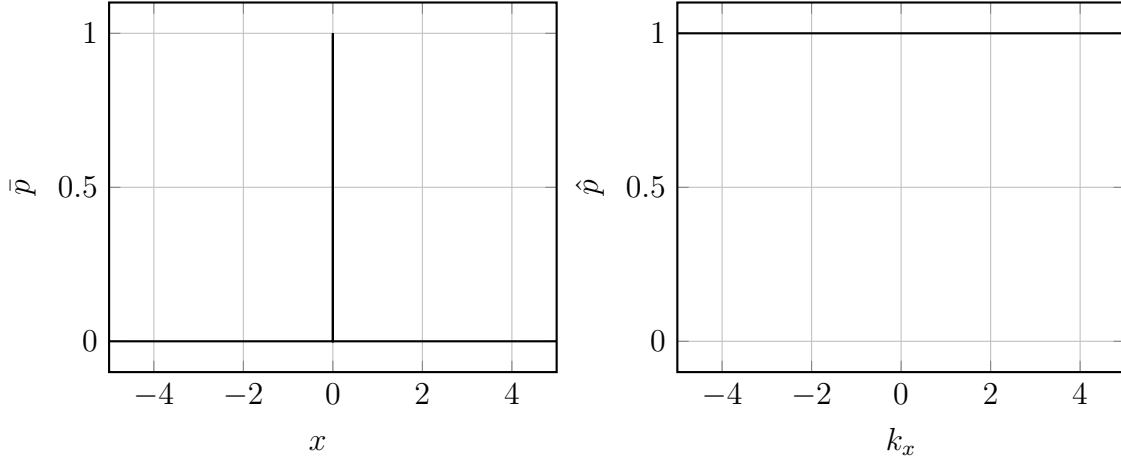
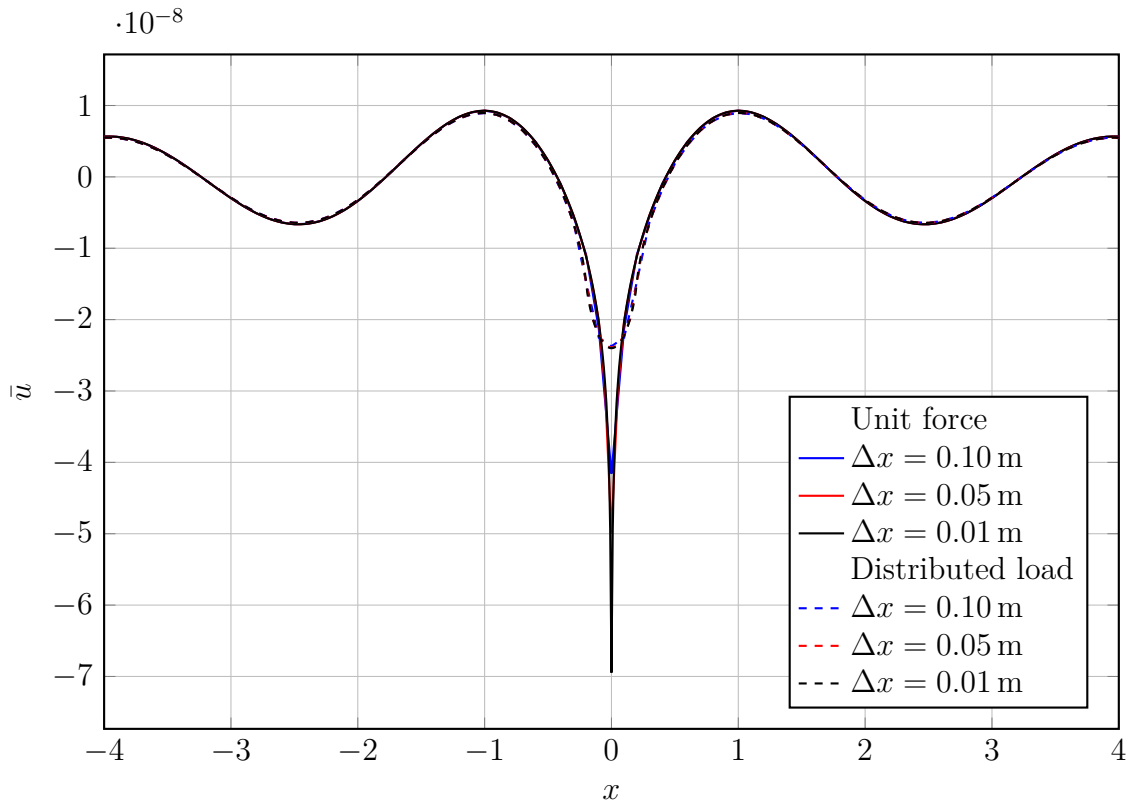


Figure 2.5: Unit force FT pair

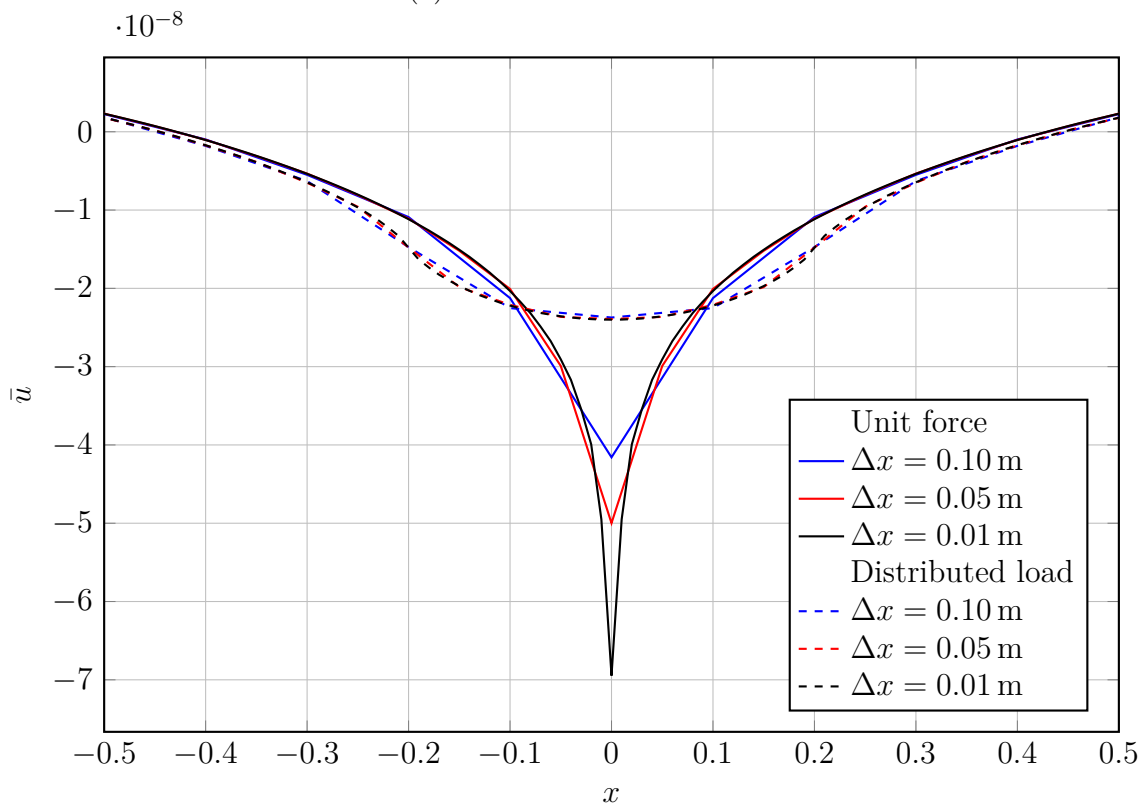
Figure 2.5 shows the FT pair $p \circ \bullet \hat{p}$ for the unit force loading pattern. The load function \hat{p} is a constant for $k_x \in (-\infty, \infty)$. The truncation of such a function is not feasible without introducing a significant numerical error into the response of the system. The transfer function of the halfspace $\widehat{\mathbf{TF}}$ is the same as in the previous example since the input parameters of the halfspace are the same. According to Equation (2.48), the multiplication of \hat{p} and $\widehat{\mathbf{TF}}_{21}$ gives \hat{u} . Concerning the distribution of \hat{p} , the displacement field \hat{u} is proportional to the transfer function $\widehat{\mathbf{TF}}_{21}$. The inverse FT of \hat{u} gives the displacement field in the original domain \bar{u} . Since \hat{u} is not a periodic function, the stability of the inverse FFT of \hat{u} , \bar{u} , is higher if \hat{u} approaches zero at the limits of the k_x domain [54]. For $k_x \rightarrow \pm\infty$ the displacement field \hat{u} approaches zero faster in the case of the distributed load. Therefore, the usage of unit force is not advisable and it should be replaced by a uniformly distributed load. The area of the distributed load should be the smallest area possible that meets the requirements imposed by FFT and provides an optimal computational effort for the calculation of the response. Unfortunately, these requirements are dependent on the type of the analysis and cannot be generalized as a fixed rule.

Figure 2.6 shows the comparison of the displacement fields of the surface of the halfspace excited by a unit force $P = 1 \text{ kN/m}$ and a distributed load $p = 2.5 \text{ kN/m}^2$ over the length of 0.4 m for different values of Δx . The magnitude of the resultant force of the distributed load p is equal to the magnitude of the unit force P . The truncation parameter B_x is fixed at 128 m . Figures 2.6a and 2.6b show the response of the same systems, but Figure 2.6b gives a detailed view of the nearfield zone. The change of Δx affects the observed wavenumber spectrum since it is inverse proportional to Δk_x , Equation (2.50): the lower the Δx , the wider the k_x spectrum. Concerning the observations mentioned in the previous paragraph, the change of Δx must affect the response of the system. Figure 2.6b shows that the differences are more pronounced in the case of the unit force, especially at the point of the excitation. In the case of the equivalent distributed load, the distribution of the displacement field is changed only in the nearfield zone. Also, the response of the system is not dependent on Δx as much as in the case of the unit force.

The displacement field \bar{u} is very important for the calculation of the flexibility/stiffness matrix of the rigid foundation (see Section 3.2). The accuracy of \bar{u} should not be significantly affected by the discretization input parameters Δx and Δk_x . This is the reason the unit force load is not used in the numerical models made for the purposes of this dissertation. However, the term *unit force* is used, as it is meaningful from the theoretical point of view, but it refers to a uniformly distributed load over a small area.



(a) Nearfield and farfield



(b) Nearfield only

Figure 2.6: Displacements of the surface of the halfspace due to a unit force and a distributed load for different Δx

2.8 Moving load

A moving load can be incorporated into ITM without changing its algorithm. This is accomplished with a help of the shifting theorem which is a property of the Fourier transform [54]. This procedure is described by many authors including Grundmann [55, 38], Müller [56], Auersch [57] and Yang and Hung [58].

Let p_z be a vertical load that moves in x -direction along the surface of a half-space with a constant speed v

$$p_z(x, y, t) = p_0(x - vt, y)f(t) \quad (2.51)$$

Applying a threefold Fourier transform on (2.51) gives

$$\hat{p}_z(k_x, k_y, \omega) = \hat{p}_0(k_x, k_y)\hat{f}(\omega + vk_x) \quad (2.52)$$

Spatial movement in the original domain leads to a frequency shift in the transformed domain. Therefore, in the transformed domain, the moving load function could be calculated as a corresponding stationary load function \hat{p}_s

$$\hat{p}_s(k_x, k_y, \bar{\omega}) = \hat{p}_0(k_x, k_y)\hat{f}(\bar{\omega}) \quad (2.53)$$

where $\bar{\omega}$ is a wavenumber dependent frequency

$$\bar{\omega} = \omega + vk_x \quad (2.54)$$

Particularly

$$\hat{p}(k_x, k_y, \omega) = \hat{p}_s(k_x, k_y, \omega + vk_x) \quad (2.55)$$

The relation between the displacement field of the halfspace $\hat{\mathbf{u}}$ and the loading vector $\hat{\mathbf{p}}$ is established with the transfer function of the soil, $\widehat{\mathbf{TF}}$:

$$\hat{\mathbf{u}}(k_x, k_y, \omega) = \widehat{\mathbf{TF}}(k_x, k_y, \omega) \hat{\mathbf{p}}(k_x, k_y, \omega) \quad (2.56)$$

Considering (2.55) and (2.54), (2.56) could be written as

$$\hat{\mathbf{u}}(k_x, k_y, \bar{\omega} - vk_x) = \widehat{\mathbf{TF}}(k_x, k_y, \bar{\omega} - vk_x) \hat{\mathbf{p}}_s(k_x, k_y, \bar{\omega}) \quad (2.57)$$

This means that the displacement field of the halfspace, $\hat{\mathbf{u}}(k_x, k_y, \omega)$, excited by a moving load $\hat{\mathbf{p}}(k_x, k_y, \omega)$ could be calculated like the displacement field of the halfspace in the moving frame of reference $\hat{\mathbf{u}}(k_x, k_y, \bar{\omega} - vk_x)$ excited by a corresponding stationary load $\hat{\mathbf{p}}_s(k_x, k_y, \bar{\omega})$. The transfer function of the soil, $\widehat{\mathbf{TF}}$, is calculated for shifted frequencies $\omega = \bar{\omega} - vk_x$.

2.8.1 Numerical example

For the purposes of verification of the presented technique a numerical model is developed using MATLAB [53]. The results are compared with the results from the literature [59].

The halfspace is modeled so that the shear waves velocity is $c_s = 120$ m/s, the longitudinal waves velocity is $c_p = 240$ m/s, the density is $\rho = 2000$ kg/m³ and the damping coefficient is $\zeta = 5\%$. The force is a half-cosine load that moves in x -direction with a constant speed v , starting from the point $x_k = 0$, Figure 2.7.

The loading function is defined as

$$P_{z_i}(x, y, t) = P_i \cos \frac{\pi \bar{x}}{l_i} \delta(x - v_i t) \delta(y) \quad (2.58)$$

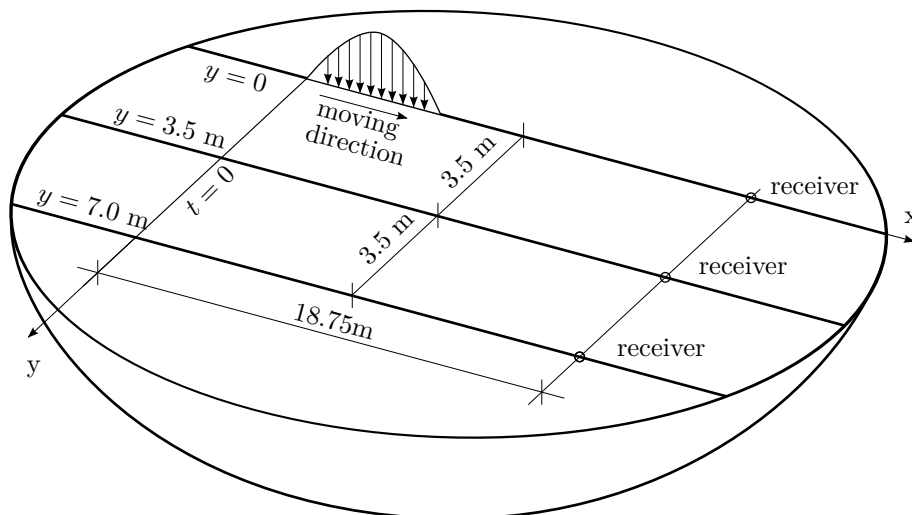


Figure 2.7: Half-cosine moving load on the surface of the halfspace. Disposition of the problem

where $P_i = P_t\pi/l_i$ is the amplitude, P_t is the load resultant force and l_i is the length of half-cosine, Figure 2.8. The duration of the load is 0.025 s . The displacement fields of the surface of the halfspace are obtained for velocities $v_i = 200, 300, 400$ and 500 km/h .

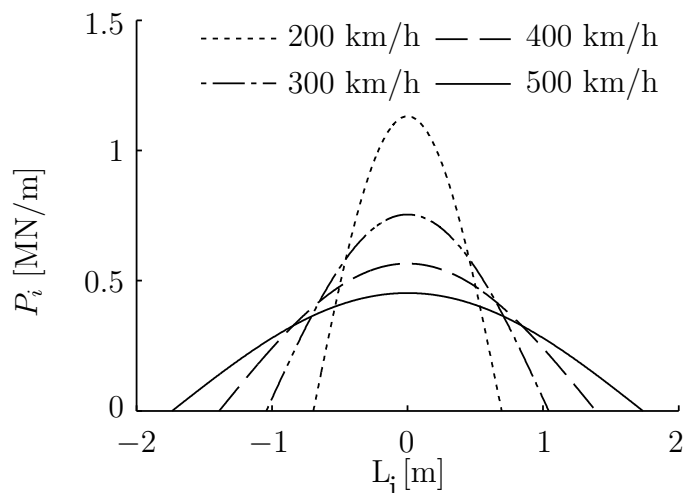


Figure 2.8: Spatial distribution of the load function P_z for different velocities v

Figure 2.9 shows the displacements in x, y and z directions at the location of the receivers placed along the line $x = 18.75\text{ m}$ at $y = 0, 3.5$ and 7 m . The higher the source speed the quicker the response occurs. The displacements decrease with increasing distances from the load path. While vertical displacement amplitudes

decrease with an increase of the source speed, horizontal displacement amplitudes increase.

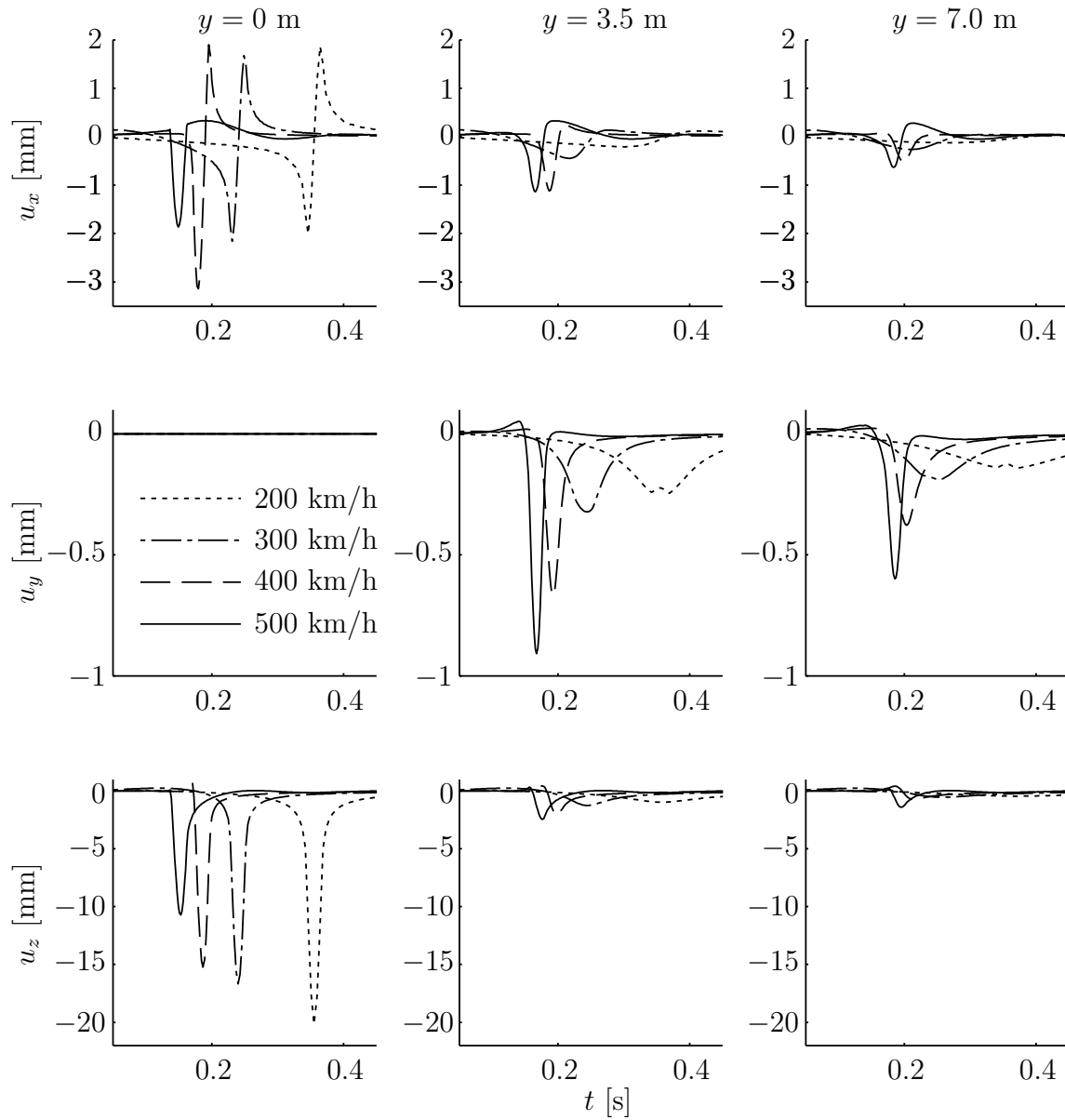


Figure 2.9: Influence of the moving force velocity on the displacements of the halfspace surface at $x = 18.75$ m

3 Dynamic Stiffness and Flexibility of Surface Foundations

This chapter presents the formulation of the method for solving the response of rigid and flexible foundations resting on halfspace. The results obtained by the proposed method in terms of displacement distributions, stress distributions, and impedance functions of the foundations, are compared with the results from the literature.

3.1 Introduction

Dynamic stiffness of the foundation is a product of the SFI analysis. It is used in the SSI analysis where it is assembled into the dynamic stiffness of the structure. Performing the SFI analysis is not a simple task. However, the response of the SFI systems could be generalized to a certain level, facilitating the implementation of SFI analysis in engineering practice.

According to Gazetas [3], Lysmer was the first to introduce the idea to represent the SFI behavior by a single degree of freedom system with lumped parameters: stiffness and damping as coefficients independent of frequency. This idea is used in the current methods of SFI analysis, where the results are presented in the form of two frequency dependent complex valued functions: impedance functions.

Impedance functions

Impedance can be any kind of resistance to wave oscillation. For example, electrical impedance can be calculated as the ratio between voltage and current, acoustic impedance as the ratio between sound pressure and particle velocity, etc.

In the field of SSI, the impedance is defined as the ratio between the dynamic force and the resulting displacement of the foundation [60]

$$K(t) = \frac{p(t)}{u(t)} \quad (3.1)$$

According to the Fourier analysis [54], any transient response can be presented as a summation of harmonic responses. Therefore, it is natural to formulate the impedance as a function of harmonic force $\bar{p}(\omega) = p_0 \exp(i\omega t)$ and harmonic displacement $\bar{u}(\omega) = u_0 \exp(i\omega t)$

$$\bar{K}(\omega) = \frac{\bar{p}(\omega)}{\bar{u}(\omega)} \quad (3.2)$$

Since the dynamic force and displacement are generally out of phase, it is useful to present them in complex notation. Thus, the impedance function is also a complex valued function

$$\bar{K}(\omega) = \bar{K}_r(\omega) + i\bar{K}_i(\omega) \quad (3.3)$$

The real part refers to the stiffness and inertia of the soil. The imaginary part refers to the radiation and material damping of the system. This is in complete accordance with the impedance of the single degree of freedom system. However, the SFI impedances depends on the geometry, stiffness and embedment of the foundation, and on the properties and profile of the soil medium. Therefore, they are usually presented as functions of dimensionless frequency [3]

$$a_0 = \frac{\omega \frac{B}{2}}{c_s} \quad (3.4)$$

where B is the width of the foundation, and c_s is the velocity of shear waves in the soil.

In order to present the impedance functions in dimensionless form, they are scaled by the value of the static stiffness of the system, $\bar{K}(\omega = 0)$, or by the coefficient C that depends on the shape of the foundation and on the observed direction of the response.

$$\frac{1}{C}\bar{K}(a_0) = \frac{1}{C}\bar{K}_r(a_0) + i\frac{1}{C}\bar{K}_i(a_0) \quad (3.5)$$

For example, in the case of square surface foundations, vertical and horizontal impedances are scaled by $C = G(B/2)$, while the scaling coefficient of rocking impedances is $C = G(B/2)^3$. The parameter G is the shear modulus of the soil.

Since the impedance functions reflect the dynamic stiffness of the system, they are also called dynamic stiffness functions.

Compliance functions

The compliance functions, also known as dynamic flexibility functions, are defined as the ratios between the dynamic displacements and the reactive forces at the base of the foundation. They are expressed in the same manner as impedance functions

$$\bar{F}(\omega) = \bar{F}_r(\omega) + i\bar{F}_i(\omega) \quad (3.6)$$

or in dimensionless form

$$C\bar{F}(a_0) = C\bar{F}_r(a_0) + iC\bar{F}_i(a_0) \quad (3.7)$$

In the case of axisymmetrical foundations the vertical and torsional compliances are inverse of the vertical and torsional impedances, respectively. Rocking and horizontal

motions are coupled. Therefore, the rocking and horizontal compliances are obtained by inverting the matrix of the system of linear equations that describes the relation between the rocking and horizontal impedances.

Usage of impedance and compliance functions

All the methods for obtaining the response of SFI systems mentioned in the Section 1.2 could be used for the calculation of impedance and compliance functions. The selection of the method depends on various parameters including the shape of the foundation, the type of the soil medium, the embedment of the foundation and the foundation stiffness/flexibility. Once the harmonic response of the foundations is obtained in terms of impedance or compliance functions, it is possible to evaluate the steady state response of any structure supported by the foundations.

A brief history of impedances with the summary of researches regarding impedances and compliances is greatly covered in the *Handbook of Impedance Functions* by Sieffert and Cevaer [60]. A detailed historical overview with theoretical basis and the discussion of the results of other researches in terms of impedance and compliance functions is published by Gazetas [3]. These publications cover the impedances and compliances of rigid foundations. The degrees of freedom of rigid foundation are defined in its centroid. The displacement profile is a constant or linear function of spatial coordinates. The impedance functions are calculated by using the displacements at the centroid of the base of the foundation and they are called the impedance functions of the foundation.

In the case of a flexible foundation every point has its own degrees of freedom. Therefore, the impedance functions are attributed to a certain point of the foundation rather than to the whole foundation. Considering the publications of Whittaker and Christiano [17] and Maravas et al. [61, 62], this dissertation analyses the compliances

of three characteristic points of flexible surface rectangular foundations: center, midway along an edge, and corner.

Numerical examples

The results of the numerical examples in this chapter are obtained using a program written in MATLAB [53]. They are presented without applying a postprocessing algorithms such as smoothing techniques or similar.

3.2 Rigid Foundation

The term *rigid foundation* refers to a rigid, massless and rectangular foundation resting on the surface of the soil. The dynamic stiffness and flexibility of the foundation is obtained using the fundamental solution of the soil calculated using the ITM and the kinematic transform [63].

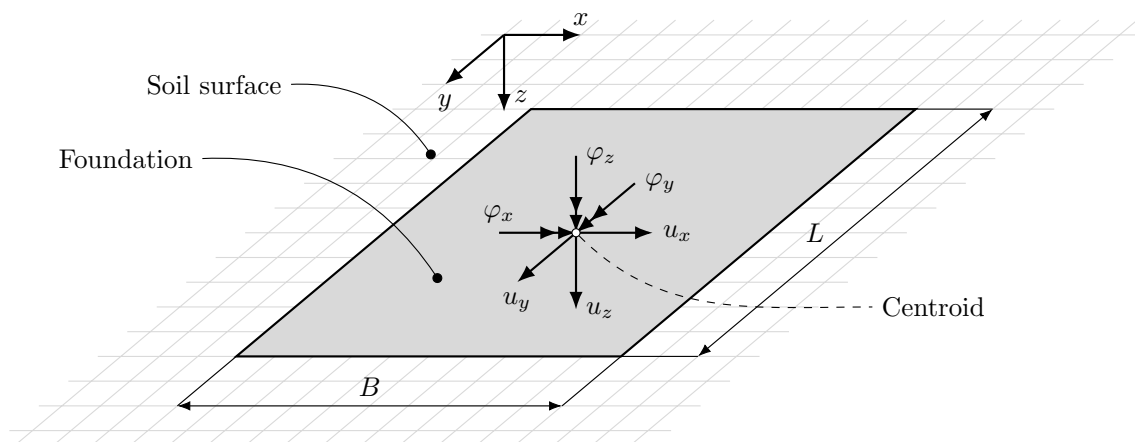


Figure 3.1: Rigid foundation resting on the surface of the soil

The disposition of the problem is shown in Figure 3.1. Symbols B and L denote the dimensions of the foundation in x and y direction, respectively. Since the foundation is surface, massless and rigid, it could be considered as the area of the surface of

the soil that acts as a rigid body. It has six degrees of freedom: three translations, \bar{u}_{rx} , \bar{u}_{ry} and \bar{u}_{rz} , and three rotations of the centroid, $\bar{\varphi}_{rx}$, $\bar{\varphi}_{ry}$ and $\bar{\varphi}_{rz}$, 3.1.

The foundation is rectangular, therefore the problem is formulated in the Cartesian, three dimensional coordinate system. The procedure of obtaining the flexibility matrix of the surface of the soil is based on the fundamental solution of the halfspace using ITM. The steps of the procedure are the following:

- Apply unit force $\bar{P} = 1$ kN in the direction of degree of freedom j .
- Obtain the displacement field of the surface of the soil, \bar{u}_s (see Section 2.7).
- The corresponding elements of displacement field \bar{u}_s represent the elements of column j of the dynamic flexibility matrix, $\bar{\mathbf{F}}_s$.

Section 2.7 explains that the calculation of the displacement field of the halfspace in rectangular coordinates implies the discretization of the soil in xy plane. At every point of discretization, the displacement field of the surface of the soil \bar{u}_s is described with three degrees of freedom

$$\bar{u}_s^T = \left\{ \bar{u}_{sx} \quad \bar{u}_{sy} \quad \bar{u}_{sz} \right\} \quad (3.8)$$

where \bar{u}_{sx} , \bar{u}_{sy} and \bar{u}_{sz} are translations in x , y and z direction. If the area of the foundation is divided into n discretization points, the number of degrees of freedom of the soil surface under the foundation is $3n$. Therefore, the size of the dynamic flexibility matrix of the surface of the soil, $\bar{\mathbf{F}}_s$, is $3n \times 3n$.

Since the displacement field has to be calculated for n different positions of unit forces in x , y and z direction, the procedure requires the ITM algorithm to be repeated $3n$ times. Section 2.7.1.2 shows that the calculation of the displacements of the surface of the soil excited by a unit force could be time consuming and resource demanding.

Fortunately, the process of obtaining the dynamic flexibility matrix, $\bar{\mathbf{F}}_s$, could be optimized.

The area of the surface of the soil is generally larger than the area of the foundation. Instead of moving the unit force from one discretization point to another, the foundation area is shifted proportionally to the discretization steps in x and y direction. In other words, the unit force excitation point is used as the frame of reference. Therefore, the ITM algorithm is performed only three times, once for every degree of freedom in only one excitation point. Figure 3.2 shows the three load cases used for the calculation of the dynamic flexibility matrix, $\bar{\mathbf{F}}_s$. Additionally,

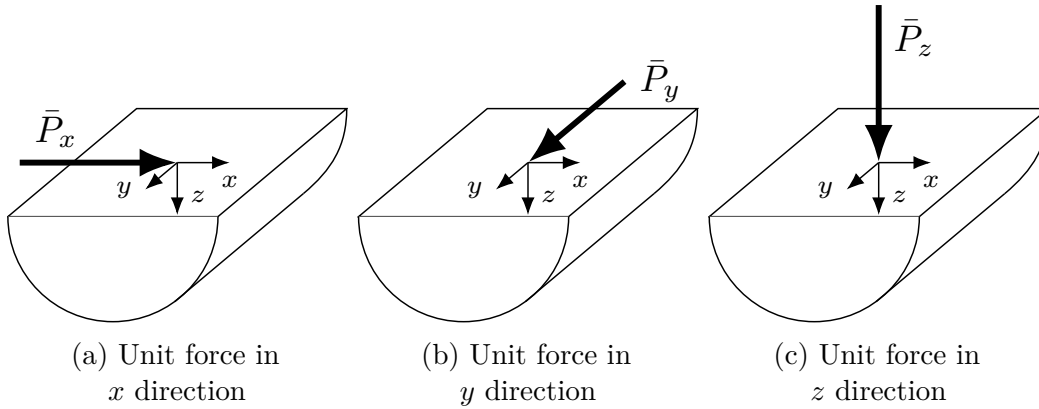


Figure 3.2: Unit force load cases for the calculation of $\bar{\mathbf{F}}_s$

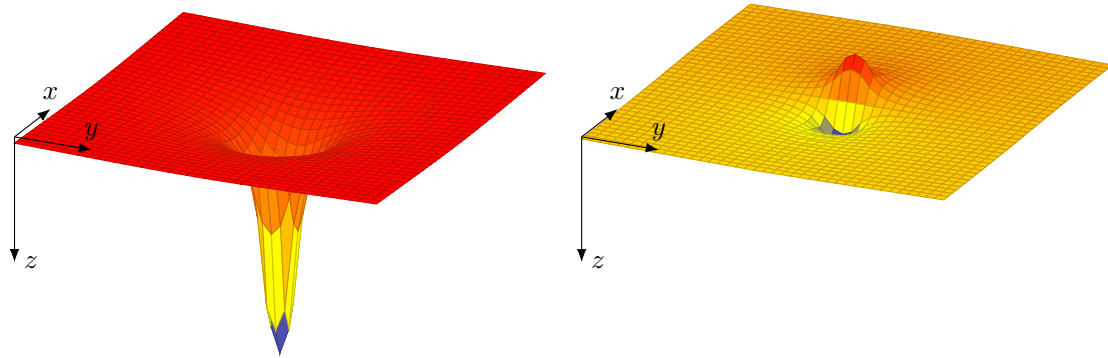
the number of ITM algorithm repetitions can be brought down to two repetitions, since the displacement field \bar{u}_s due to $\bar{P}_y = 1$ kN, Figure 3.2b, could be obtained by performing the 90 degrees rotation of the displacement field \bar{u}_s due to $\bar{P}_x = 1$ kN, Figure 3.2a, along the z axis.

Figure 3.3 depicts two steps of the shifting procedure for calculating the soil displacements at the surface of the soil under the foundation due to unit force in z direction. The displacement field components in z and x direction, \bar{u}_{sz} and \bar{u}_{sx} , due to a unit force state $\bar{P}_z = 1$ kN are shown in Figures 3.3a and 3.3b. The first step is when the first node of the foundation area 1 is the point of excitation, Figures 3.3c and 3.3d. The displacements in x , y and z direction, inside the foundation area, due

to $P_z = 1$ kN, represent $(j, 3)$ elements of $\bar{\mathbf{F}}_s, \bar{F}_s^{j,3}$. The last shifting step is when the last node of the foundation area n is the point of excitation, Figures 3.3e and 3.3f. The displacements in x, y and z directions inside the foundation area represent $(j, 3n)$ elements of dynamic stiffness matrix $\bar{\mathbf{F}}_s, \bar{F}_s^{j,3n}$. If m is an excitation point loaded with unit force P_z , the displacements in x, y and z direction, inside the foundation area, represent $(j, 3m)$ elements of $\bar{\mathbf{F}}_s$. As mentioned before, number j takes values from 1 to $3n$. To calculate all elements of dynamic stiffness matrix $\bar{\mathbf{F}}_s$ the analogous procedure should be performed for the case of a unit force $\bar{P}_x = 1$ kN and $\bar{P}_y = 1$ kN.

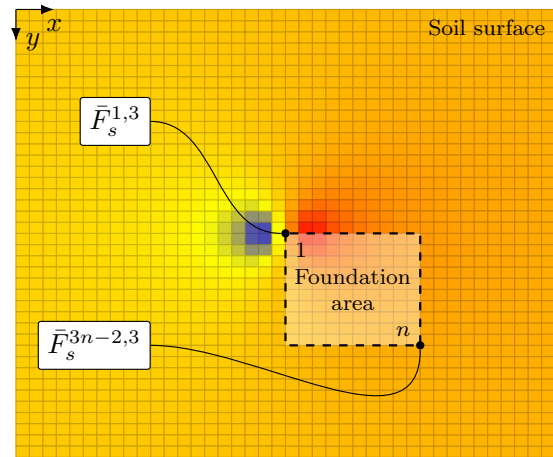
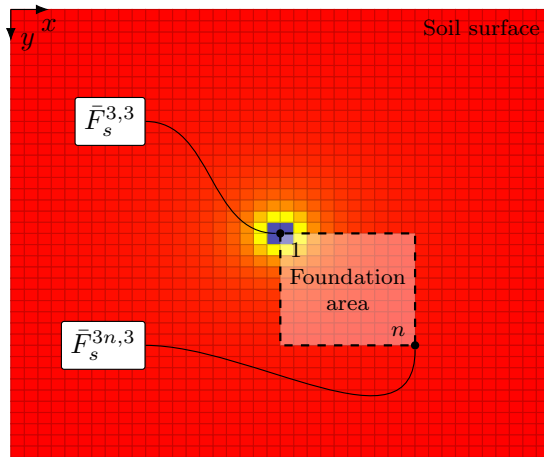
In calculating the elements of the dynamic flexibility matrix certain numerical problems arise. The usage of a distributed load instead of a unit force (see Section 2.7.1.2) combined with a small step in numerical analysis leads to an ill-conditioning of the dynamic stiffness matrix $\bar{\mathbf{F}}_s$ making its inversion non accurate. The excitation load distributed over a small area occupies several discretization nodes. The shifting of the load by one discretization node is not big enough to make a significant change of the displacement field \bar{u}_s under the foundation area. Since each column of matrix $\bar{\mathbf{F}}_s$ is obtained using the shifting procedure, the nearby columns of matrix $\bar{\mathbf{F}}_s$ becomes similar enough to cause its ill condition. This is solved by introducing a new, coarser discretization grid for the purpose of calculating matrix $\bar{\mathbf{F}}_s$. Figure 3.4 shows the displacement fields \bar{u}_{sz} in $x0z$ plane of two adjacent shifting steps, before and after introducing a new discretization grid. Figure 3.5 shows the overlay of the areas occupied by the unit load in all shifting steps before and after introducing a new discretization grid. Furthermore, instead of a single point value at the node location, the elements of the flexibility matrix are calculated as a mean value of the displacement \bar{u}_s over the chosen area A

$$\bar{F}_s^{i,j} = \frac{\int \bar{u}_s(x, y) dA}{\int_A dA} \quad (3.9)$$



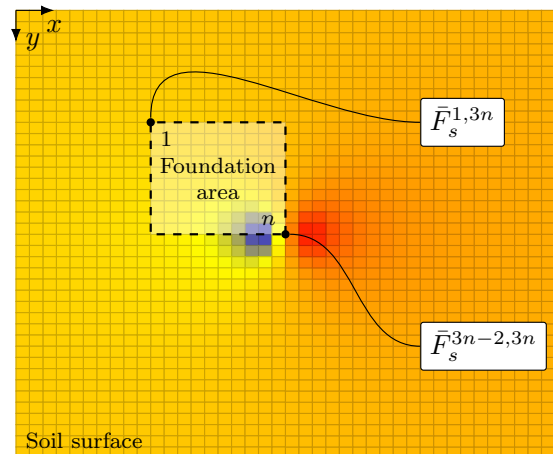
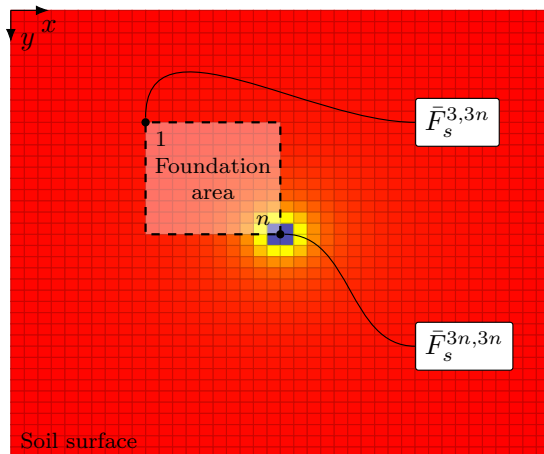
(a) Displacement field \bar{u}_{sz} due to $P_z = 1$ kN

(b) Displacement field \bar{u}_{sx} due to $P_z = 1$ kN



(c) \bar{u}_{sz} with the foundation area in the first shifting step

(d) \bar{u}_{sx} with the foundation area in the first shifting step



(e) \bar{u}_{sz} with the foundation area in the last shifting step

(f) \bar{u}_{sx} with the foundation area in the last shifting step

Figure 3.3: The procedure of populating the flexibility matrix of the soil by shifting the area of the foundation

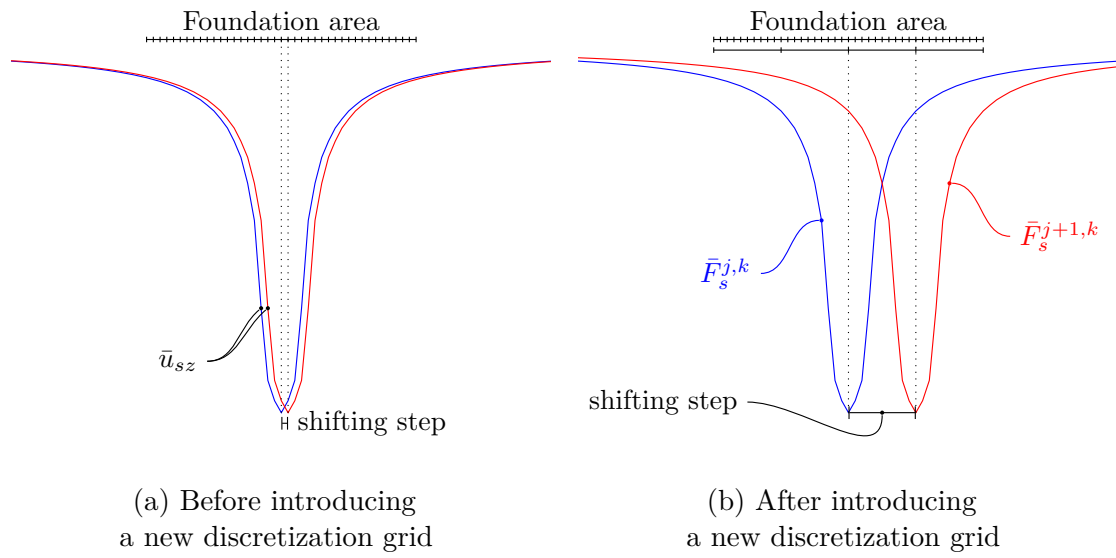


Figure 3.4: The displacement fields \bar{u}_{sz} in x_0z plane of two adjacent shifting steps

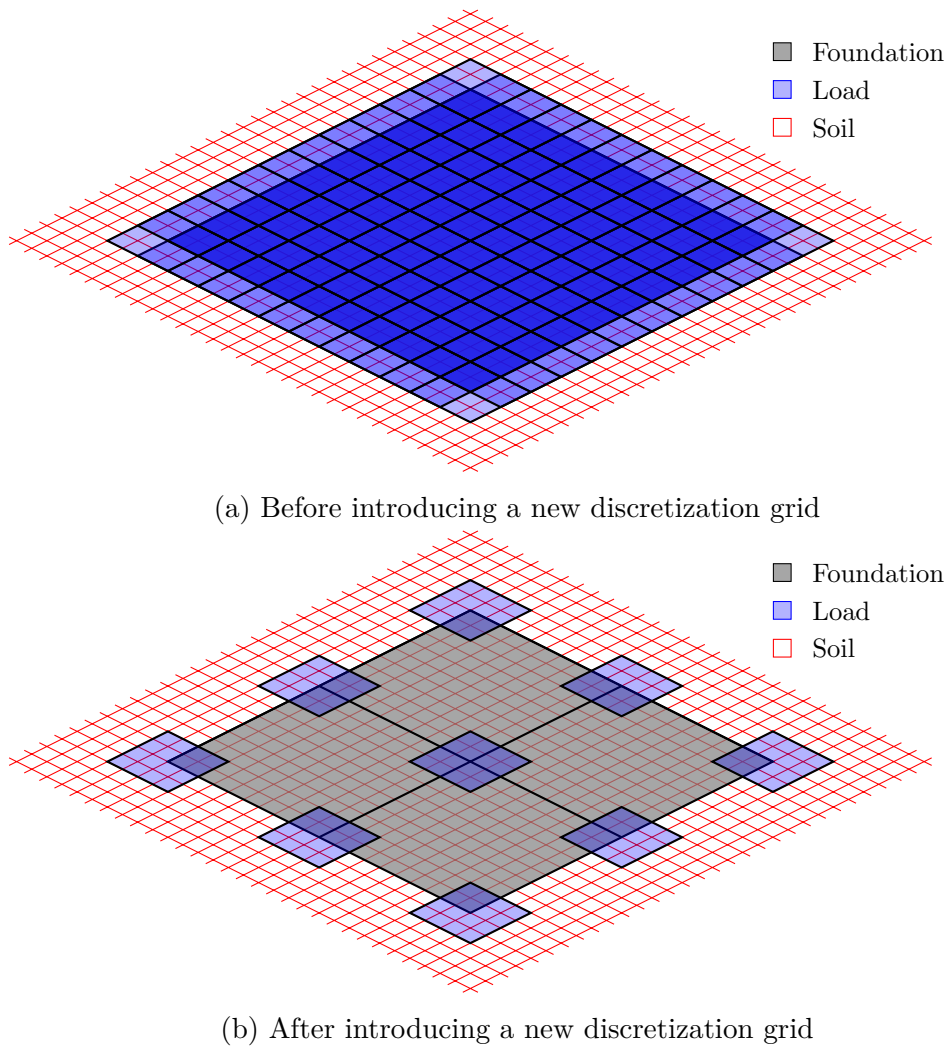


Figure 3.5: Overlay of the areas occupied by the unit load in all shifting steps

The dynamic stiffness matrix of the soil $\bar{\mathbf{K}}_s$ is obtained by inverting the flexibility matrix $\bar{\mathbf{F}}_s$:

$$\bar{\mathbf{K}}_s = \bar{\mathbf{F}}_s^{-1} \quad (3.10)$$

It establishes the connection between the displacements and the forces that corresponds to $3n$ degrees of freedom of the soil surface under the foundation. This matrix is used for obtaining the dynamic stiffness matrix of the rigid foundation, $\bar{\mathbf{K}}_r$. Matrix $\bar{\mathbf{K}}_r$ establishes the connection between the displacements and the forces that corresponds to six degrees of freedom of the rigid foundation, shown in Figure 3.6.

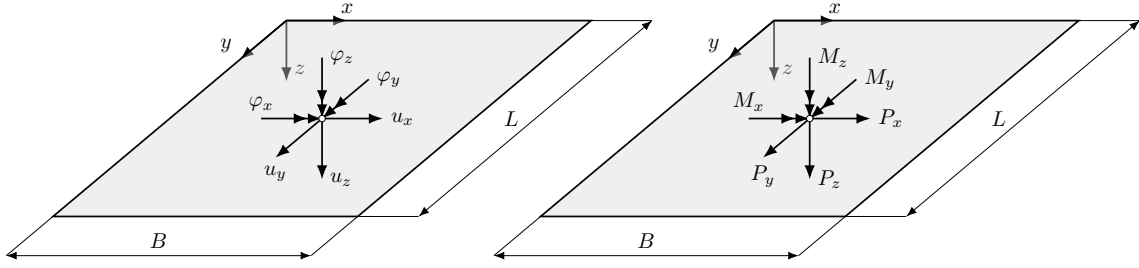


Figure 3.6: Displacements and forces of the rigid foundation

According to Figure 3.6 the displacement vector, $\bar{\mathbf{u}}_r$, and the force vector of centroid of the rigid foundation, $\bar{\mathbf{P}}_r$, are defined as

$$\bar{\mathbf{u}}_r^T = \{ \bar{u}_x \quad \bar{u}_y \quad \bar{u}_z \quad \bar{\varphi}_x \quad \bar{\varphi}_y \quad \bar{\varphi}_z \} \quad (3.11)$$

$$\bar{\mathbf{P}}_r^T = \{ \bar{P}_x \quad \bar{P}_y \quad \bar{P}_z \quad \bar{M}_x \quad \bar{M}_y \quad \bar{M}_z \} \quad (3.12)$$

The relation between matrices $\bar{\mathbf{K}}_s$ and $\bar{\mathbf{K}}_r$ is obtained using the energy principle that equates the deformation energy of the foundation area of the soil and the rigid foundation in the following form

$$\bar{\mathbf{P}}_s^T \bar{\mathbf{u}}_s = \bar{\mathbf{P}}_r^T \bar{\mathbf{u}}_r \quad (3.13)$$

The vectors of the nodal displacements of the soil $\bar{\mathbf{u}}_s$ and the foundation $\bar{\mathbf{u}}_r$ are related with kinematic matrix \mathbf{a} :

$$\bar{\mathbf{u}}_s = \mathbf{a}\bar{\mathbf{u}}_r \quad (3.14)$$

where

$$\mathbf{a}^\top = \{\mathbf{a}_1 \quad \mathbf{a}_2 \quad \cdots \quad \mathbf{a}_i \quad \cdots \quad \mathbf{a}_{n \times n}\} \quad (3.15)$$

The submatrices \mathbf{a}_i are obtained by the kinematic consideration

$$\mathbf{a}_i = \begin{bmatrix} 1 & 0 & 0 & 0 & 0 & -y_i \\ 0 & 1 & 0 & 0 & 0 & x_i \\ 0 & 0 & 1 & y_i & -x_i & 0 \end{bmatrix} \quad (3.16)$$

where x_i and y_i are coordinates of the node A_i and O is the centroid of the foundation, as shown in Figure 3.7. The size of matrix \mathbf{a} is $(3n, 6)$. The relation between the

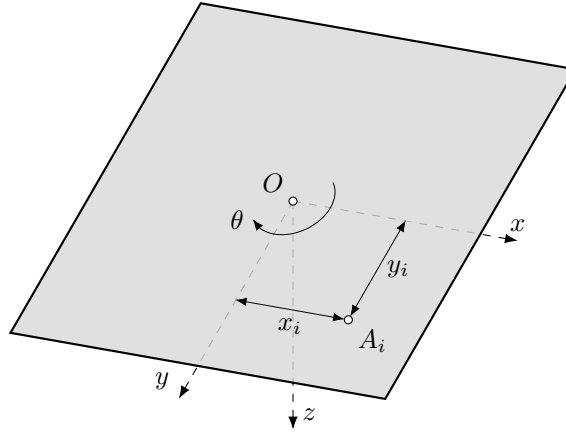


Figure 3.7: Kinematic transformation

nodal displacements and the corresponding force vectors for the flexible and rigid foundation is given by equations

$$\bar{\mathbf{P}}_s = \bar{\mathbf{K}}_s \cdot \bar{\mathbf{u}}_s \quad (3.17)$$

$$\bar{\mathbf{P}}_r = \bar{\mathbf{K}}_r \cdot \bar{\mathbf{u}}_r \quad (3.18)$$

Taking into account equations (3.13) and (3.14) the dynamic stiffness matrix of the rigid foundation, $\bar{\mathbf{K}}_r$, can be obtained as

$$\bar{\mathbf{K}}_r = \mathbf{a}^T \bar{\mathbf{K}}_s \mathbf{a} \quad (3.19)$$

Regarding previously adopted assumptions, the sizes of the matrices $\bar{\mathbf{K}}_s$ and $\bar{\mathbf{K}}_r$ are $(3n, 3n)$ and $(6, 6)$, respectively. The stiffness matrix of the rigid foundation, $\bar{\mathbf{K}}_r$, has a form of a diagonal matrix with non-diagonal elements regarding additional rotational stiffnesses, \bar{K}_{mx} and \bar{K}_{my} , to the horizontal translational stiffnesses, \bar{K}_{xx} and \bar{K}_{yy} , and vice versa.

$$\bar{\mathbf{K}}_r = \begin{bmatrix} \bar{K}_{xx} & 0 & 0 & 0 & \bar{K}_{x,my} & 0 \\ 0 & \bar{K}_{yy} & 0 & \bar{K}_{y,mx} & 0 & 0 \\ 0 & 0 & \bar{K}_{zz} & 0 & 0 & 0 \\ 0 & \bar{K}_{mx,y} & 0 & \bar{K}_{mx} & 0 & 0 \\ \bar{K}_{my,x} & 0 & 0 & 0 & \bar{K}_{my} & 0 \\ 0 & 0 & 0 & 0 & 0 & \bar{K}_{mz} \end{bmatrix} \quad (3.20)$$

Analogous, the flexibility matrix of the rigid foundation is the following

$$\bar{\mathbf{F}}_r = \begin{bmatrix} \bar{F}_{xx} & 0 & 0 & 0 & \bar{F}_{x,my} & 0 \\ 0 & \bar{F}_{yy} & 0 & \bar{F}_{y,mx} & 0 & 0 \\ 0 & 0 & \bar{F}_{zz} & 0 & 0 & 0 \\ 0 & \bar{F}_{mx,y} & 0 & \bar{F}_{mx} & 0 & 0 \\ \bar{F}_{my,x} & 0 & 0 & 0 & \bar{F}_{my} & 0 \\ 0 & 0 & 0 & 0 & 0 & \bar{F}_{mz} \end{bmatrix} \quad (3.21)$$

3.2.1 Numerical example: Square foundation on a homogeneous halfspace

This example analyses a square rigid surface massless foundation resting on a homogeneous halfspace, Figure 3.8. The results are compared with the results obtained by Wong [60]. The assumed Poisson's coefficient of the soil is $\nu = 1/3$. The damping coefficient of the soil is $\xi = 2\%$. The problem is axisymmetrical which means that dynamic stiffnesses in x and y directions are equal, i.e. $K_{xx} = K_{yy}$ and $K_{mx} = K_{my}$.

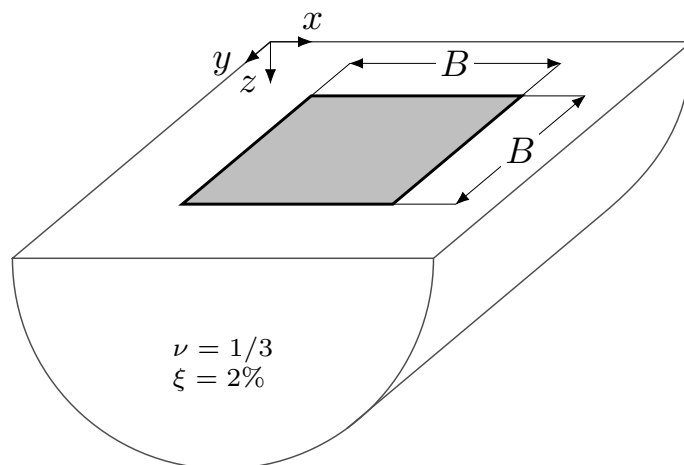


Figure 3.8: Square foundation resting on a homogeneous halfspace

Figures 3.9-3.10 show the real and imaginary part of the vertical, horizontal and rocking compliance functions of the square rigid foundation resting on a homogeneous halfspace obtained using the proposed method together with the results from the literature, Wong [60]. The discrepancies between the results are negligible, except for the real part of the rocking compliance. That might be due to the fact that Wong did not introduce damping in his model, while the proposed method requires damping in order to avoid aliasing phenomena. Since the adopted damping coefficient is $\xi = 2\%$, the proposed method gives the lower amplitudes of the compliance functions in general.

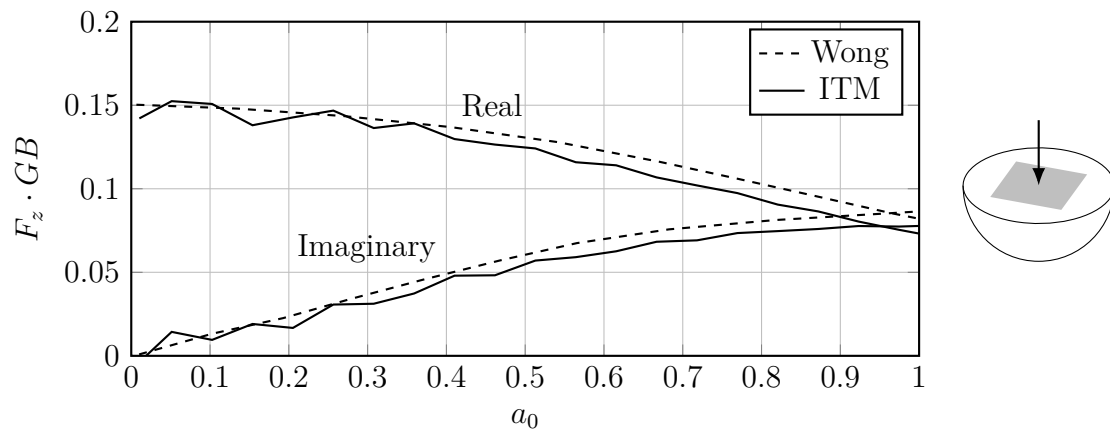


Figure 3.9: Vertical compliance of a square foundation on a homogeneous halfspace in comparison with Wong [60]

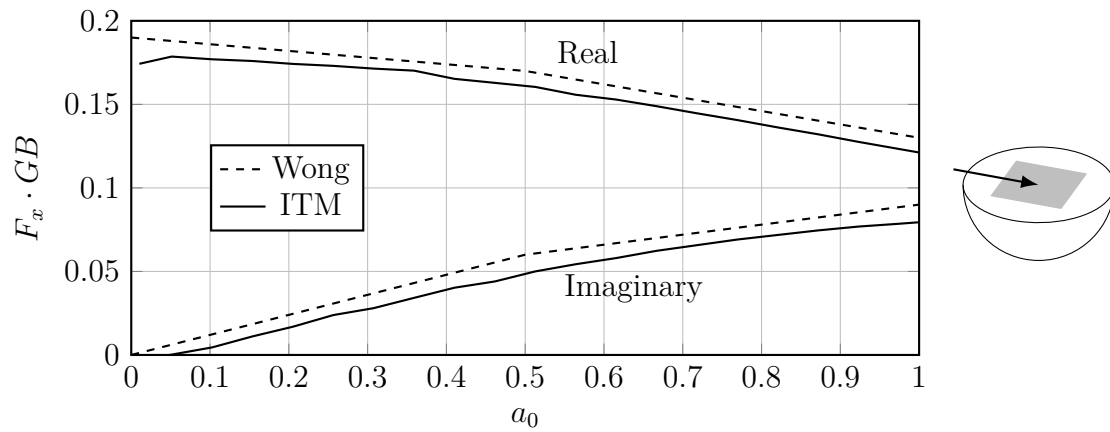


Figure 3.10: Horizontal compliance of a square foundation on a homogeneous halfspace in comparison with Wong [60]

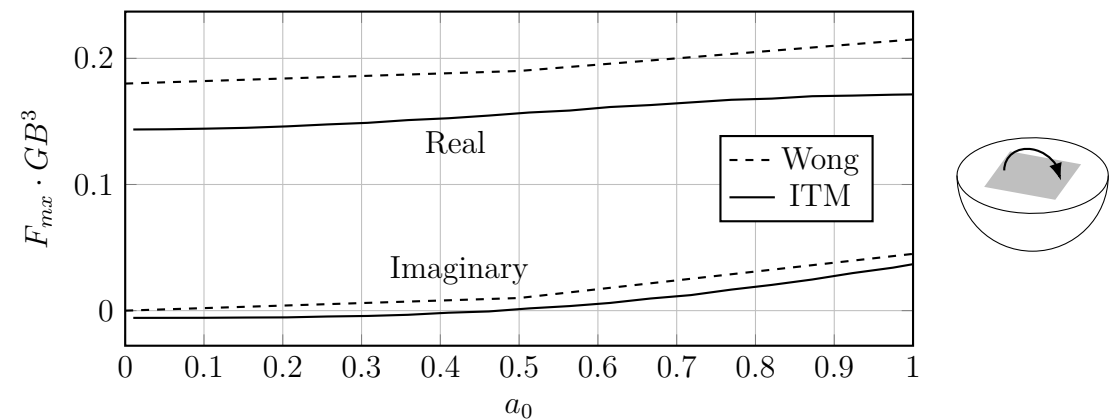


Figure 3.11: Rocking compliance of a square foundation on a homogeneous halfspace in comparison with Wong [60]

3.2.2 Group of rigid foundations

The problem of obtaining the dynamic stiffness matrix of the group of foundations is analogous to the problem that involves a single foundation. The disposition of the problem that involves a group of two foundations is shown in Figure 3.12.

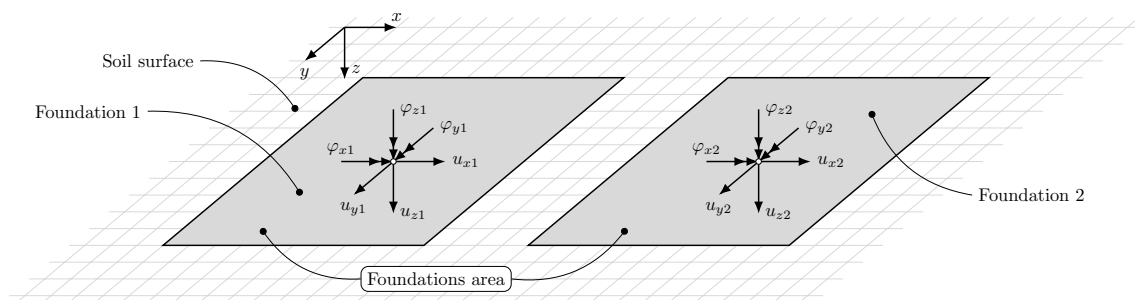


Figure 3.12: A group of two rigid foundations resting on the surface of the soil

Once again, the solution of the problem is based on the fundamental solution of the soil by ITM and the kinematic transformation [63]. The steps of the procedure are following:

- Calculate the dynamic flexibility matrix of the soil area covered by the foundations, $\bar{\mathbf{F}}_s$, using ITM.
- Obtain the dynamic stiffness matrix $\bar{\mathbf{K}}_s$ by inverting dynamic flexibility matrix $\bar{\mathbf{F}}_s$.
- Calculate the dynamic stiffness matrix of the system of foundations using the kinematic transform.

Let M be the number of the foundation and $3n$ the number of degrees of freedom of the soil surface occupied by the foundation area of each foundation. Matrix $\bar{\mathbf{F}}_s$ is obtained using the shifting method (see Section 3.2, Figure 3.3). In this case, the foundations area is the union of the foundation areas of all foundations, Figure 3.12. The size of $\bar{\mathbf{K}}_s$ is $(M \times 3n, M \times 3n)$. The dynamic stiffness matrix of the group of

rigid foundations is calculated using the same kinematic principle as in Section 3.2

$$\bar{\mathbf{K}}_r = \mathbf{A}^\top \bar{\mathbf{K}}_s \mathbf{A} \quad (3.22)$$

where \mathbf{A} is a diagonal block matrix

$$\mathbf{A} = \begin{bmatrix} \mathbf{a}_1 & 0 & \cdots & 0 \\ 0 & \mathbf{a}_2 & \cdots & 0 \\ \vdots & \vdots & \ddots & \vdots \\ 0 & 0 & 0 & \mathbf{a}_M \end{bmatrix} \quad (3.23)$$

that consists of the kinematic matrices \mathbf{a}_i four each foundation i . Matrices \mathbf{a}_i are defined in equations (3.15) and (3.16). The size of the matrix \mathbf{A} is $(M \times 3n, M \times 6)$. Regarding equation (3.22), the size of the stiffness matrix of the system of rigid foundations is $(M \times 6, M \times 6)$.

3.2.3 Numerical example: Group of foundations on a layer over bedrock

This example presents the analysis of two square $B \times B$ foundations resting on the layer of depth H over the bedrock, Figure 3.13. The distance between the centroids of the foundations is denoted with X . The soil damping coefficient is $\xi = 5\%$, the Poisson's coefficient $\nu = 1/3$.

The compliances are calculated for various layer depths, $H = B, 2B, 4B, \infty$. The results are given in terms of absolute values of the compliance functions. The compliances in the vertical direction are presented against the results obtained by Karabalis and Mohammadi (K&M) [19], Figure 3.14. Figures 3.15-3.18 shows horizontal and rocking compliance functions obtained using the proposed method.

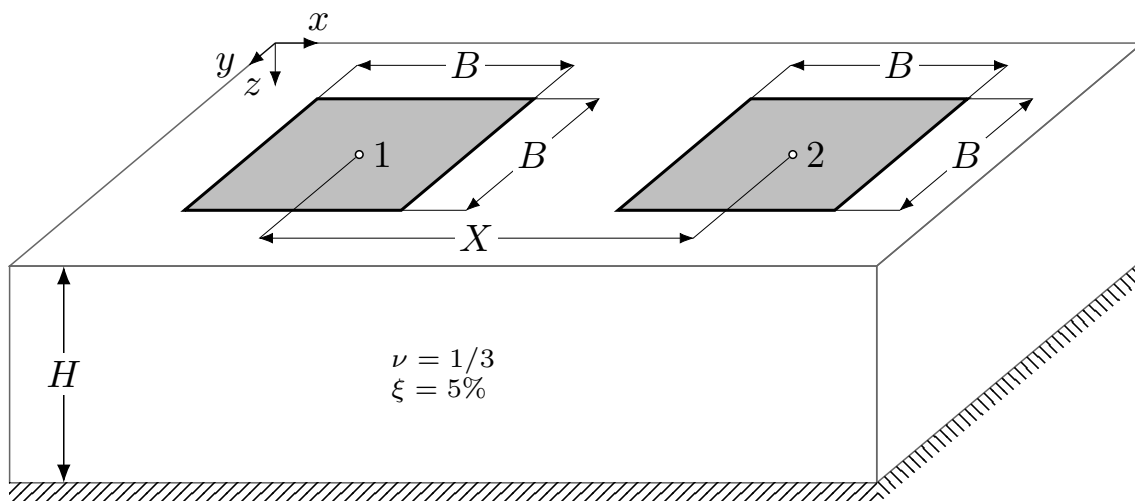


Figure 3.13: FSFI - layer over bedrock

The notation of the compliance functions of the system of the foundations is a bit different than the notation of the compliance function of the single foundation. F_{kl}^{ij} represents the compliance function of foundation i in direction k due to the force acting on foundation j in direction l . The presented compliances are calculated for the case of the load acting on the foundation 1.

The effect of the natural frequency of the layer on the compliance functions of the foundations is manifested through the resonant peaks which occur at non dimensional frequencies $a_{0n} = (\pi B(1 + 2n))/(2H)$ [52]. In the comparison with K&M, the proposed method gives significantly higher amplification of the compliance function at the first resonant frequency ($n = 0$) of the layer, but lower at the other resonant frequencies. The resonant peaks of the layer are more pronounced in the case of horizontal compliances F_{xx} and F_{yy} shown in Figures 3.15 and 3.16 respectively. The amplitudes of the adjacent foundation are more pronounced when the force is acting in x direction, Figure 3.15 (e)-(h), than in y direction, Figure 3.16 (e)-(h). This behavior is expected, since the foundations are placed along the x axis. The rocking movement of the loaded foundation around x axis, Figure 3.17 (a)-(d), excites the adjacent foundation to rock around x axis significantly, Figure 3.17 (e)-(h). The rocking of the adjacent foundation along y axis, Figure 3.18 (e)-(h), when the

foundation 1 is subjected to a rocking movement along y axis, Figure 3.18 (a)-(d), is almost neglectable. In contrast with the vertical and horizontal compliances, the rocking compliances became independent of the layer depth, for $H \geq 4B$. In general, the influence of the loaded foundation on the adjacent one is more pronounced than the influence of the adjacent foundation on the loaded one.

The influence of the distance between the foundations on the compliance functions is shown in Figures 3.19-3.23. The compliance functions are calculated for $X/B = 1.2, 2.0$ and 4.0 and for $H = B$ and ∞ . The influence of the loaded foundation on the adjacent ones decays with the increase of the distance between the foundations. The decay factor is the lowest for horizontal compliances F_{xx} and F_{yy} and rocking compliance $F_{rx,rx}$. If close enough, the adjacent foundation could reduce the amplification of the compliance of the loaded foundation around the first resonant frequency of the soil. This is more pronounced in the case of horizontal compliances, Figures 3.20(a,c) and 3.21(a,c), and rocking compliances, Figures 3.22(a,c) and 3.23(a,c), than in the case of vertical compliance, Figure 3.19(a,c).

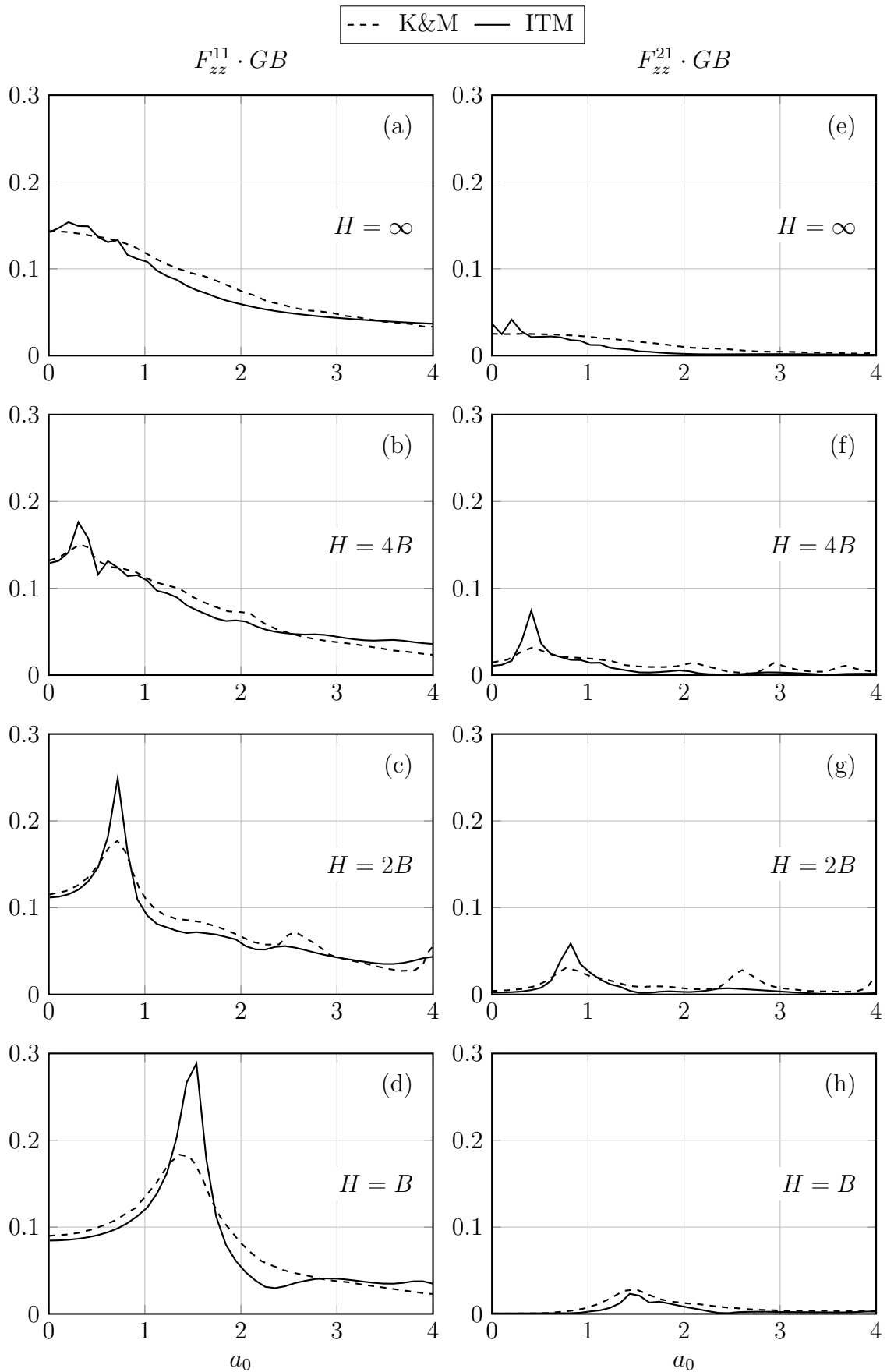


Figure 3.14: Vertical compliance F_{zz} of the foundations for varying depths of the layer

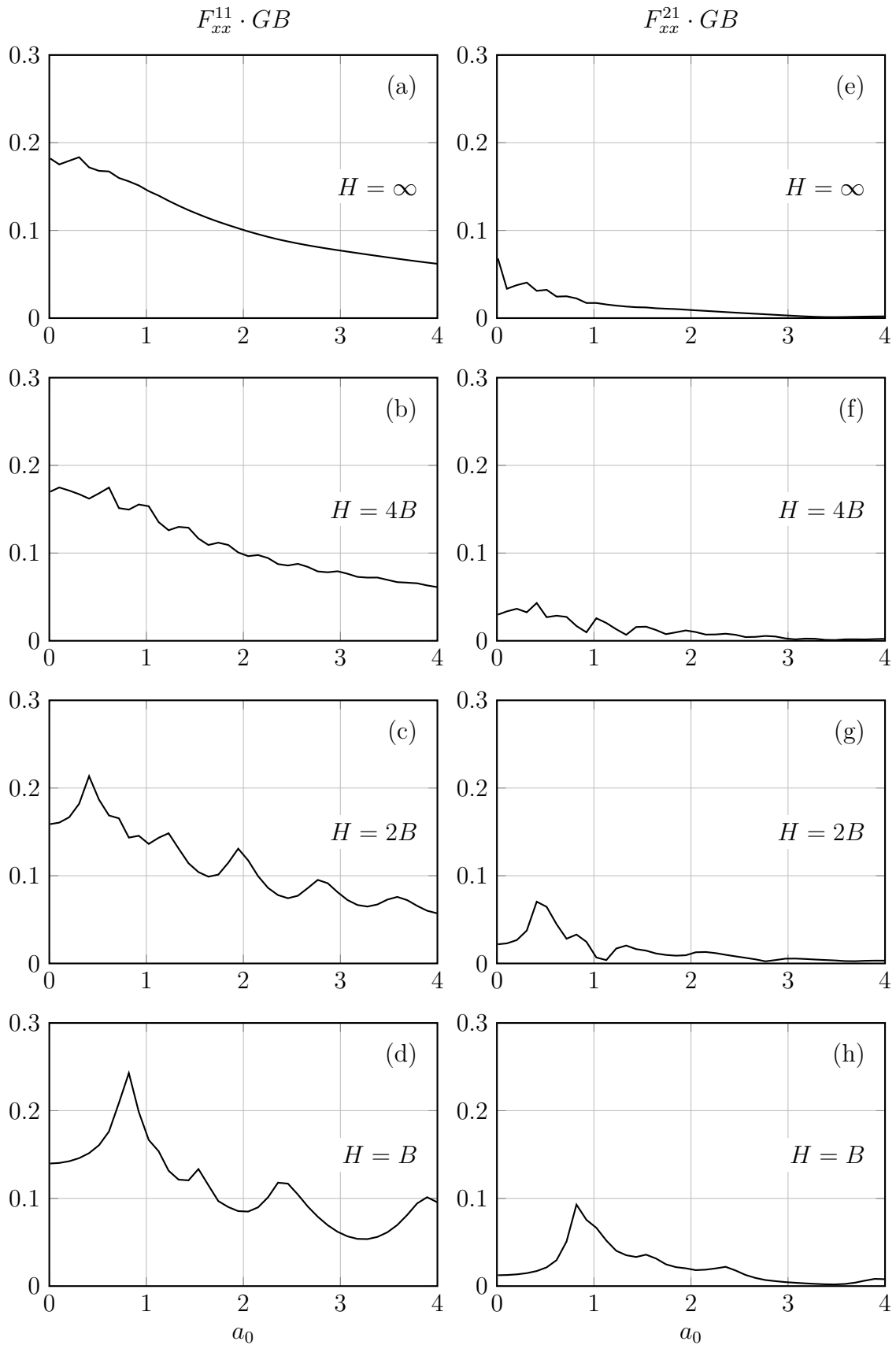


Figure 3.15: Horizontal compliance F_{xx} of the foundations for varying depths of the layer

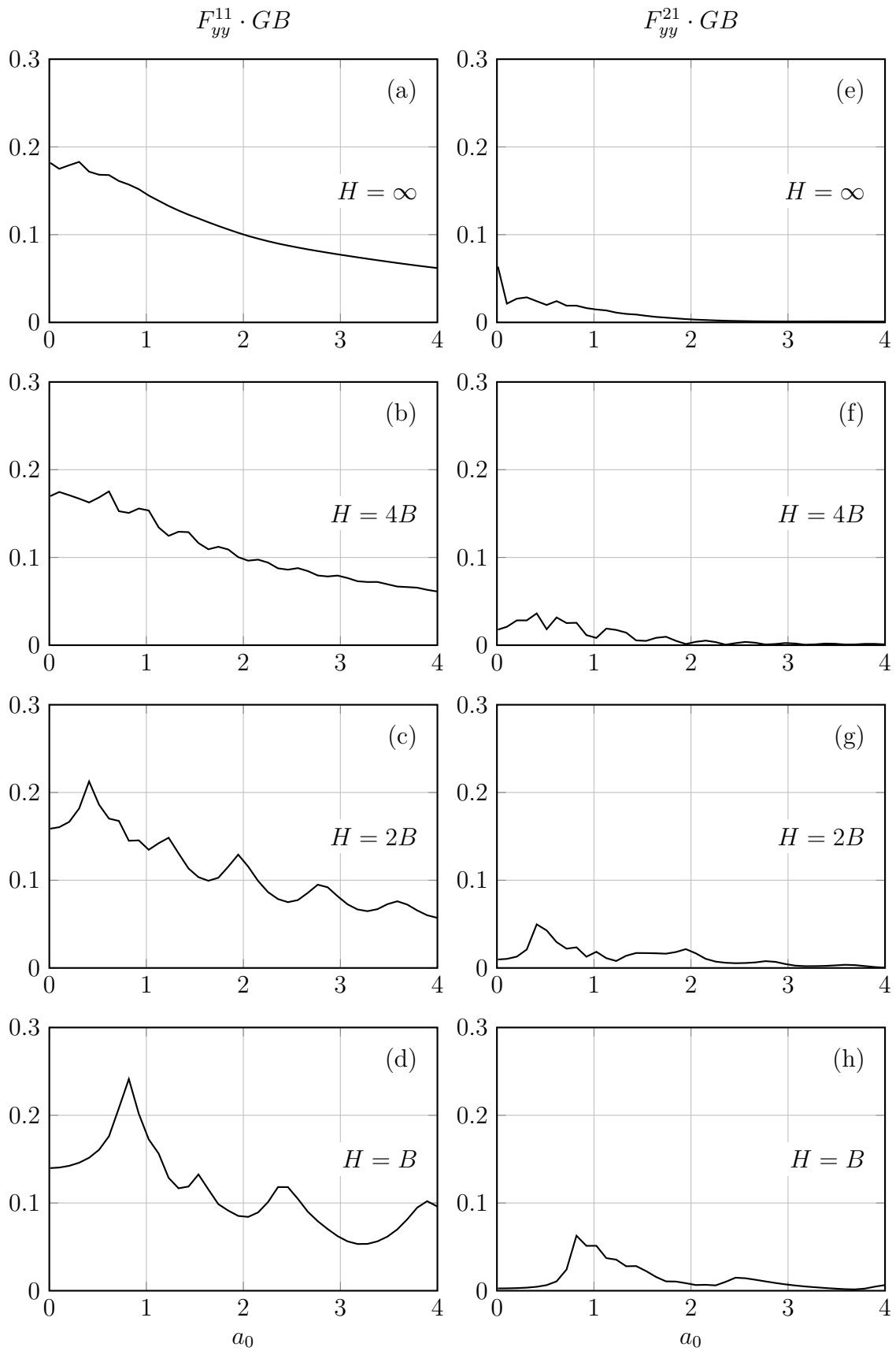


Figure 3.16: Horizontal compliance F_{yy} of the foundations for varying depths of the layer

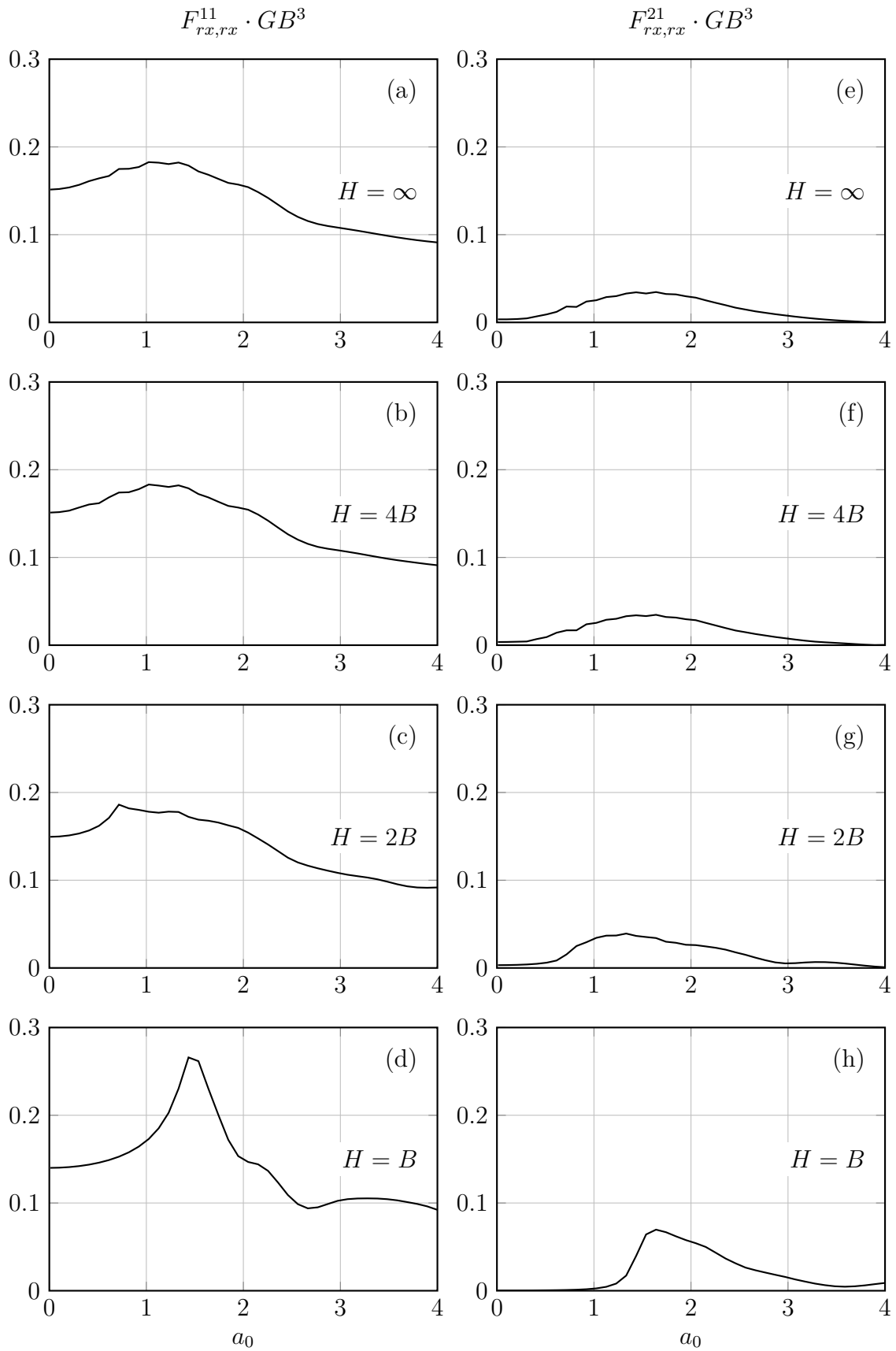


Figure 3.17: Rocking compliance $F_{rx,rx}$ of the foundations for varying depths of the layer

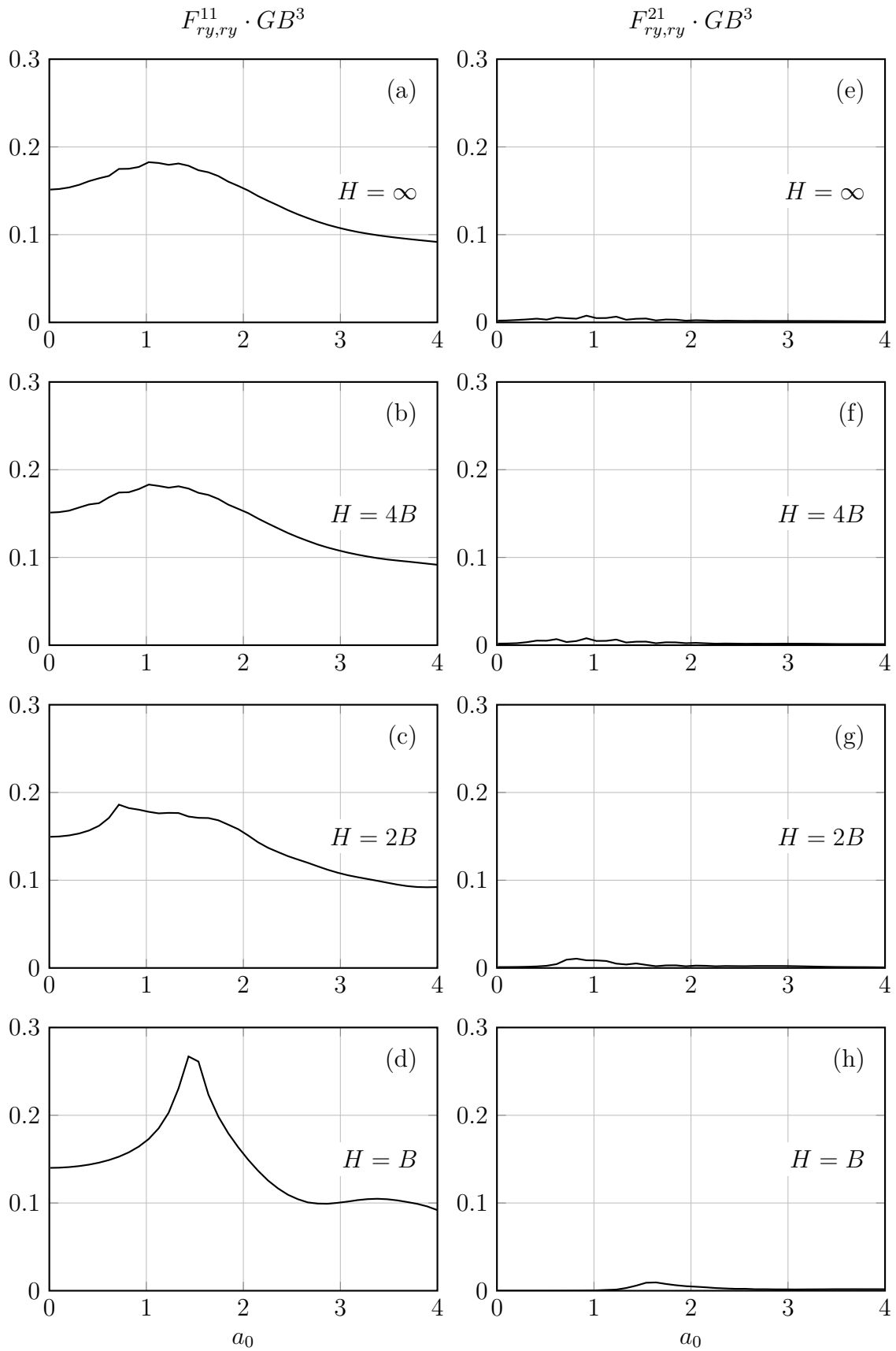


Figure 3.18: Rocking compliance $F_{ry,ry}$ of the foundations for varying depths of the layer

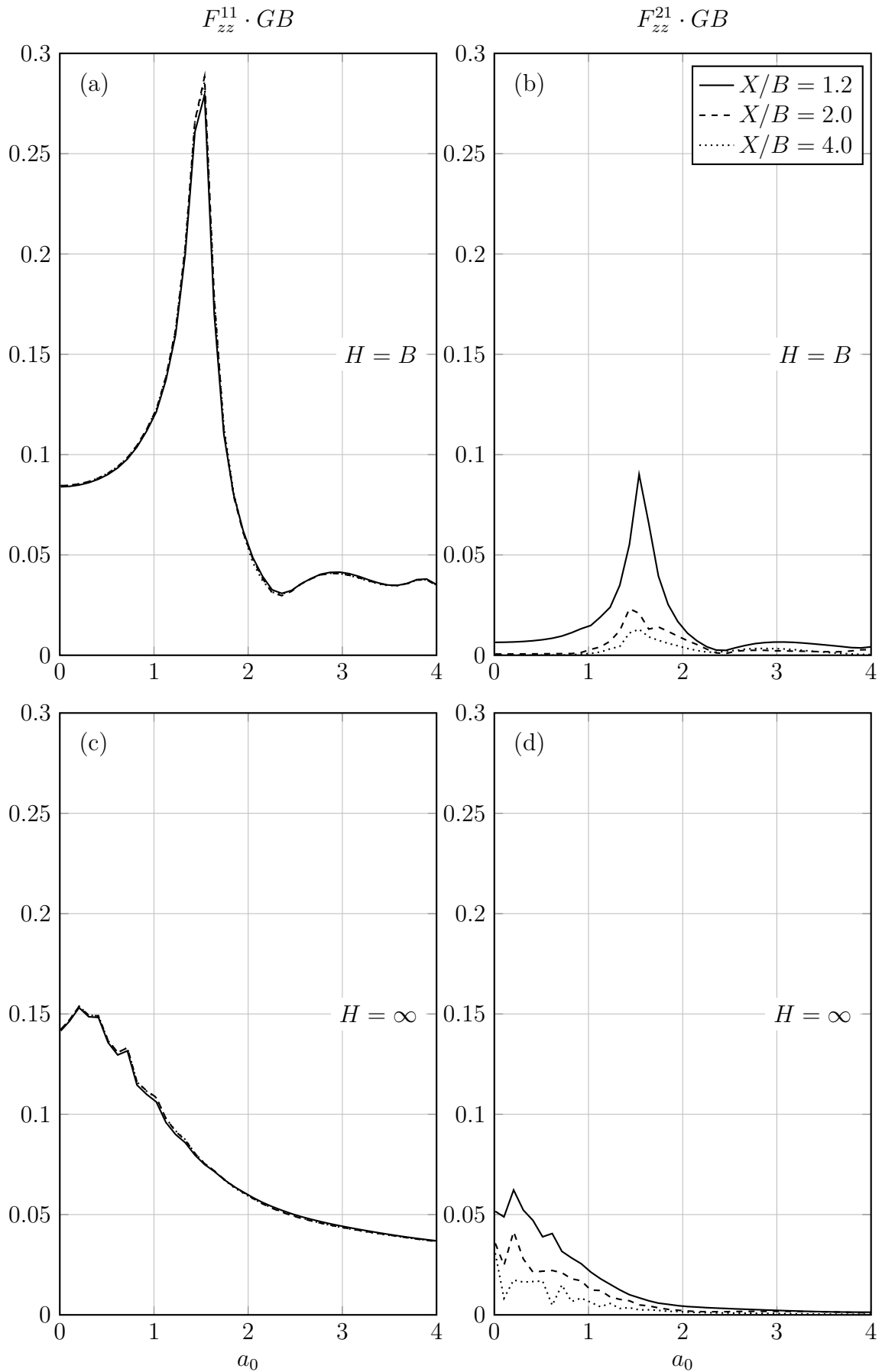


Figure 3.19: Vertical compliance F_{zz} of the foundations for varying X/B ratio and layer depth H

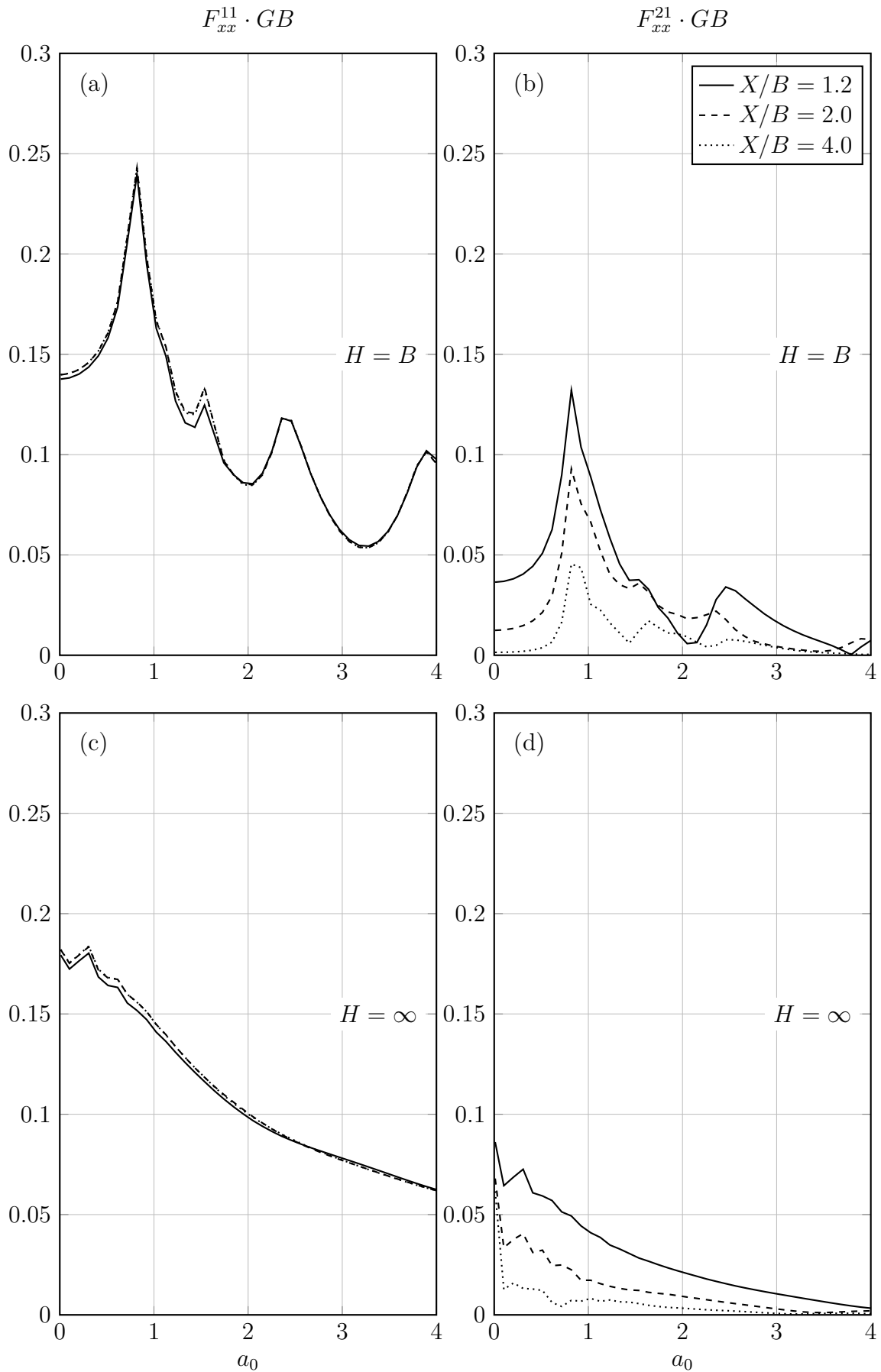


Figure 3.20: Horizontal compliance F_{xx} of the foundations for varying X/B ratio and layer depth H

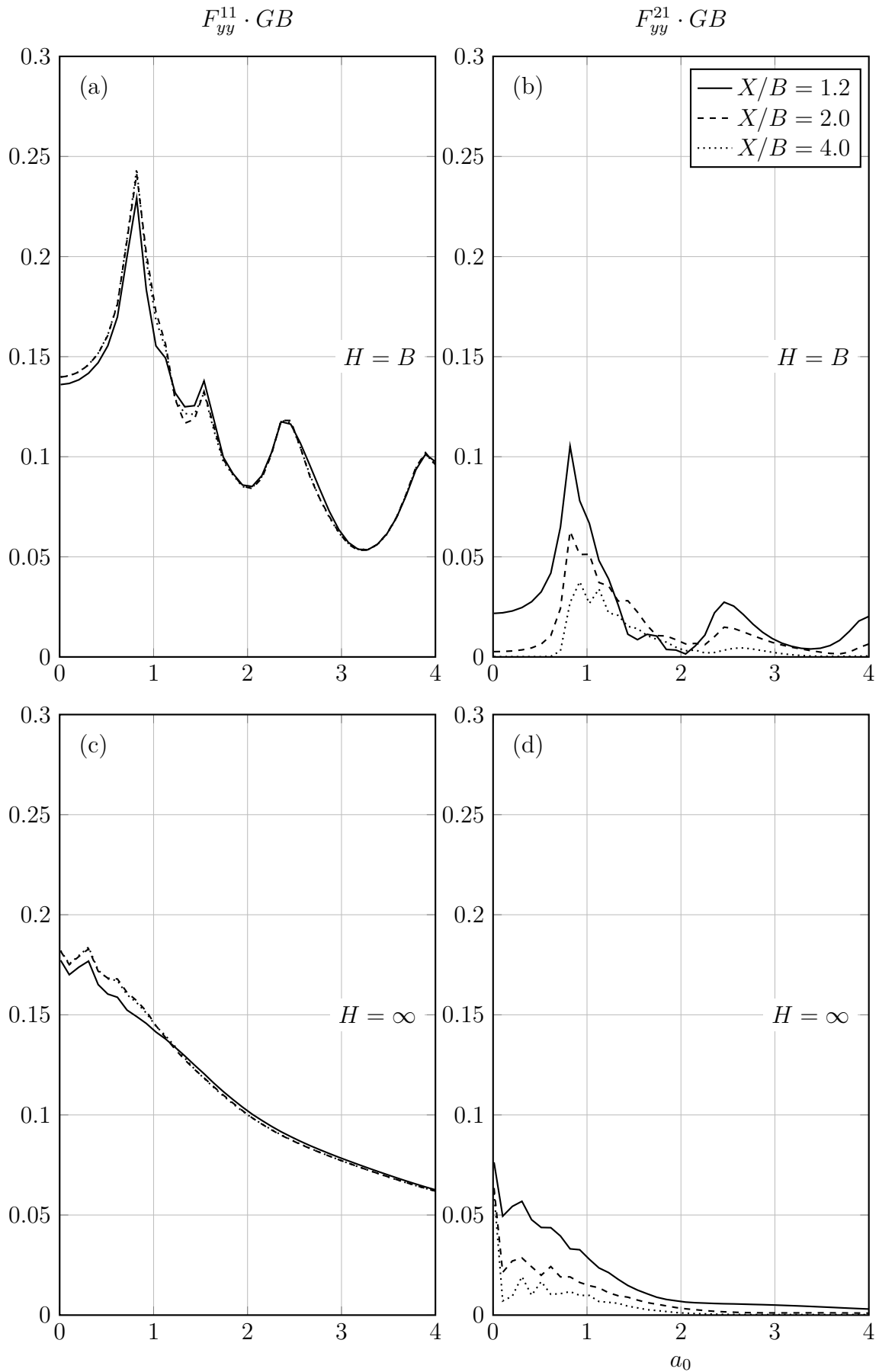


Figure 3.21: Horizontal compliance F_{yy} of the foundations for varying X/B ratio and layer depth H

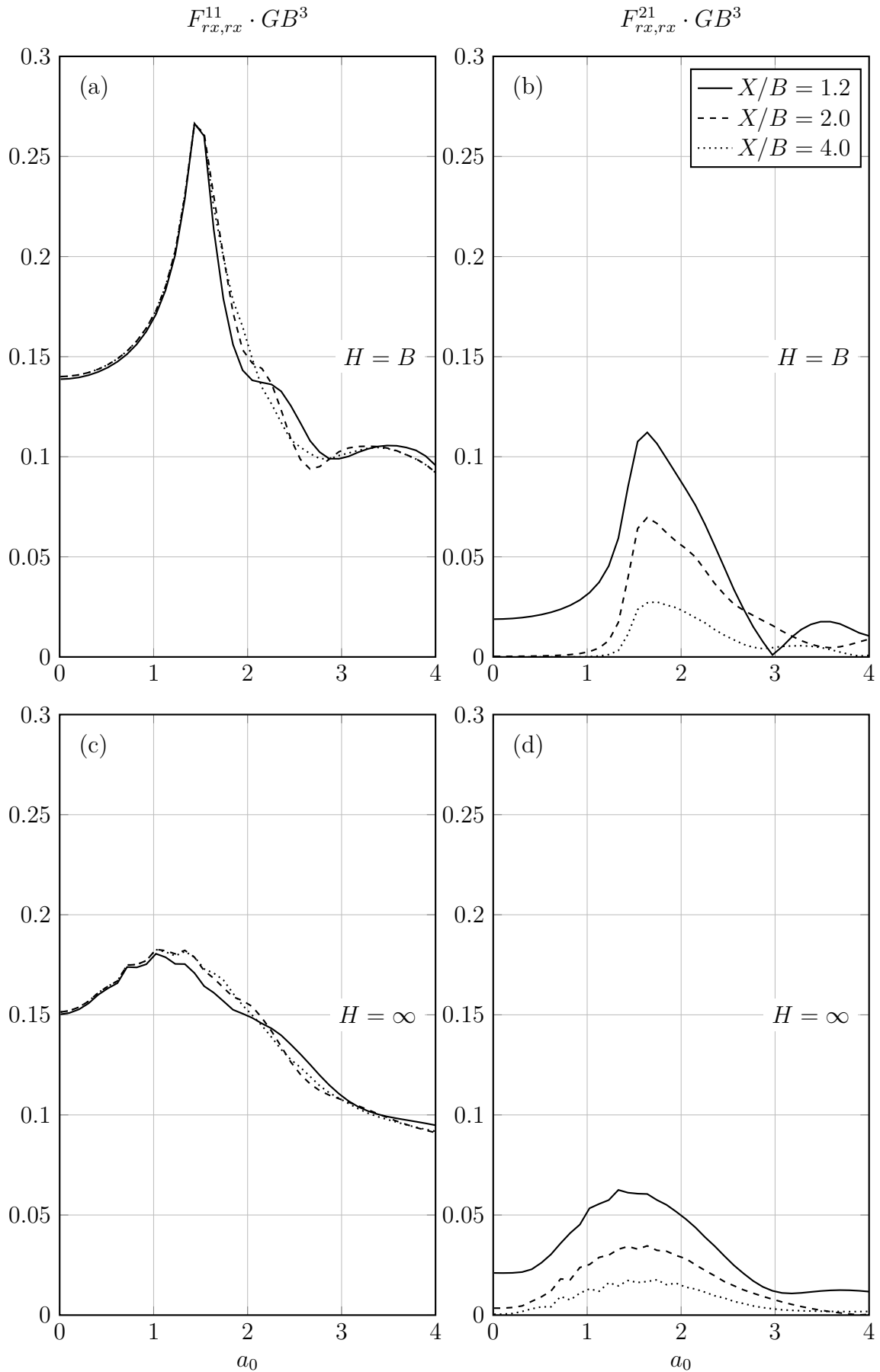


Figure 3.22: Rocking compliance $F_{rx,rx}$ of the foundations for varying X/B ratio and layer depth H

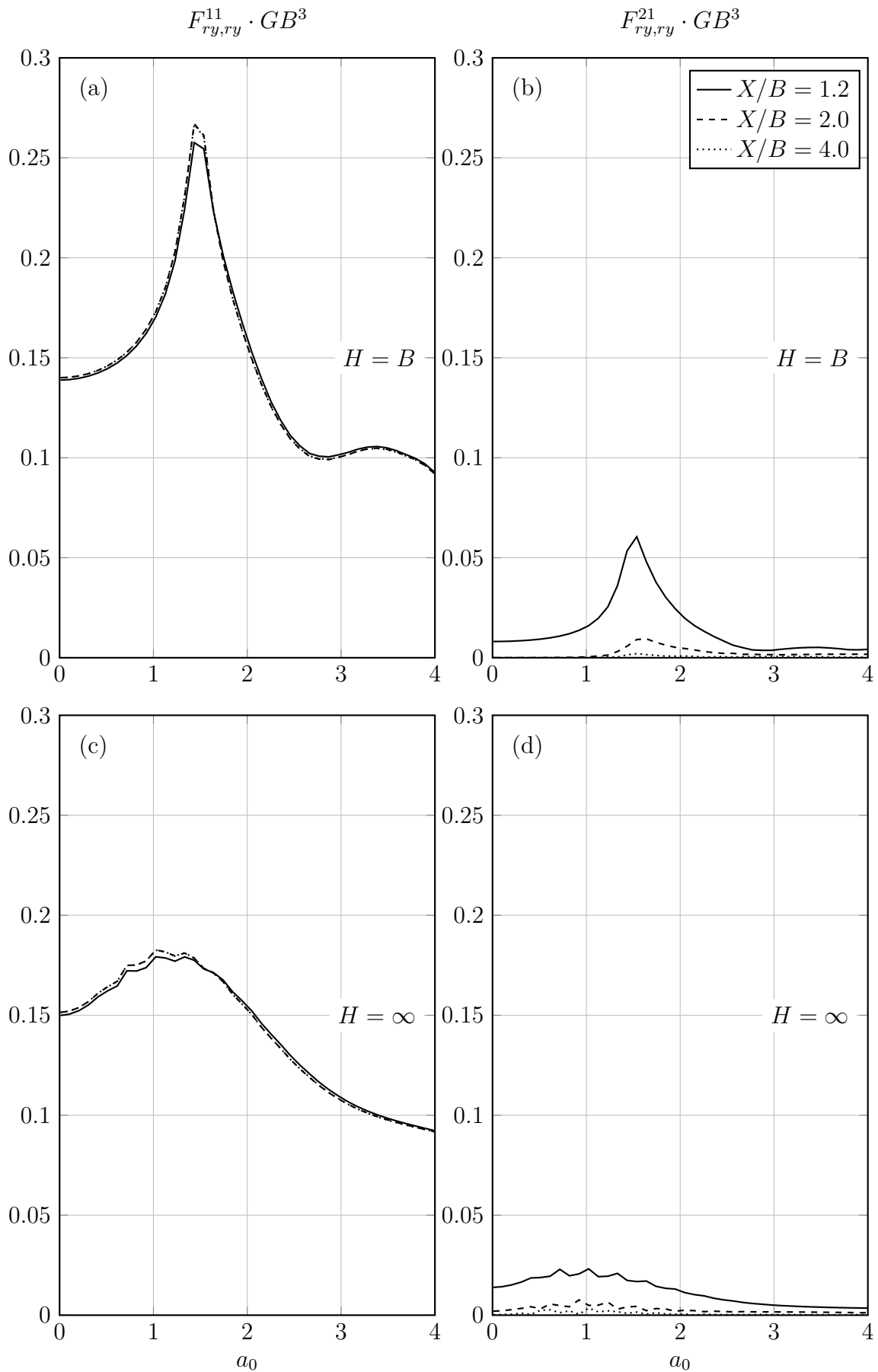


Figure 3.23: Rocking compliance $F_{ry,ry}$ of the foundations for varying X/B ratio and layer depth H

3.3 Flexible Foundation

The process of determining the compliances of flexible foundation is more complex than in the case of rigid ones, since the flexibility of the foundation must be taken into account and the foundation should be treated as a plate of limited rigidity. The analysis of the response of such a plate resting on the soil is convenient for the usage of substructuring method, considering the different nature of the substructures, the plate and the soil. Each substructure is modeled separately, using different methods suitable for obtaining the solution of the differential equation of the substructure. The coupling of the system of differential equations is challenging. The most common approach of solving this problem in the literature considers BEM-FEM coupling, where the soil is modeled using BEM and the foundation is modeled using FEM, [22, 21, 20, 19]. This coupling is well developed and widely used, but it is based on a weak formulation, and it inherits all the deficiencies of FEM in the field of dynamic analysis. The literature offers an analytical solution of the response of the flexible foundation on the halfspace [16], but it is limited to problems described in polar coordinates only.

This chapter presents the main contribution of the dissertation: formulation of a semi-analytical approach for the solution of the rectangular flexible foundation resting on the homogeneous halfspace. The approach is formulated in the Cartesian coordinate system. It is based on ITM used for obtaining the fundamental solution of the soil and SEM used for obtaining the fundamental solution of the foundation. The differential equation of the system is solved by using the modal approach [16]. The connection between the foundation model and the soil model is established using the modal impedance matrix of the soil.

Based on the presented formulation, a computer code for calculating the response of a strip and rectangular foundations on halfspace has been developed using MAT-

LAB [53]. The results obtained using the proposed approach are verified against the results obtained using SASSI [10], a commercial software package for SSI analysis based on FEM, and the results from the literature. The proposed method deals with vertical vibrations only, although its formulation could be generalized to all directions, which will be the subject of further research. The coupling assumes relaxed boundary conditions [64]: the coupling of shear stresses along the interface zone is neglected.

3.3.1 Flexible strip foundation

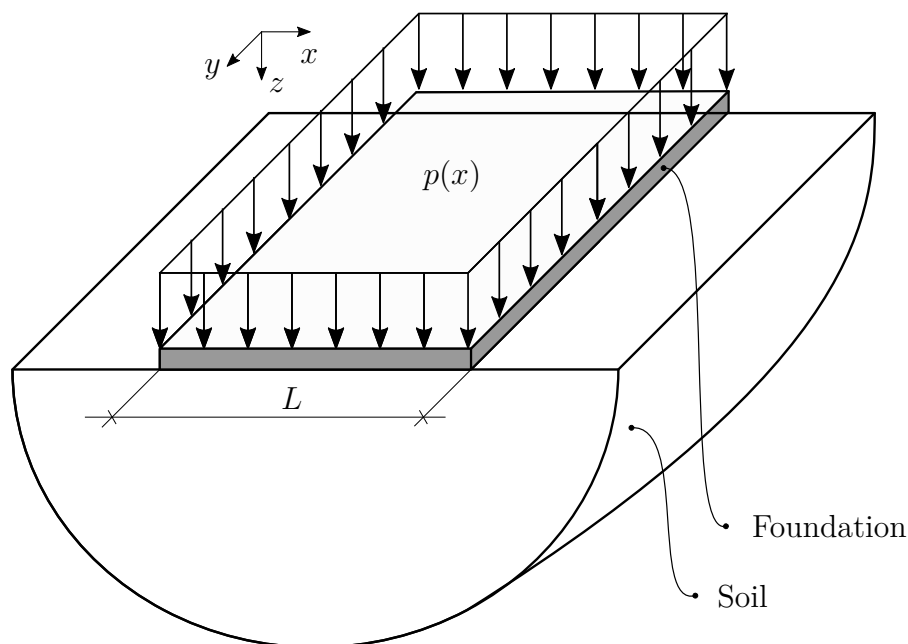


Figure 3.24: Flexible y -wise infinite strip foundation resting on a homogeneous halfspace

The following formulation describes a flexible y -wise infinite strip foundation resting on a homogeneous and isotropic halfspace. The problem is formulated in the Cartesian coordinate xyz system. The load, the geometry of the foundation and the boundary conditions are not y dependent. The cross section of the foundation lays in the xz plane, as shown in Figure 3.25. The foundation behaves as an Euler-Bernoulli

beam of length L and height H in xz direction. Accordingly, the formulation of the problem considers a plane strain analysis.

The steady state response analysis of the beam is performed in the frequency domain, (x, y, z, ω) . The response of the soil medium is obtained in the wavenumber-frequency domain (k_x, k_y, z, ω) using ITM. It is considered that all functions are ω dependent, therefore, the ω variable is omitted in the notation of the functions. For example, $f(x, \omega)$ is $f(x)$.

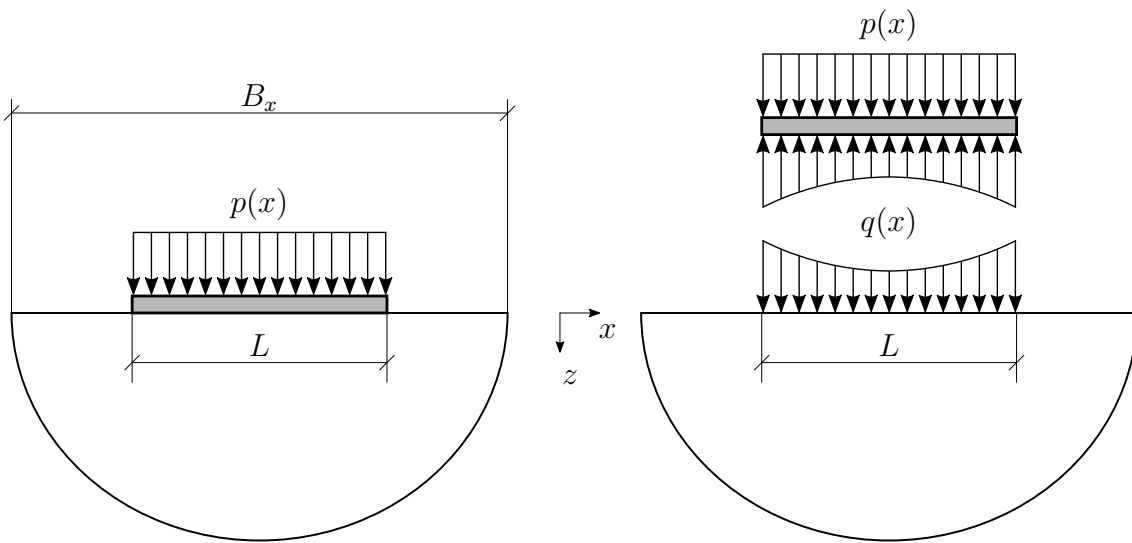


Figure 3.25: Flexible y-wise infinite strip foundation resting on a homogeneous halfspace

The differential equation of the problem of the strip foundation resting on the surface of the soil in (x, ω) domain is given by

$$E_f I_f \frac{d^4 w(x)}{dx^4} - \omega^2 m_f w(x) = p(x) - q(x) \quad (3.24)$$

where E_f , I_f and m_f are the Young's modulus, the moment of inertia and the mass per unit area of the foundation, respectively. $w(x)$, $p(x)$ and $q(x)$ are the transverse deflection of the foundation, the vertical load and the soil reaction, respectively.

They can be expanded in a series of free vibration modes as follows:

$$\begin{aligned}
 w(x) &= \sum_{n=0}^N Y_n \phi_n(x) \\
 p(x) &= \sum_{n=0}^N P_n \phi_n(x) \\
 q(x) &= \sum_{n=0}^N Q_n \phi_n(x)
 \end{aligned} \tag{3.25}$$

where $\phi_n(x)$ represents the orthonormalized mode shape of the foundation for the n^{th} mode and Y_n , P_n and Q_n are modal coefficients.

$$\begin{aligned}
 Y_n &= \int_0^L w(x) \phi_n(x) dx \\
 P_n &= \int_0^L p(x) \phi_n(x) dx \\
 Q_n &= \int_0^L q(x) \phi_n(x) dx
 \end{aligned} \tag{3.26}$$

The mode shapes of the foundation are obtained by analyzing free vibrations of a free-free beam element. The differential equation of motion of the beam element is given by

$$E_f I_f \frac{d^4 w(x)}{dx^4} - \omega^2 m_f w(x) = 0 \tag{3.27}$$

The exact solution of the equation (3.27) leads to [48]

$$w(x) = C_1 \sin(kx) + C_2 \cos(kx) + C_3 \sinh(kx) + C_4 \cosh(kx) \tag{3.28}$$

where k is a pure bending wavenumber of a beam element

$$k = \sqrt{\omega} \left(\frac{m_f}{E_f I_f} \right)^{1/4} \tag{3.29}$$

The boundary conditions of a free-free beam are following

$$\frac{d^2w}{dx^2}(0) = 0, \quad \frac{d^3w}{dx^3}(0) = 0, \quad \frac{d^2w}{dx^2}(L) = 0, \quad \frac{d^3w}{dx^3}(L) = 0 \quad (3.30)$$

Substituting (3.28) into (3.30) gives

$$\begin{bmatrix} 0 & -1 & 0 & 1 \\ -1 & 0 & 1 & 0 \\ -\sin(kL) & -\cos(kL) & \sinh(kL) & \cosh(kL) \\ -\cos(kL) & \sin(kL) & \cosh(kL) & \sinh(kL) \end{bmatrix} \begin{Bmatrix} C_1 \\ C_2 \\ C_3 \\ C_4 \end{Bmatrix} = \begin{Bmatrix} 0 \\ 0 \\ 0 \\ 0 \end{Bmatrix} \quad (3.31)$$

The system of equations (3.31) could be transformed to

$$\begin{bmatrix} \sinh(kL) - \sin(kL) & \cosh(kL) - \cos(kL) \\ \cosh(kL) - \cos(kL) & \sin(kL) + \sinh(kL) \end{bmatrix} \begin{Bmatrix} C_1 \\ C_2 \end{Bmatrix} = \begin{Bmatrix} 0 \\ 0 \end{Bmatrix} \quad (3.32)$$

A non trivial solution of the system of equations (3.32) gives

$$\cosh(kL) \cos(kL) = 1 \quad (3.33)$$

The transcendental equation (3.33) has infinite solutions k_n , $n = 0, 1, 2, \dots \infty$ and it is solved numerically. Every solution k_n gives one mode shape

$$\phi_n^*(x) = (\sinh(k_n x) + \sin(k_n x)) + \frac{\sin(k_n L) - \sinh(k_n L)}{\cosh(k_n L) - \cos(k_n L)} (\cosh(k_n x) + \cos(k_n x)) \quad (3.34)$$

The mode shapes ϕ_n^* are orthonormalized as follows

$$\phi_n = \frac{\phi_n^*}{\int_0^L |\phi_n^*|^2 dx} \quad \text{so that} \quad \int_0^L \phi_n(x) \phi_m(x) dx = \begin{cases} 1, & m = n \\ 0, & m \neq n \end{cases} \quad (3.35)$$

Figure 3.26 shows the first three mode shapes of a free-free beam. The first mode is a translational mode ($k_1 = 0$).

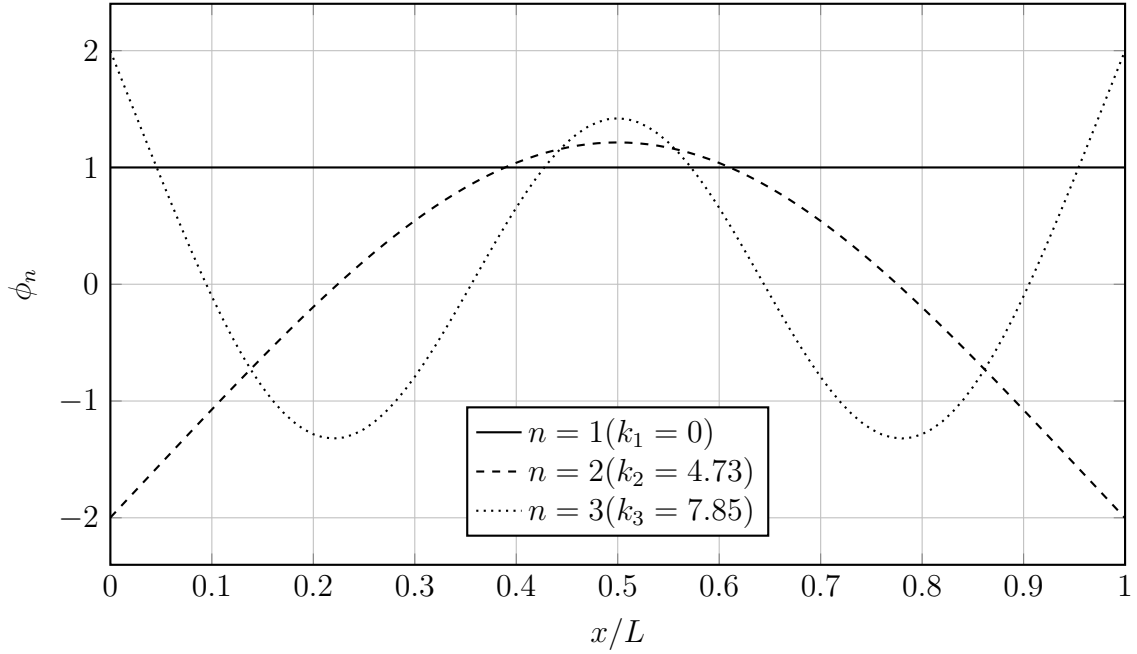


Figure 3.26: Free vibrations mode shapes of a strip foundation for $n = 1, 2, 3$

Substituting (3.25) into (3.24) gives

$$\sum_{n=0}^N (E_f I_f k_n^4 - m_f \omega^2) \phi_n(x) Y_n = \sum_{n=0}^N \phi_n(x) P_n - \sum_{n=0}^N \phi_n(x) Q_n \quad (3.36)$$

Since modes $\phi_n(x)$ are orthonormal, equation (3.36) can be decoupled into N equations by multiplying with mode shape $\phi_m(x)$ and integrating over the length of the beam, L . That gives the system of N equations:

$$(E_f I_f k_m^4 - m_f \omega^2) Y_m = P_m - Q_m, \quad m = 0, 1, 2, \dots, N \quad (3.37)$$

Equation (3.37) can be expressed in matrix form as follows

$$\left(E_f I_f [\mathbf{k}^4] - m_f \omega^2 [\mathbf{I}] \right) \{\mathbf{Y}\} = \{\mathbf{P}\} - \{\mathbf{Q}\} \quad (3.38)$$

where $\{\mathbf{Y}\}$, $\{\mathbf{P}\}$ and $\{\mathbf{Q}\}$ are coefficient vectors of modal displacement, load and soil reaction, respectively, $[\mathbf{I}]$ is identity matrix and $[\mathbf{k}^4]$ is the pure bending wavenumber matrix of the beam

$$[\mathbf{k}^4] = \begin{bmatrix} 0 & 0 & \cdots & 0 \\ 0 & k_1^4 & & \vdots \\ \vdots & & \ddots & 0 \\ 0 & \cdots & 0 & k_N^4 \end{bmatrix} \quad (3.39)$$

Relation between displacements and soil reaction coefficient vectors can be defined as follows

$$[\mathbf{K}_s]\{\mathbf{Y}\} = \{\mathbf{Q}\} \quad (3.40)$$

where $[\mathbf{K}_s]$ is the modal impedance matrix of the soil. Substituting (3.40) into (3.38) the equation of motion becomes

$$\left\{ E_f I_f [\mathbf{k}^4] - m_f \omega^2 [\mathbf{I}] + [\mathbf{K}_s] \right\} \{\mathbf{Y}\} = \{\mathbf{P}\} \quad (3.41)$$

The element of the modal impedance matrix $K_{s,ij}$ can be defined as the required modal load in the i^{th} modal component that produces a unit soil displacement profile within the j^{th} mode shape. It is not possible to solve this problem directly by using the ITM. However, it is possible to obtain the modal impedance matrix as an inverse modal compliance matrix $[\mathbf{F}_s]$. The element of the modal compliance matrix $F_{s,ij}$ is the soil displacement in the i^{th} modal component induced by a unit modal load of the j^{th} shape. The steps for obtaining the modal soil compliance are the following:

1. Applying a unit modal load of the n^{th} mode on the soil, $q_n(x)$, that leads $Q_n = 1$
2. Transforming the modal load into wavenumber domain $\tilde{q}_n(k_x)$

3. Solving the soil displacement field in wavenumber domain $\tilde{w}_n(k_x)$ with the help of ITM, where the accuracy of the results depends on the discretization in the k_x domain
4. Transforming the soil displacement field into the spatial domain $w_n(x)$
5. Obtaining elements of the modal soil compliance matrix $F_{s,mn}$ as follows

$$F_{s,mn} = \int_0^L w_n(x)\phi_m(x)dx \quad (3.42)$$

Once the modal compliance matrix of the soil is formed, the displacement coefficient vector $\{Y\}$ is obtained by solving the system of equations (3.41) and finally the displacement field $w(x)$ is obtained by using equation (3.25). To obtain the displacement field spectrum, one should repeat the procedure for every frequency in a desired frequency range.

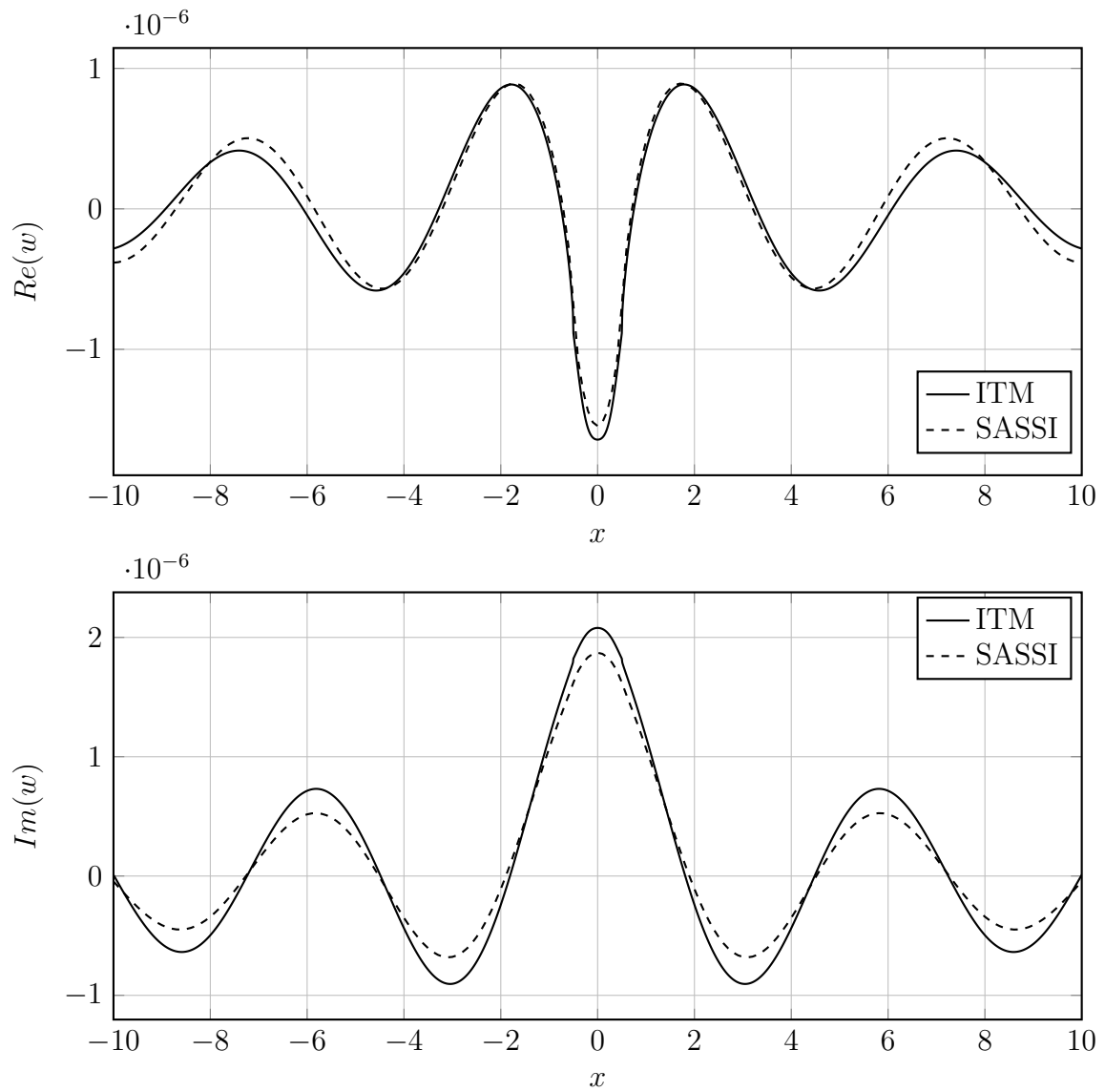
3.3.1.1 Numerical examples

The solution procedure for the proposed method is coded in MATLAB [53]. The results are compared with the numerical solution obtained by using a commercial software package for SSI analysis based on FEM, SASSI2000 [10].

In order to verify the proposed method, two limit states are considered: (1) the soft, $E_f = 0$ and (2) the rigid strip foundation, $E_f = 3e15 \text{ N/m}^2$. The properties of the elastic halfspace are: elastic modulus $E_s = 5e8 \text{ N/m}^2$, damping coefficient $\xi = 0.05$, Poisson's coefficient $\nu = 0.3$ and density $\rho = 2000 \text{ kg/m}^3$. The properties of the strip foundation are: width $L = 1 \text{ m}$, thickness $H = 0.1 \text{ m}$, damping coefficient $\xi = 0.05$, Poisson's coefficient $\nu = 0.3$ and density $\rho = 2000 \text{ kg/m}^3$. The foundation is loaded with the uniformly distributed load acting in z direction $q(x) = 10 \text{ N/m}^2$, as shown

in Figure 3.25. The results of the steady state plane strain analysis are given for the radial frequency $\omega = 50$ rad/s. The number of modes used for the analysis is three.

Figures 3.27 and 3.28 shows the real and the imaginary part of the displacement field of the surface of the soil medium for soft and rigid foundation, respectively. In SASSI2000 the soil medium model uses the FEM and the substructure subtraction method, solving the system of more than 1000 equations for the particular problem. The halfspace is simulated using the thin layer method with the variable depth method and the viscous boundary at the base [10]. Discrepancies in the results exist in both cases. ITM gives higher amplitudes of the displacement at the point of excitation, especially for higher values of E_f . Even though both approaches are using the same damping model, its impact is higher in the proposed method. It is manifested through the lower values of the real part of the displacement field, and the higher values of the imaginary part of the displacement field with the increase of the distance from the point of excitation.

Figure 3.27: Displacement field of the surface of the soil medium, $E_f = 0$

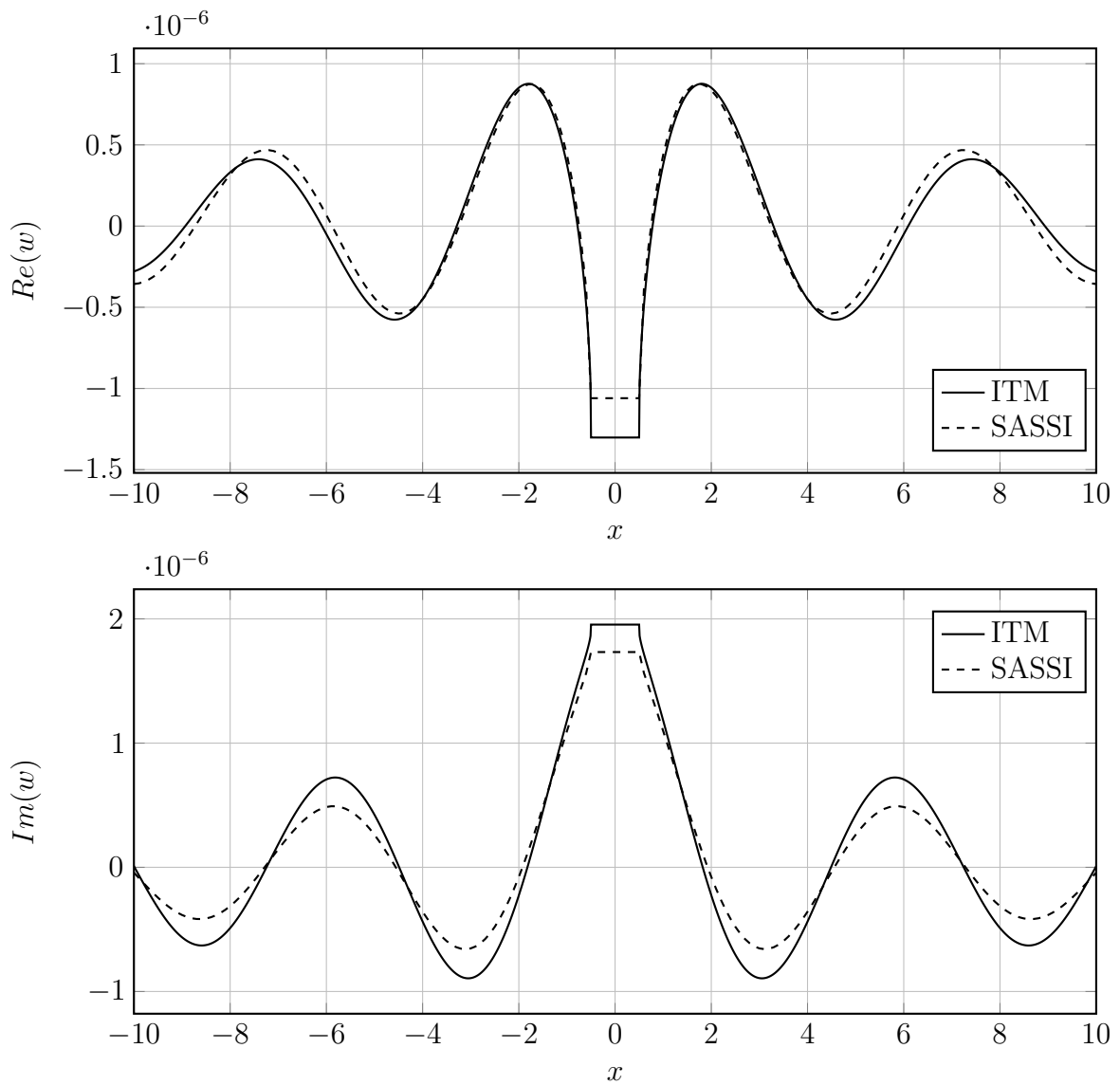


Figure 3.28: Displacement field of the surface of the soil medium,
 $E_f = 3 \times 10^{15} \text{ kN/m}^2$

3.3.2 Flexible square foundation

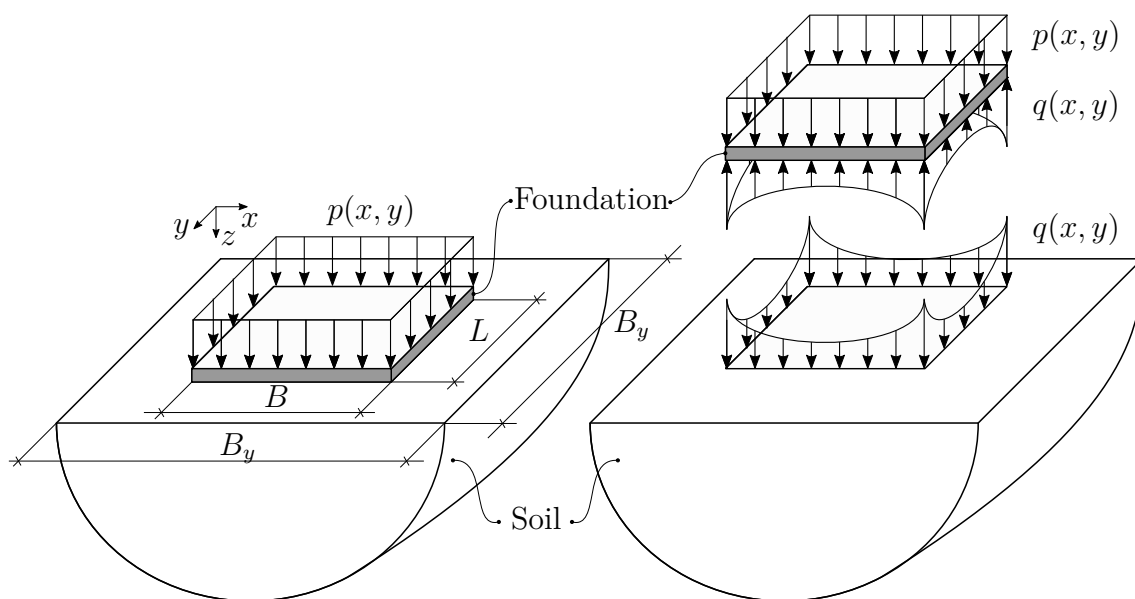


Figure 3.29: Flexible square foundation resting on halfspace

The procedure of obtaining the solution of the square flexible foundation resting on the halfspace is similar to the 2D analysis but more complex since the differential equation of the rectangular foundation is a partial differential equation.

The differential equation of the problem is solved by using the modal superposition method [16] after obtaining mode shape functions of a completely free spectral plate element [48]. The foundation is considered a Kirchhoff plate. The analysis is performed as a steady state analysis. This chapter deals with vertical vibrations of the foundation excited by an axisymmetrical loading function. The possibilities of extending the formulation to problems of horizontal vibrations and arbitrary functions of excitation is a subject of future research.

3.3.2.1 Mode shapes of the foundation

Mode shape functions of the foundations are obtained by analyzing free vibrations of a completely free plate using SEM. First, the general solution of the differential

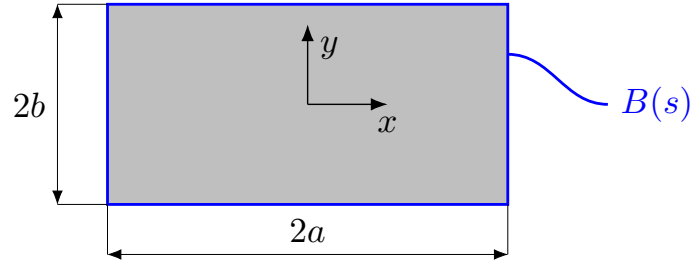


Figure 3.30: Spectral plate element

equation of the problem is generated. That leads to the development of the dynamic stiffness matrix of the plate. The natural frequencies of the plate are obtained using the dynamic stiffness matrix and respecting the boundary conditions of the plate. For every natural frequency, one mode shape is generated.

The differential equation of free vibrations of the plate is the following

$$D \left(\frac{\partial^4 w(x, y)}{\partial x^4} + 2 \frac{\partial^4 w(x, y)}{\partial x^2 \partial y^2} + \frac{\partial^4 w(x, y)}{\partial y^4} \right) - \rho h \omega^2 w(x, y) = 0 \quad (3.43)$$

where D denotes the bending stiffness, $w(x, y)$ is the displacement field, ρ is the material density and h is the thickness of the plate. The bending stiffness of the Kirchhoff plate is defined as

$$D = \frac{Eh^3}{12(1 - \nu^2)} \quad (3.44)$$

where E is Young's modulus and ν is Poisson's coefficient of the plate.

The general solution of the differential equation is of the form

$$w(x, y) = e^{k_x x} e^{k_y y} \quad (3.45)$$

where k_x and k_y are wavenumbers. Substituting (3.45) into (3.43) gives the characteristic equation of the differential equation

$$k_x^2 + k_y^2 = \pm \omega \sqrt{\frac{\rho h}{D}} \quad (3.46)$$

Kulla [43] concluded that it is possible to generate an infinite series of base solution in (k_x^2, k_y^2) plane. The solutions are generated by introducing k_x^2 and k_y^2 series

$$k_{xm}^2 = - \left(\frac{i\pi}{a} \right)^2, \quad m = 0, 1, 2, \dots \quad (3.47)$$

$$k_{ym}^2 = - \left(\frac{i\pi}{b} \right)^2, \quad m = 0, 1, 2, \dots \quad (3.48)$$

where a and b are half-length and half-width of the plate, respectively, Figure 3.30. The square root of (3.47) and (3.48) gives

$$k_{xm} = \pm i \left(\frac{i\pi}{a} \right) \quad (3.49)$$

$$k_{ym} = \pm i \left(\frac{i\pi}{b} \right) \quad (3.50)$$

where $i = \sqrt{-1}$. Inserting (3.49) and (3.50) into (3.45) leads to a conclusion that every term k_{xm}^2 represents a pair of functions in x direction, one symmetric and one antisymmetric [43]. Analogous conclusion is made for every k_{ym}^2 term concerning y direction. Therefore, every (k_{xm}^2, k_{ym}^2) pair represents four solutions of the differential equation (3.43). Every solution represents one of the following four symmetry cases:

- symmetric - symmetric (SS),
- antisymmetric - antisymmetric (AA),
- symmetric - antisymmetric (SA) and
- antisymmetric - symmetric (AS).

The deflection of the plate can be written as a superposition of the four symmetry cases:

$$w(x, y) = w_{SS}(x, y) + w_{AA}(x, y) + w_{SA}(x, y) + w_{AS}(x, y) \quad (3.51)$$

The letters in the subscript of the displacement field w in (3.51) denote the type of symmetry along y and x axis, respectively.

The detailed algorithm of derivation of the displacement field $w(x, y)$ is presented by Nefovska-Danilović [48]. This section analyses only double symmetry contribution, SS, since the loading function is axisymmetrical. The displacement field of the plate for the double symmetry case is given by

$$w_{SS}(x, y) = \sum_{m=0}^M {}^1W_{SS,m}(y) \cos \frac{m\pi x}{a} + \sum_{m=0}^M {}^2W_{SS,m}(x) \cos \frac{m\pi y}{b} \quad (3.52)$$

where ${}^1W_{SS,m}(y)$ and ${}^2W_{SS,m}(x)$ are even functions obtained by substituting Eq. (3.52) into Eq. (3.43) omitting the odd contributions of the solution

$${}^1W_{SS,m}(y) = C_m \cosh \beta_{1m}y + D_m \cos \beta_{2m}y \quad (3.53)$$

$${}^2W_{SS,m}(x) = A_m \cosh \alpha_{1m}x + B_m \cos \alpha_{2m}x \quad (3.54)$$

Coefficients A_m, B_m, C_m and D_m represents integration constants, while β_{im} and α_{im} are

$$\beta_{1m}^2 = \omega \sqrt{\frac{\rho h}{D}} + k_{xm}^2, \quad \beta_{2m}^2 = \omega \sqrt{\frac{\rho h}{D}} - k_{xm}^2, \quad k_{xm} = \frac{m\pi}{a} \quad (3.55)$$

$$\alpha_{1m}^2 = \omega \sqrt{\frac{\rho h}{D}} + k_{ym}^2, \quad \alpha_{2m}^2 = \omega \sqrt{\frac{\rho h}{D}} - k_{ym}^2, \quad k_{ym} = \frac{m\pi}{b} \quad (3.56)$$

Substituting Eqs (3.53) and (3.54) into Eq (3.52) gives

$$w_{SS}(x, y) = \sum_{m=0}^M (A_m f_{1m}(x, y) + B_m f_{2m}(x, y)) + \sum_{m=0}^M (C_m f_{3m}(x, y) + D_m f_{4m}(x, y)) \quad (3.57)$$

where

$$f_{1m}(x, y) = \cosh(\alpha_{1m}x) \cos\left(\frac{m\pi y}{b}\right) \quad (3.58)$$

$$f_{2m}(x, y) = \cos(\alpha_{2m}x) \cos\left(\frac{m\pi y}{b}\right) \quad (3.59)$$

$$f_{3m}(x, y) = \cosh(\beta_{1m}y) \cos\left(\frac{m\pi x}{a}\right) \quad (3.60)$$

$$f_{4m}(x, y) = \cos(\alpha_{2m}y) \cos\left(\frac{m\pi x}{a}\right) \quad (3.61)$$

Equation (3.52) could be written in matrix form as

$$\mathbf{u}(x, y) = \mathbf{\Phi}(x, y) \mathbf{C} \quad (3.62)$$

where $\mathbf{u}(x, y)$ is a vector of the displacement field of the plate, $\mathbf{\Phi}(x, y)$ is matrix of functions $f_m(x, y)$ and \mathbf{C} is the vector of integration constants [48]. According to the Kirchhoff's plate theory, the force vector $\mathbf{f}(x, y)$ is a function of derivatives of the displacement field $\mathbf{u}(x, y)$ and can be expressed as

$$\mathbf{f}(x, y) = \mathbf{G}(x, y) \mathbf{C} \quad (3.63)$$

where $\mathbf{G}(x, y)$ is a matrix of the derivatives of the components of matrix $\mathbf{\Phi}(x, y)$ [48].

Let s be a spatial coordinate and $B(s)$ a function that defines the boundary of a plate. In the case of the rectangular plate shown in Figure 3.30, $B(s)$ is defined as following:

$$B(s) = \begin{cases} y|y \in [-b, b] \text{ for } x = a \text{ and } x = -a \\ x|x \in [-a, a] \text{ for } y = b \text{ and } y = -b \end{cases} \quad (3.64)$$

The dynamic stiffness matrix of the plate is derived as a relation between the displacements along the boundary $\mathbf{q}(s)$ and the forces along the boundary $\mathbf{Q}(s)$.

The relations between boundary displacement $\mathbf{q}(s)$ force vectors $\mathbf{Q}(s)$ and vector of integration constants \mathbf{C} are derived in the following form:

$$\mathbf{q}(s) = \mathbf{\Phi}_b(s) \mathbf{C} \quad (3.65)$$

$$\mathbf{Q}(s) = \mathbf{G}_b(s) \mathbf{C} \quad (3.66)$$

Matrices $\mathbf{\Phi}_b(s)$ and $\mathbf{G}_b(s)$ could not be found directly since $\mathbf{q}(s)$ and $\mathbf{Q}(s)$ are continuous functions of the spatial coordinate s . This problem is solved by using the Projection method [65]. Elements $q_n(s)$ and $Q_n(s)$ of vectors $\mathbf{q}(s)$ and $\mathbf{Q}(s)$ are projected on the boundary using a set of projection functions $h(s)$ [48]

$$q_n(s) = \sum_{m=1}^M \left(\int_{B(s)} q_n(s) h_m(s) ds \right) h_m(s), \quad n = 1, 2, \dots, N \quad (3.67)$$

$$Q_n(s) = \sum_{m=1}^M \left(\int_{B(s)} Q_n(s) h_m(s) ds \right) h_m(s), \quad n = 1, 2, \dots, N \quad (3.68)$$

If $h(s)$ are trigonometric functions, the projection is equivalent to the Fourier series.

The projections are collected into two $(1 \times NM)$ vectors

$$\bar{\bar{\mathbf{q}}} = \left[\int_{B(s)} q_n(s) h_m(s) ds \right], \quad n = 1, 2, \dots, N, \quad m = 1, 2, \dots, M \quad (3.69)$$

$$\bar{\bar{\mathbf{Q}}} = \left[\int_{B(s)} Q_n(s) h_m(s) ds \right], \quad n = 1, 2, \dots, N, \quad m = 1, 2, \dots, M \quad (3.70)$$

The elements of vectors $\bar{\bar{\mathbf{q}}}$ and $\bar{\bar{\mathbf{Q}}}$ represent the coefficients of the Fourier series of $\mathbf{q}(s)$ and $\mathbf{Q}(s)$. Using (3.69), (3.70), (3.65) and (3.66) one can obtain the relation between the projections $\bar{\bar{\mathbf{q}}}$ and $\bar{\bar{\mathbf{Q}}}$ and the integration constants \mathbf{C} . The relation

matrices are denoted with $\bar{\bar{\mathbf{D}}}$ and $\bar{\bar{\mathbf{F}}}$

$$\bar{\bar{\mathbf{q}}} = \bar{\bar{\mathbf{D}}}\mathbf{C} \quad (3.71)$$

$$\bar{\bar{\mathbf{Q}}} = \bar{\bar{\mathbf{F}}}\mathbf{C} \quad (3.72)$$

The relation between $\bar{\bar{\mathbf{q}}}$ and $\bar{\bar{\mathbf{Q}}}$ is derived from Eq. (3.71) and Eq. (3.72), eliminating \mathbf{C}

$$\bar{\bar{\mathbf{Q}}} = \bar{\bar{\mathbf{F}}}\bar{\bar{\mathbf{D}}}^{-1}\bar{\bar{\mathbf{q}}} = \mathbf{K}_{\mathbf{D}}\bar{\bar{\mathbf{q}}} \quad (3.73)$$

where $\mathbf{K}_{\mathbf{D}}$ is the dynamic stiffness matrix of the plate

$$\mathbf{K}_{\mathbf{D}} = \bar{\bar{\mathbf{F}}}\bar{\bar{\mathbf{D}}}^{-1} \quad (3.74)$$

A detailed analysis of obtaining matrix $\mathbf{K}_{\mathbf{D}}$ is given in the literature [48].

Natural frequencies of the plate are calculated using the condition that

$$\det \mathbf{K}_{\mathbf{D}} = 0 \quad (3.75)$$

Equation (3.75) cannot be solved analytically. It is solved using Wittrick-Williams algorithm [46]. The algorithm counts the number of natural frequencies from zero frequency up to the chosen one. If the increase of the chosen frequency by a small amount increases the number of natural frequencies by one, the chosen frequency is declared as the natural frequency.

For every natural frequency a family of displacement fields can be obtained. By proclaiming one of the displacement along the boundary a unit displacement, the family of displacement fields is reduced to a single displacement field - mode shape. This can lead to error, the displacement that should be zero is adopted for unit

displacement. This problem can be overcome using Wittrick-Williams algorithm. The detailed explanation of the solution could be found in the literature [46].

3.3.2.2 Dynamic stiffness matrix of the system

If we assume that the foundation is Kirchhoff plate, the differential equation of the steady state problem (ω is omitted) is the following

$$D \left(\frac{\partial^4 w(x, y)}{\partial x^4} + 2 \frac{\partial^4 w(x, y)}{\partial x^2 \partial y^2} + \frac{\partial^4 w(x, y)}{\partial y^4} \right) - \rho h \omega^2 w(x, y) = p(x, y) - q(x, y) \quad (3.76)$$

where $p(x, y)$ is the active and $q(x, y)$ is the reactive plate load function.

Analogous to the 2D problem, we assume that the displacement field, the active load and the reactive load can be expanded in a series of free vibration modes as follows

$$\begin{aligned} w(x, y) &= \sum_{n=0}^N Y_n \phi_n(x, y) \\ p(x, y) &= \sum_{n=0}^N P_n \phi_n(x, y) \\ q(x, y) &= \sum_{n=0}^N Q_n \phi_n(x, y) \end{aligned} \quad (3.77)$$

where $\phi_n(x, y)$ represents the orthonormalized mode shape of the foundation for the n^{th} mode and Y_n , P_n and Q_n are modal coefficients

$$\begin{aligned} Y_n &= \int_{x=0}^B \int_{y=0}^L w(x, y) \phi_n(x, y) \, dx dy \\ P_n &= \int_{x=0}^B \int_{y=0}^L p(x, y) \phi_n(x, y) \, dx dy \\ Q_n &= \int_{x=0}^B \int_{y=0}^L q(x, y) \phi_n(x, y) \, dx dy \end{aligned} \quad (3.78)$$

The mode shapes φ_n^* are orthonormalized as follows

$$\phi_n = \frac{\phi_n^*}{\int_{x=0}^B \int_{y=0}^L |\phi_n^*|^2 dx} \quad \text{so that} \quad \int_{x=0}^B \int_{y=0}^L \phi_n(x, y) \phi_m(x, y) dx = \begin{cases} 1, & m = n \\ 0, & m \neq n \end{cases} \quad (3.79)$$

Substituting (3.77) into (3.76) gives

$$\sum_{n=0}^N (D(k_x^4 + 2k_x^2 k_y^2 + k_y^4) - \rho h \omega^2) \phi_n(x, y) Y_n = \sum_{n=0}^N \phi_n(x, y) P_n - \sum_{n=0}^N \phi_n(x, y) Q_n \quad (3.80)$$

Multiplying Eq. (3.80) with each of N mode shapes and integrating over the domain $x \in [0, B]$ and $y \in [0, L]$, the system of N algebraic equations is obtained. The system could be written in matrix form as follows

$$D [\mathbf{k}^4] - \rho h \omega^2 [\mathbf{I}] \{\mathbf{Y}\} = \{\mathbf{P}\} - \{\mathbf{Q}\} \quad (3.81)$$

where $\{\mathbf{Y}\}$, $\{\mathbf{P}\}$ and $\{\mathbf{Q}\}$ are coefficient vectors of modal displacement, load and soil reaction, respectively, $[\mathbf{I}]$ is identity matrix and $[\mathbf{k}^4]$ is the pure bending wavemode wavenumber matrix of the plate

$$[\mathbf{k}^4] = \begin{bmatrix} 0 & 0 & \cdots & 0 \\ 0 & \rho h \omega_{f1}^2 & & \vdots \\ \vdots & & \ddots & 0 \\ 0 & \cdots & 0 & \rho h \omega_{fN}^2 \end{bmatrix} \quad (3.82)$$

In Eq. (3.82) $\omega_{f1}, \omega_{f2}, \dots, \omega_{fN}$ are natural frequencies of the foundation.

Relation between displacements and soil reaction coefficient vectors can be defined as follows

$$[\mathbf{K}_s] \{\mathbf{Y}\} = \{\mathbf{Q}\} \quad (3.83)$$

where $[\mathbf{K}_s]$ is the modal impedance matrix of the soil.

Using Eq. (3.83), Eq. (3.81) could be written as

$$\left\{ D [\mathbf{k}^4] - m_f \omega^2 [\mathbf{I}] + [\mathbf{K}_s] \right\} \{\mathbf{Y}\} = \{\mathbf{P}\} \quad (3.84)$$

The modal impedance matrix of the soil $[\mathbf{K}_s]$ is obtained as inverse matrix of the modal compliance matrix of the soil $[\mathbf{F}_s]$. The steps for obtaining the modal soil compliance matrix elements are the following:

1. Applying a unit modal load of the n^{th} mode on the soil, $q_n(x, y)$, that leads $Q_n = 1$
2. Transforming the modal load into wavenumber domain $\tilde{q}_n(k_x, k_y)$ using two-dimensional FT.
3. Solving the soil displacement field in wavenumber domain $\tilde{w}_n(k_x, k_y)$ with the help of ITM, where the accuracy of the results depends on the discretization in the (k_x, k_y) domain
4. Transforming the soil displacement field into the spatial domain $w_n(x, y)$
5. Obtaining elements of the modal soil compliance matrix $F_{s,mn}$ as follows

$$F_{s,mn} = \int_{x=0}^B \int_{y=0}^L w_n(x, y) \phi_m(x, y) dx dy \quad (3.85)$$

Computer program based on this formulation are developed in MATLAB [53]. The code is consisted of subroutines for

- obtaining the solution of the halfspace using ITM,
- obtaining the natural frequencies and the mode shapes of the foundation using SEM and

- obtaining the solution of the coupled system soil-foundation using the proposed modal superposition method.

The results of the analysis will be presented in terms of compliance, in order to verify the response of the system with the results from the literature.

3.3.3 Numerical examples

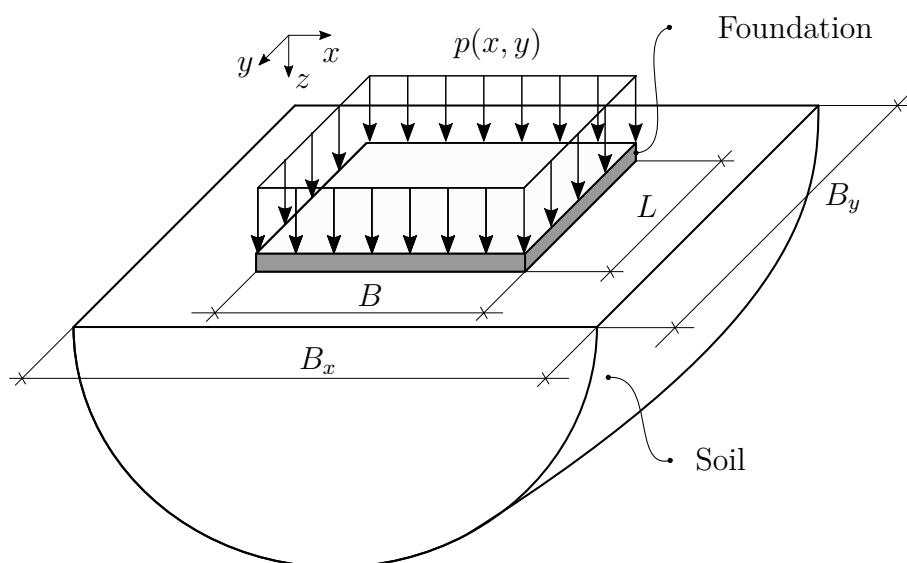


Figure 3.31: Square massless surface foundation excited by a uniformly distributed load

This section presents vertical displacements and contact stresses of a square massless surface foundation excited by a uniformly distributed load, presented in Figure 3.31.

The numerical model considers the foundation of size $B \times L = 2 \text{ m} \times 2 \text{ m}$ and the soil of size $B_x \times B_y = 40 \text{ m} \times 40 \text{ m}$. The domain is discretized using the discretization units $dx = 0.1 \text{ m}$ and $dy = 0.1 \text{ m}$. The damping mechanism is introduced by using a complex modulus with the damping coefficient $\xi = 1 \%$. The analysis is performed taking into account eight shape modes of the foundation shown in Figure 3.32. Since the problem is axisymmetrical, only axisymmetrical mode shapes are used.

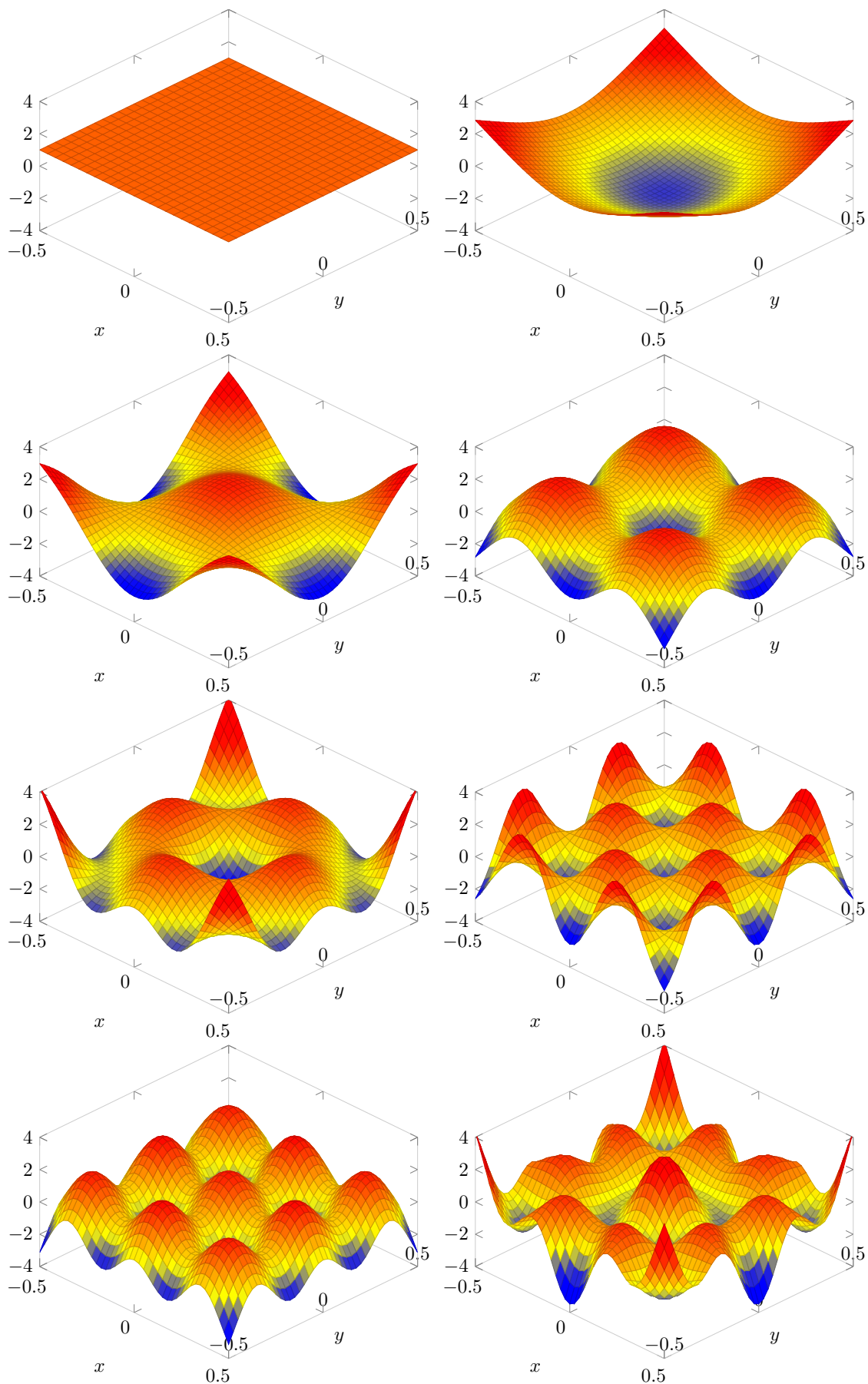


Figure 3.32: Shape modes

3.3.3.1 Compliance functions

The vertical displacements fields of the foundation obtained using the proposed method are compared with the results obtained by Whittaker and Christiano (W&C) [17]. They have modeled the foundation using thin plate finite elements. The boundary value problem of the subgrade is solved using the Green's function. They observed a uniformly loaded plate displacements in three points: center (1), edge midway (2) and corner (3), Figure 3.33. The results are presented in a dimensionless

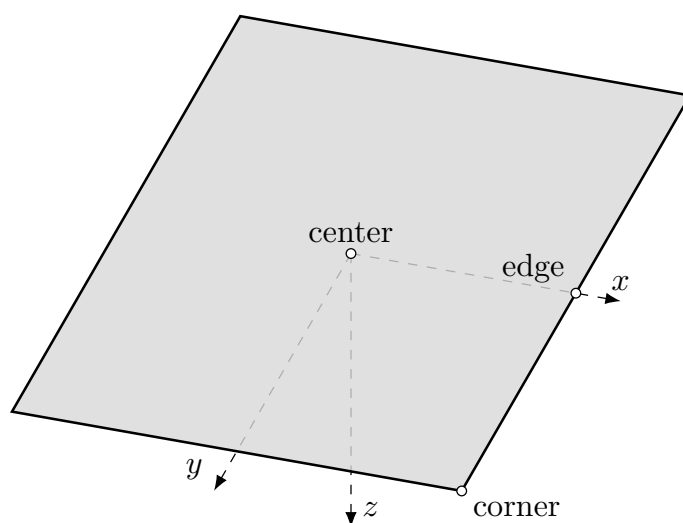


Figure 3.33: Characteristic points of the flexible square foundation resting on the soil

form, $\Delta_i(a_0)$, where Δ_i is the dimensionless vertical displacement at the point i

$$\Delta_i = \frac{wG_s B}{(1 - \nu_s) \sum F_{ext}} \quad (3.86)$$

and a_0 is the dimensionless frequency

$$a_0 = \frac{\omega B}{c_s} \quad (3.87)$$

In Eq (3.86) w is the displacement, G_s is the shear modulus of the soil, ν_s is Poisson's coefficient of the soil and $\sum F_{ext}$ is the resultant of the external force in z direction.

The results are obtained for different stiffness ratios K introduced by Whittaker and Christiano

$$K = \frac{Eh^3(1 - \nu_s^2)}{12(1 - \nu^2)G_s B^3}, \quad (3.88)$$

where E is Young's modulus of the plate and ν is Poisson's coefficient of the plate.

Spatial distribution of vertical load over the foundation surface affects the responses at the observed points. This is analyzed in detail by Riggs and Waas [66], Spyarakos and Beskos [22] and Chen and Hou [16]. Two different types of load distribution are considered:

- a uniformly distributed load, $p(x, y) = p = 1/(BL)$ and
- a modified uniformly distributed load, $p^*(x, y)$.

The load types are presented in Figure 3.34. The active load $p^*(x, y)$ differs from the active load $p(x, y)$ along the edges of the foundation where the amplitude of $p^*(x, y)$ is $p/2$ and at the corners of the foundation where the amplitude of $p^*(x, y)$ is $p/4$. The idea behind the definition of $p^*(x, y)$ comes from the formulation of the problem written by Whittaker and Christiano [17], where the subgrade compliances and impedances are concentrated in discrete points of the domain with the amplitude calculated considering the associated area of each point. That means that inner nodes have the largest amplitude p , the edge nodes $p/2$ and the corner nodes $p/4$.

Figure 3.35 shows the real and imaginary part of the compliance functions for the stiffness ratio $K = 0$ obtained for different types of active load together with the results from the literature [17]. The results obtained using the active load $p^*(x, y)$ show better agreement with the results from the literature, especially regarding the corner point.

Maravas et al. [62] made a comparison with the results obtained by Whittaker and Christiano [17]. In their paper, the foundation-soil stiffness ratio K is defined by

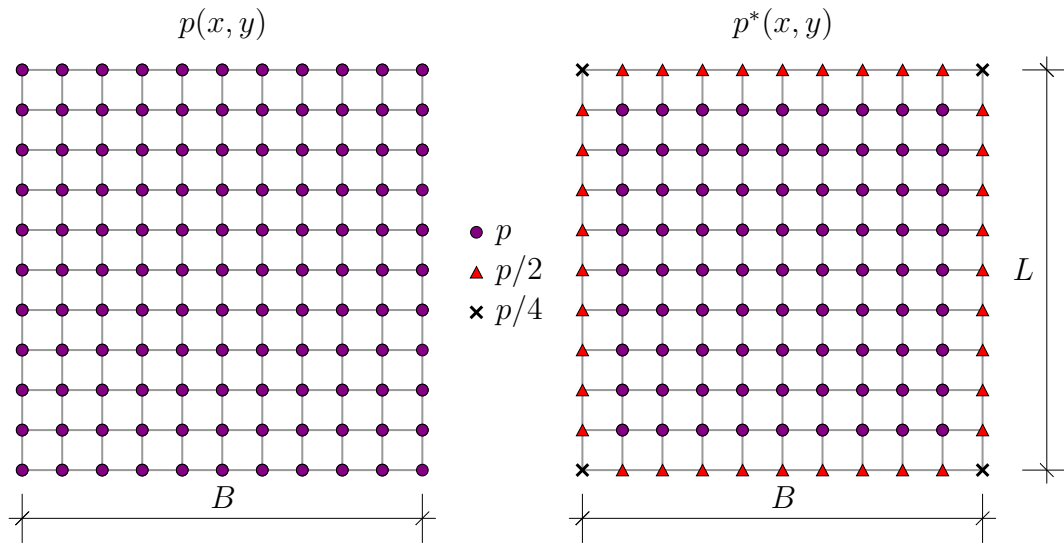


Figure 3.34: Active load type cases

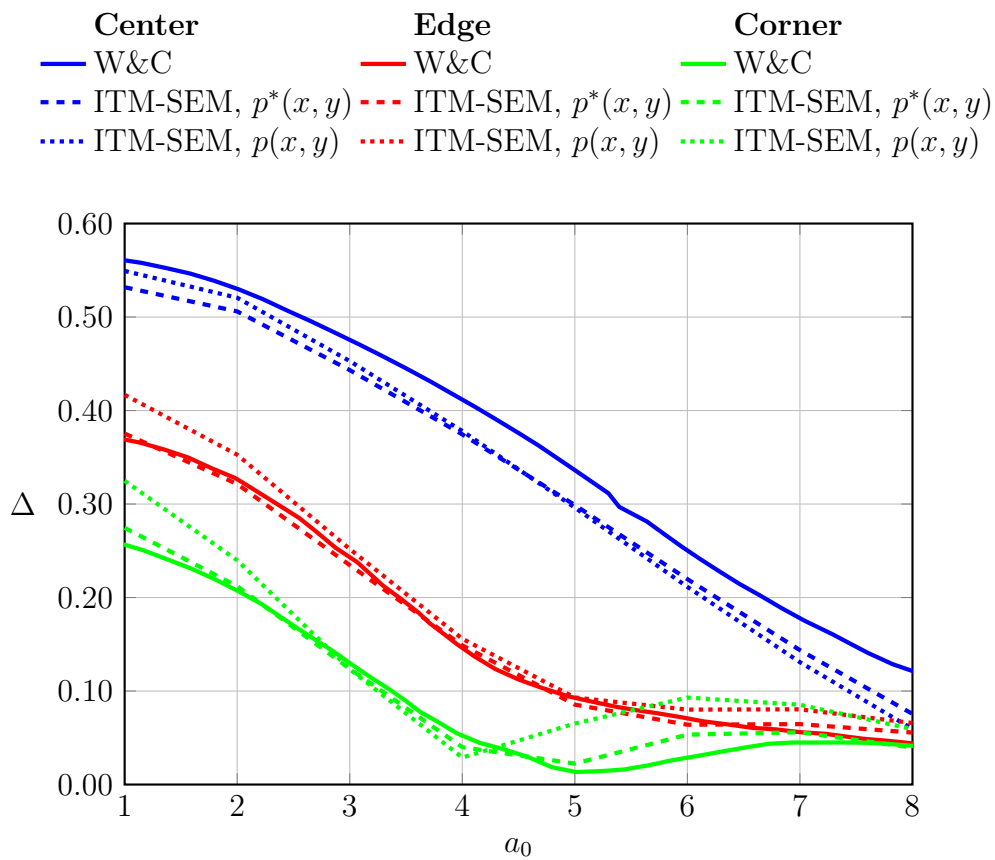


Figure 3.35: Compliance functions for different load types, $K = 0$

using the half-width of the foundation, $B/2$

$$K^* = \frac{Eh^3(1 - \nu_s^2)}{12(1 - \nu^2)G_s \left(\frac{B}{2}\right)^3}. \quad (3.89)$$

The relation between K and K^* could be interpreted as following: the stiffness of the foundation of the SFI model for which $K = 0.004$ is eight times greater than the stiffness of the foundation of the SFI model for which $K^* = 0.004$.

Using the proposed method, the analysis is performed for $K = 0, 0.004, 0.06, 3.3$ and for $K^* = 0, 0.004, 0.06, \text{ and } 3.3$. The results of the analyses involving the ratio K are presented in Figures 3.36-3.39. The results of the analyses involving the ratio K^* are presented in Figures 3.40-3.43.

The foundation stiffness has no influence on the results of the analysis in the case of $K = 0$ and $K^* = 0$. In other words, if $K = 0$ or $K^* = 0$ the results represent the response of the halfspace surface subjected to the load p^* . For $K^* = 3.3$, the foundation is already acting like a rigid plate. Therefore, the results are the same as if the foundation is eight times stiffer, $K = 3.3$. However, by comparing the response of the soil-foundation system in the case of $K = 0.004, 0.06$ and $K^* = 0.004, 0.06$, it is noticeable that the results obtained for K^* corresponds to the W&C results better. Therefore, the results obtained for K^* and presented in Figures 3.40-3.43 are used for the further analysis.

Although the results obtained by the proposed method are in a good agreement with the results obtained by W&C, there are few differences that should be mentioned. In the following discussion, the comparisons of the results are expressed in terms of the compliance amplitudes obtained using the proposed method with regard to the compliance amplitudes obtained by W&C. In the frequency range $0 < a_0 < 4$, for $K^* = 0$, the proposed method gives lower amplitudes of the compliance for the center point of the foundation. For $K^* > 0$, the compliance amplitudes of the center

point of the foundation tend to be higher, as opposed to the compliance amplitudes of the edge and corner point of the foundation. The differences between the results increase with the increase of K^* and a_0 . In the frequency range $a_0 > 4$, the highest discrepancies are observed at the corner of the foundation. This is the point of significant stress concentration that is very difficult to model properly and it should be analyzed in detail in future research. W&C did not provide the compliance amplitude of the edge point for $K^* = 0.06$. However, it is interesting to notice that for $K^* = 0.06$ the center of the foundation modeled by W&C behaves like the edge of the foundation modeled using the proposed method.

In general, with an increase of the relative stiffness K^* , the displacements of the foundation become less spatially dependent.

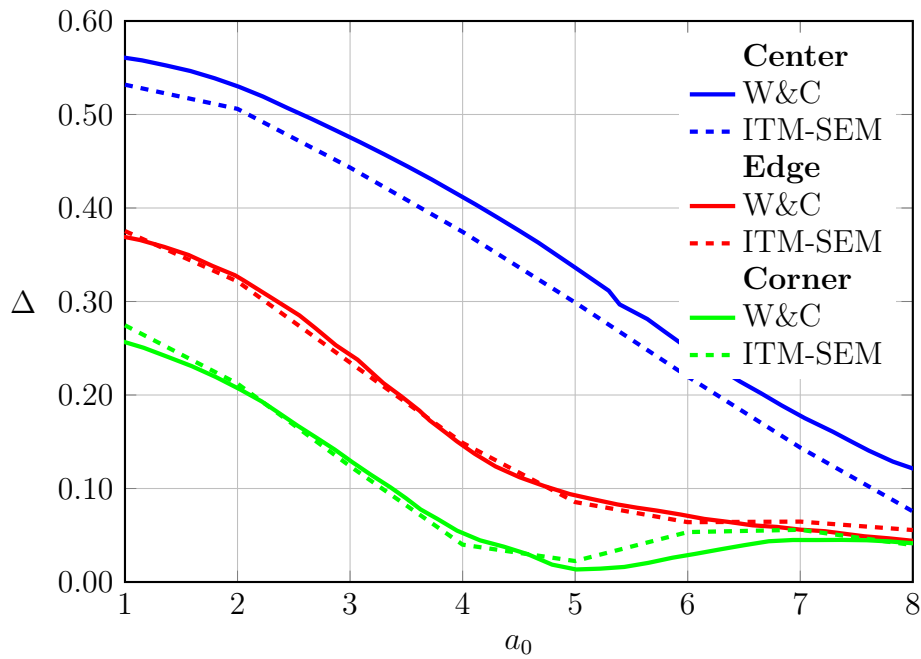


Figure 3.36: W&C - ITM-SEM comparison of the displacements of the foundation at the characteristic points, $K = 0$

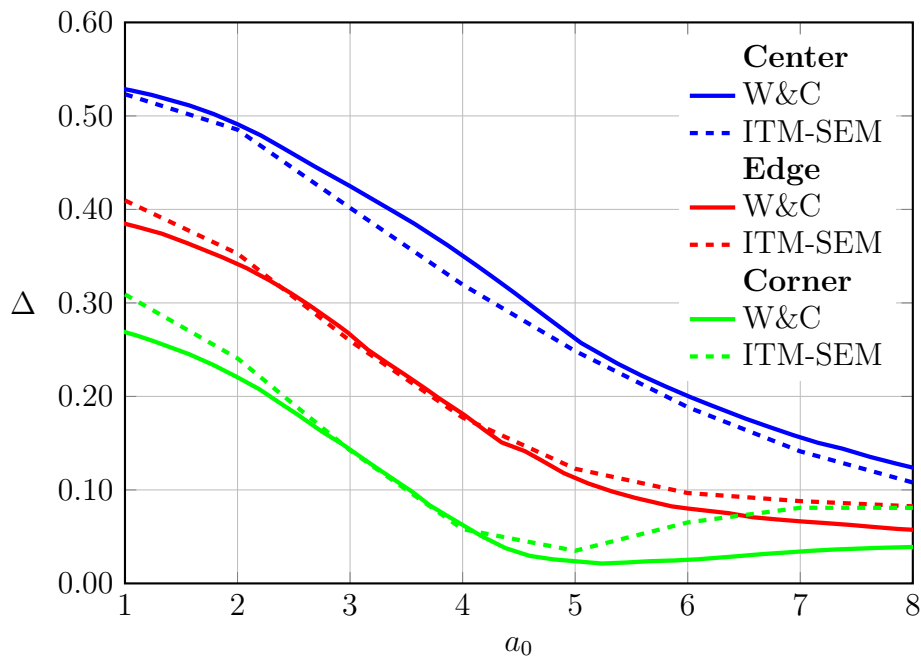


Figure 3.37: W&C - ITM-SEM comparison of the displacements of the foundation at the characteristic points, $K = 0.004$

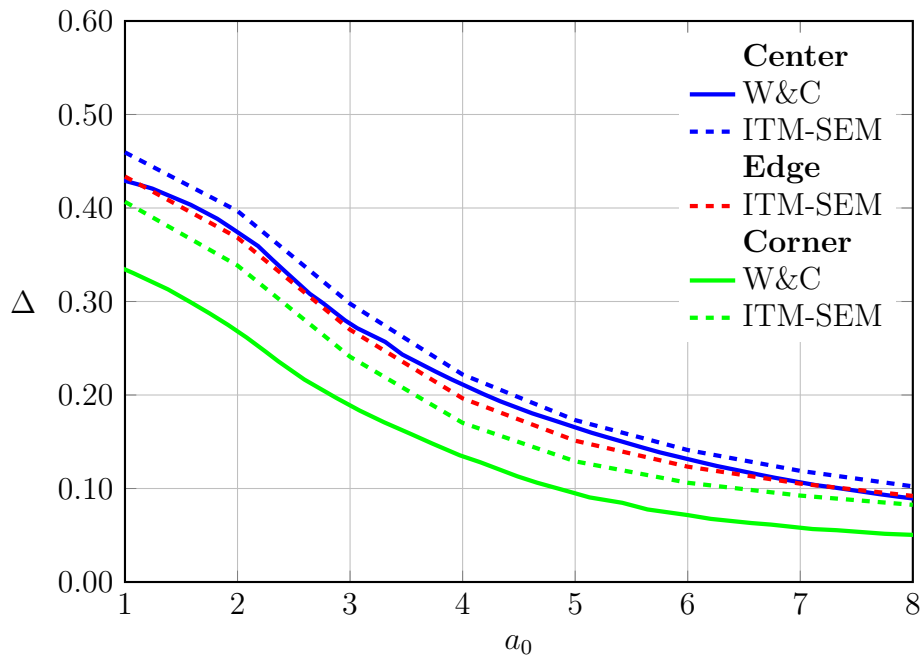


Figure 3.38: W&C - ITM-SEM comparison of the displacements of the foundation at the characteristic points, $K = 0.06$

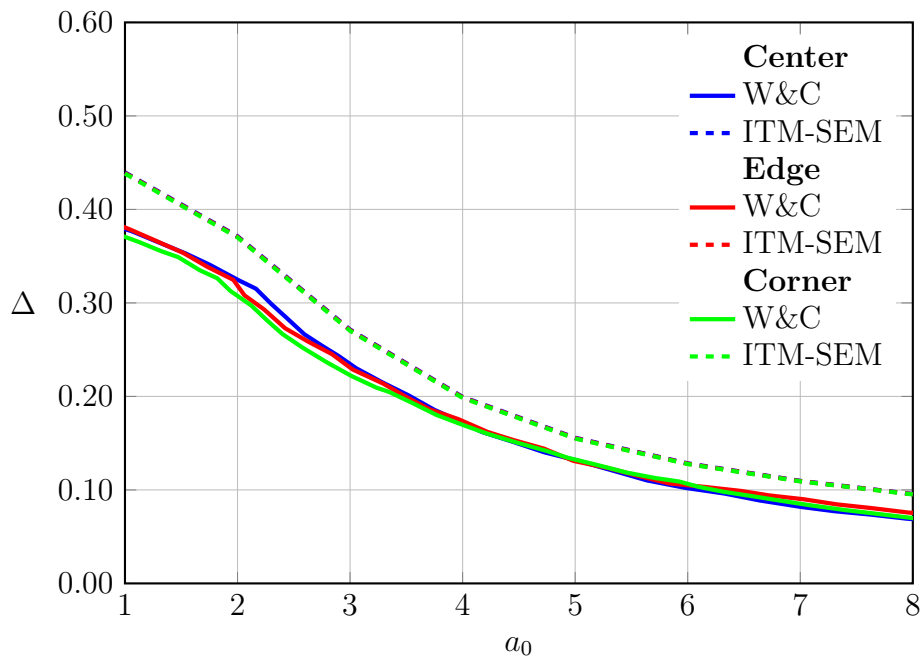


Figure 3.39: W&C - ITM-SEM comparison of the displacements of the foundation at the characteristic points, $K = 3.3$

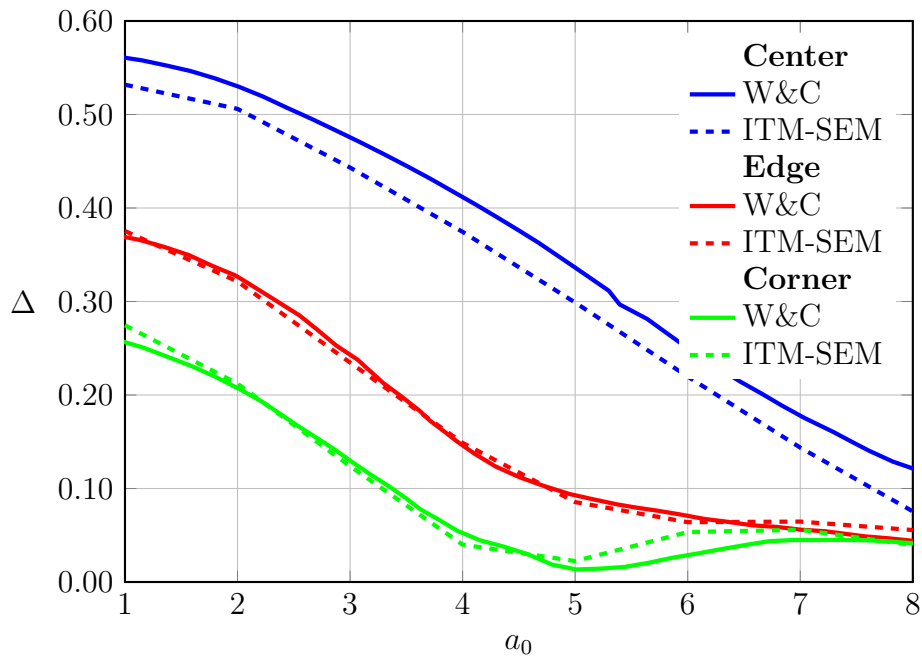


Figure 3.40: W&C - ITM-SEM comparison of the displacements of the characteristic points of the foundation, $K^* = 0$

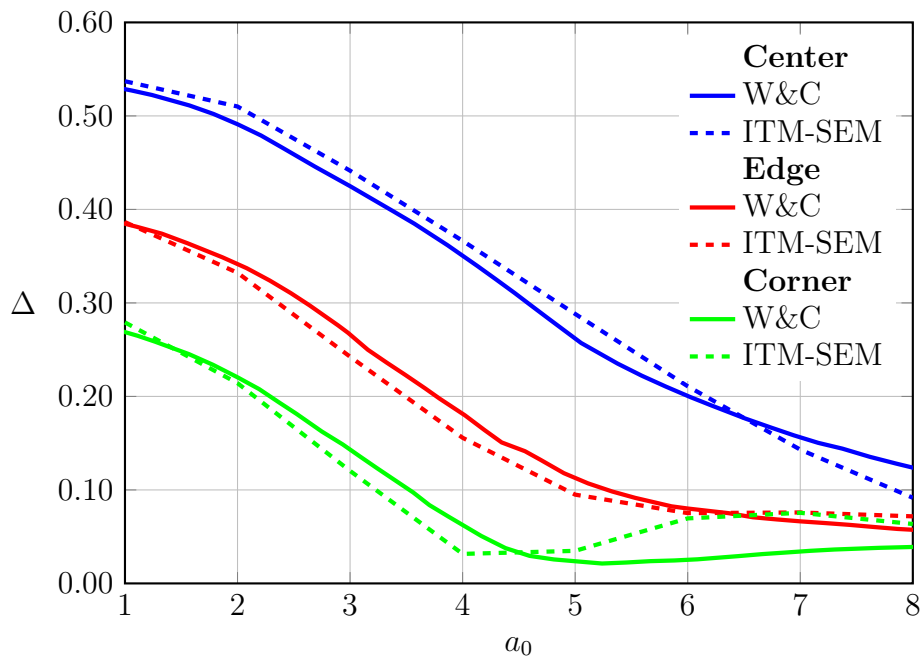


Figure 3.41: W&C - ITM-SEM comparison of the displacements of the foundation at the characteristic points, $K^* = 0.004$

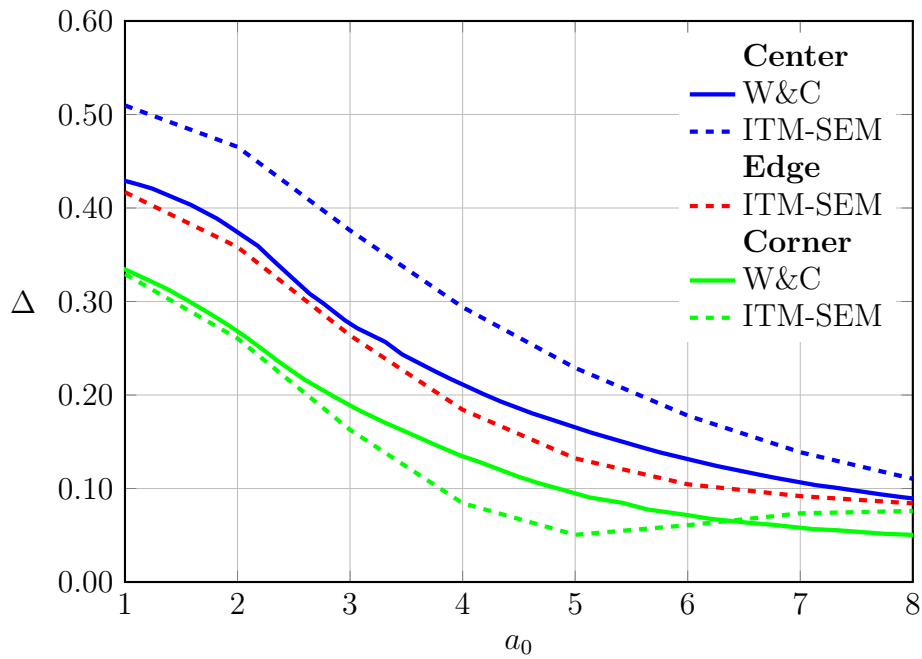


Figure 3.42: W&C - ITM-SEM comparison of the displacements of the characteristic points of the foundation, $K^* = 0.06$

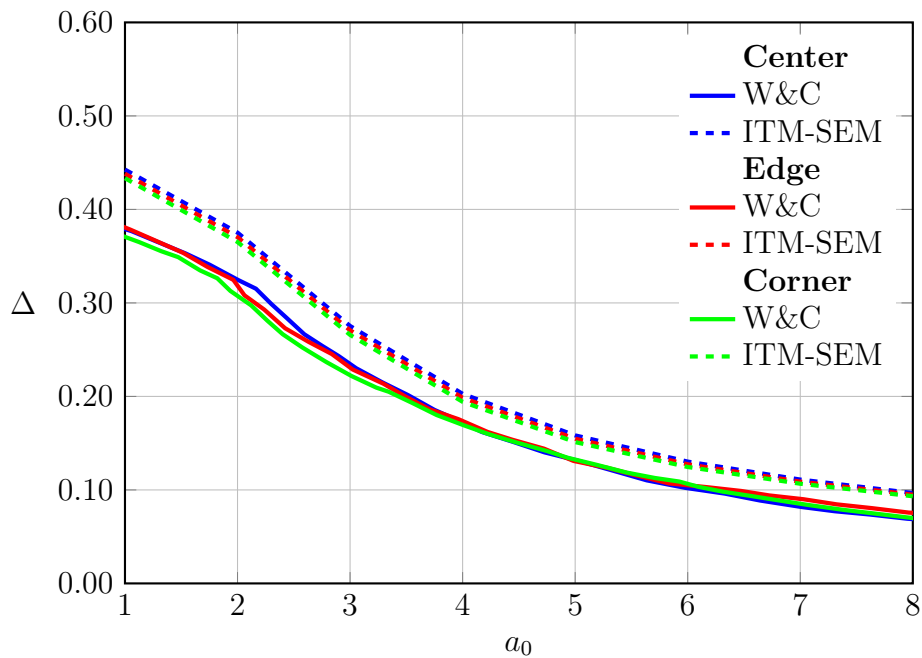


Figure 3.43: W&C - ITM-SEM comparison of the displacements of the characteristic points of the foundation, $K^* = 3.3$

For further verification, the amplitudes of the compliance function calculated by Whittaker & Christiano [17], and obtained using the proposed method for the case of $K^* = 3.3$, are compared with the amplitudes of the compliance function of rigid foundation obtained by Wong [60]. Wong obtained the response of the soil-foundation system by solving the boundary integral problem using the Green's function. Figure 3.44 shows the comparison. The trend of all the lines is similar. However, the compliance amplitudes in the case of W&C analysis are the lowest over the whole observed frequency range. The compliance amplitudes obtained using the proposed method match up to the displacements obtained by Wong, except for $a_0 < 3$ where they become significantly higher.

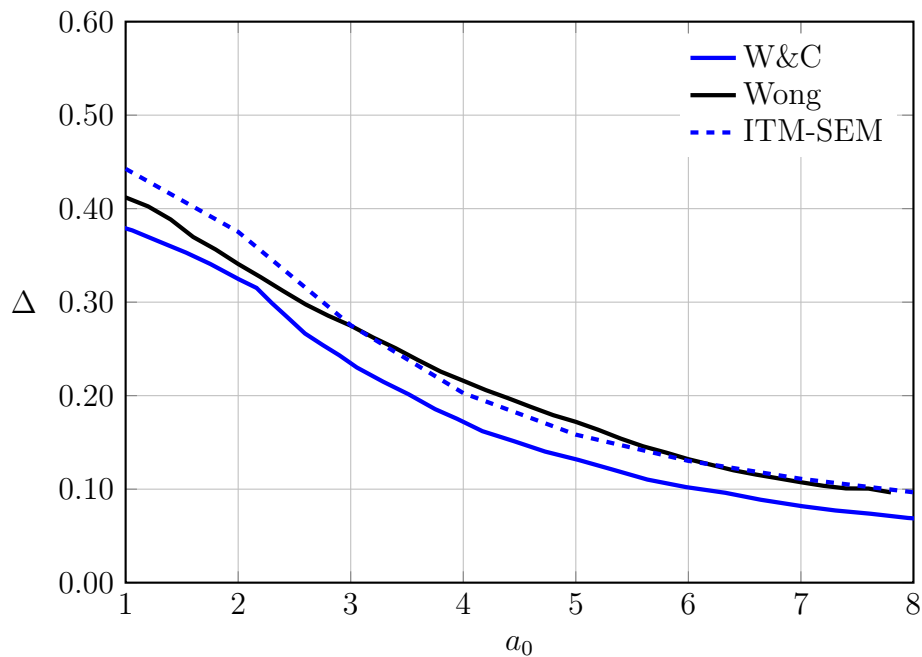


Figure 3.44: W&C - Wong - ITM-SEM comparison, $K^* = 3.3$

3.3.3.2 Displacement field

In this chapter, the displacement field of the square flexible foundation is presented for different values of a_0 and K^* . Since the displacement field is axisymmetrical the results are presented for one quarter of the foundation along the line between the edge point and the center point. The response of the system is obtained for $a_0 = 2.5, 5, 10$ and for different stiffness ratios $K^* = 0, 0.004, 0.06, 3.3$. The results are compared with the results presented by W&C [17]. The real and the imaginary part of the displacement field are shown on Figures 3.45-3.47. The dashed lines denote the results obtained using the proposed method, while the results from the literature are denoted by the solid lines.

The values of the real and the imaginary part of the displacement field obtained by using the proposed method are generally lower than the amplitudes obtained by W&C except in the case of the rigid foundation $K^* = 3.3$ for the frequency $a_0 \geq 5$. The difference between the displacements fields obtained for two stiffness ratios $K^* = 0$ and $K^* = 0.004$ are more pronounced in the results obtained by W&C than in the solution obtained using the ITM-SEM coupling. The real parts of the displacement field shows that the distribution along the center-edge line is almost independent of the stiffness ratio K^* for high frequencies, $a_0 \geq 5$. The imaginary part reaches the maxima at the center of the foundation for $K^* \leq 0.06$, regardless of the frequency.

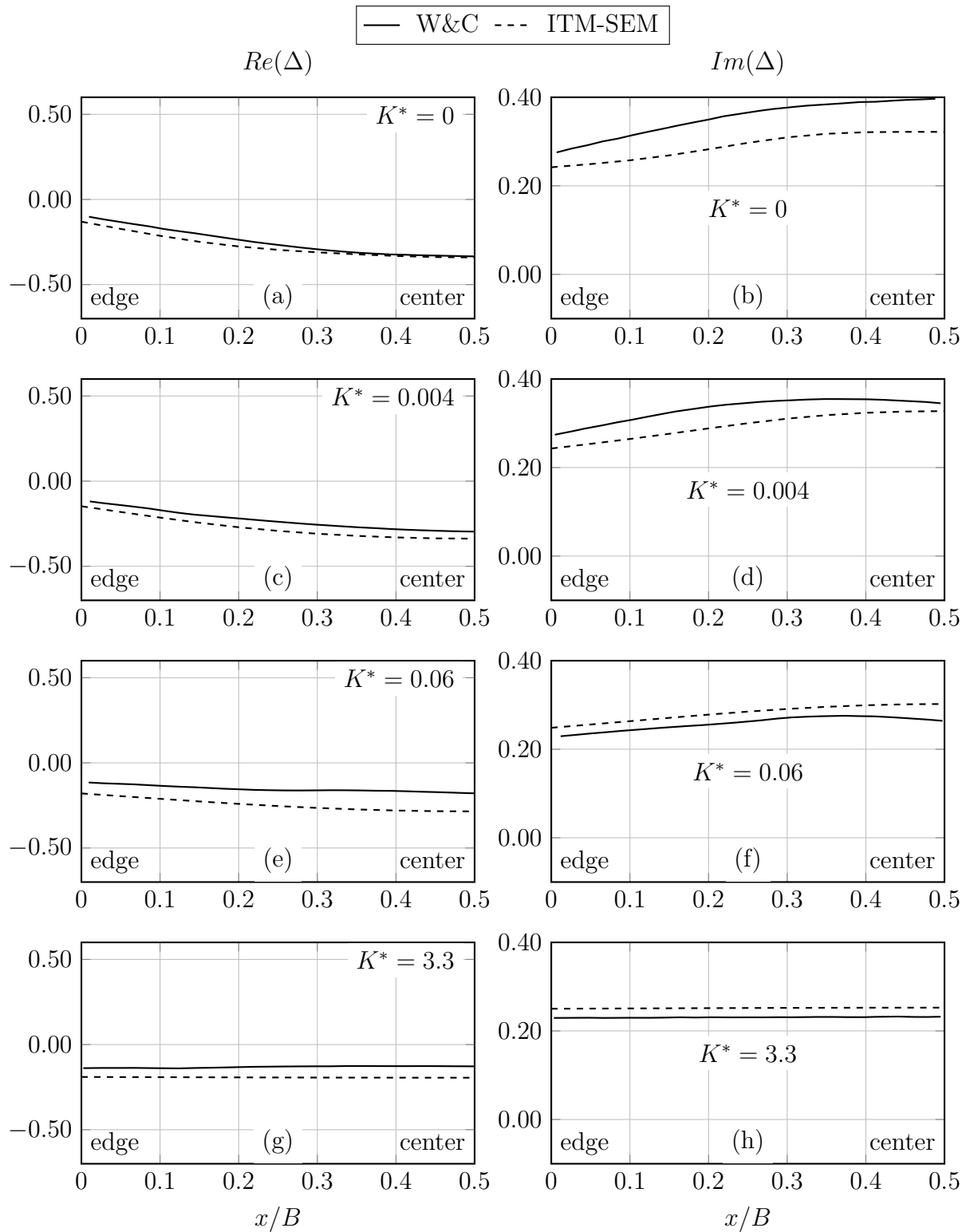


Figure 3.45: Displacement profile, $a_0 = 2.5$

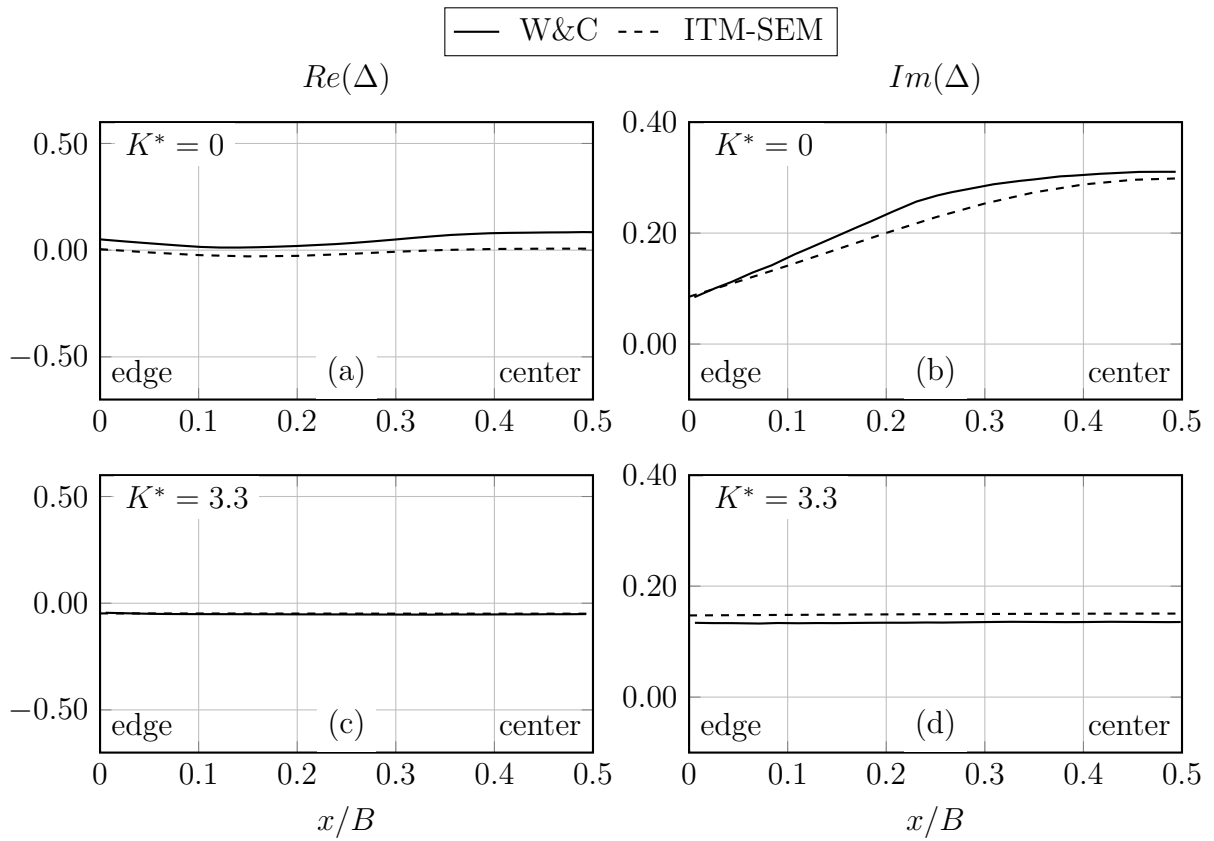


Figure 3.46: Displacement profile, $a_0 = 5$

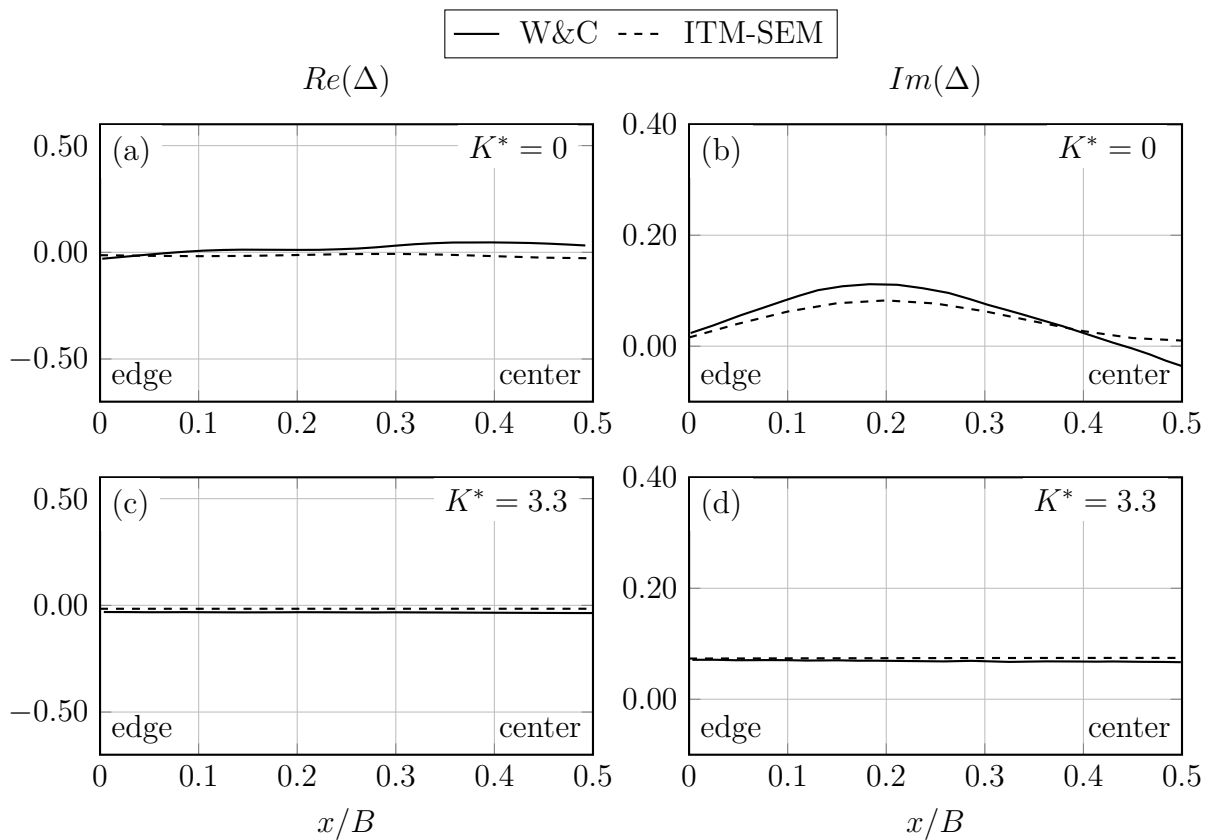


Figure 3.47: Displacement profile, $a_0 = 10$

3.3.3.3 Contact stress

The numerical model introduced in Section 3.3.3.2 is used for the analysis of the contact stress field between the foundation and the soil. The obtained results are presented in form of dimensionless stress

$$\bar{\sigma} = \frac{\sigma BL}{\sum F_{ext}} \quad (3.90)$$

The contact stress fields are obtained for dimensionless frequency $a_0 = 2.5$, and 5 and foundation-soil stiffness ratio $K^* = 0.0007, 0.004, 0.06$ and 3.3. The real and the imaginary parts of the contact stress field are presented in Figures 3.48-3.51 together with the results obtained by Whittaker & Christiano [17]. The dashed lines denote the results obtained using the proposed method, while the results from the literature are denoted by the solid lines.

Even a small plate stiffness leads to a concentration of the contact stress at the edges. The concentration zone is considerably narrow for the coarse discretization used in the proposed numerical model. However, a finer discretization would require a significant computational effort and more powerful hardware. Mohammadi and Karabalis [64] have tried to solve this problem by introducing the adaptive discretization scheme to their numerical model consisted of boundary elements. The scheme considers a non-uniform element discretization. It gives very good results for low frequencies, but it is incapable of producing good results at high frequencies. Implementation of the adaptive discretization scheme in the proposed method would require usage of Non-Uniform Discrete Fourier Transformation. It is a task that is out of the scope of this dissertation, but it will be investigated in future research.

The discrepancies between the obtained contact stresses and the results from the literature are more pronounced for higher frequencies and for stiffer plate, indicating

a great influence of the plate stiffness on the response. It might seem that in the case of considerably small values of K^* , there is a decrease of the contact stress $\bar{\sigma}$ along the edges of the foundation obtained using the proposed method ($\bar{\sigma} < 1$). However, the dimensionless contact stress along the edges should be compared to $\bar{\sigma} = 0.5$, concerning the active load pattern p^* that assumes the reduction of the loading force along the edges by half, Figure 3.34.

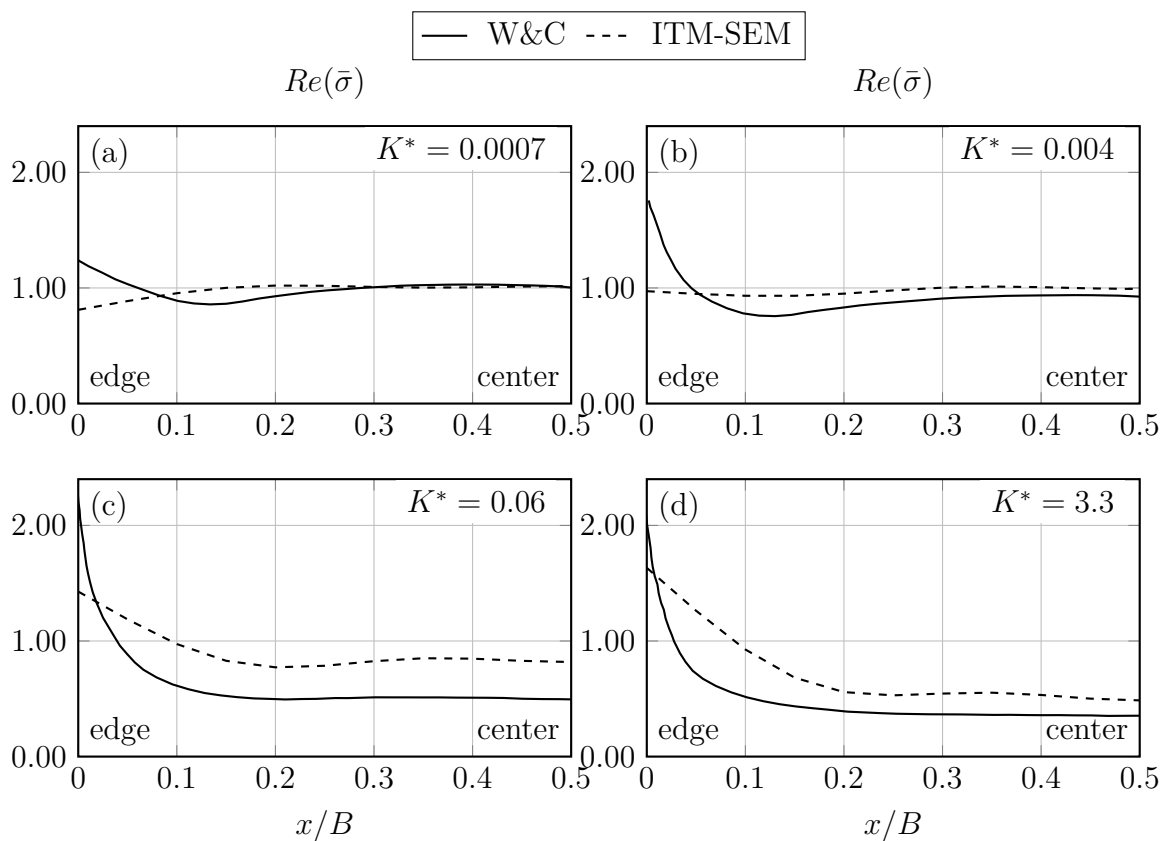


Figure 3.48: Contact stress, real part, $a_0 = 2.5$

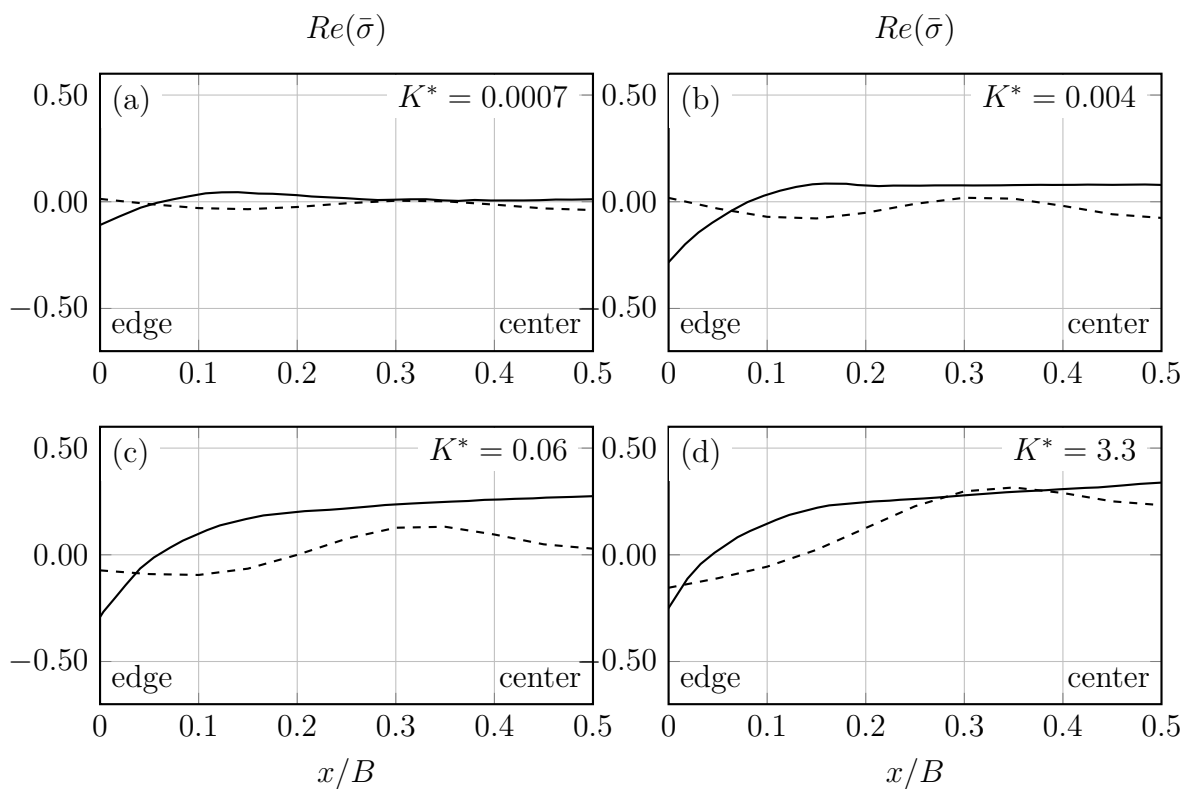


Figure 3.49: Contact stress, imaginary part, $a_0 = 2.5$

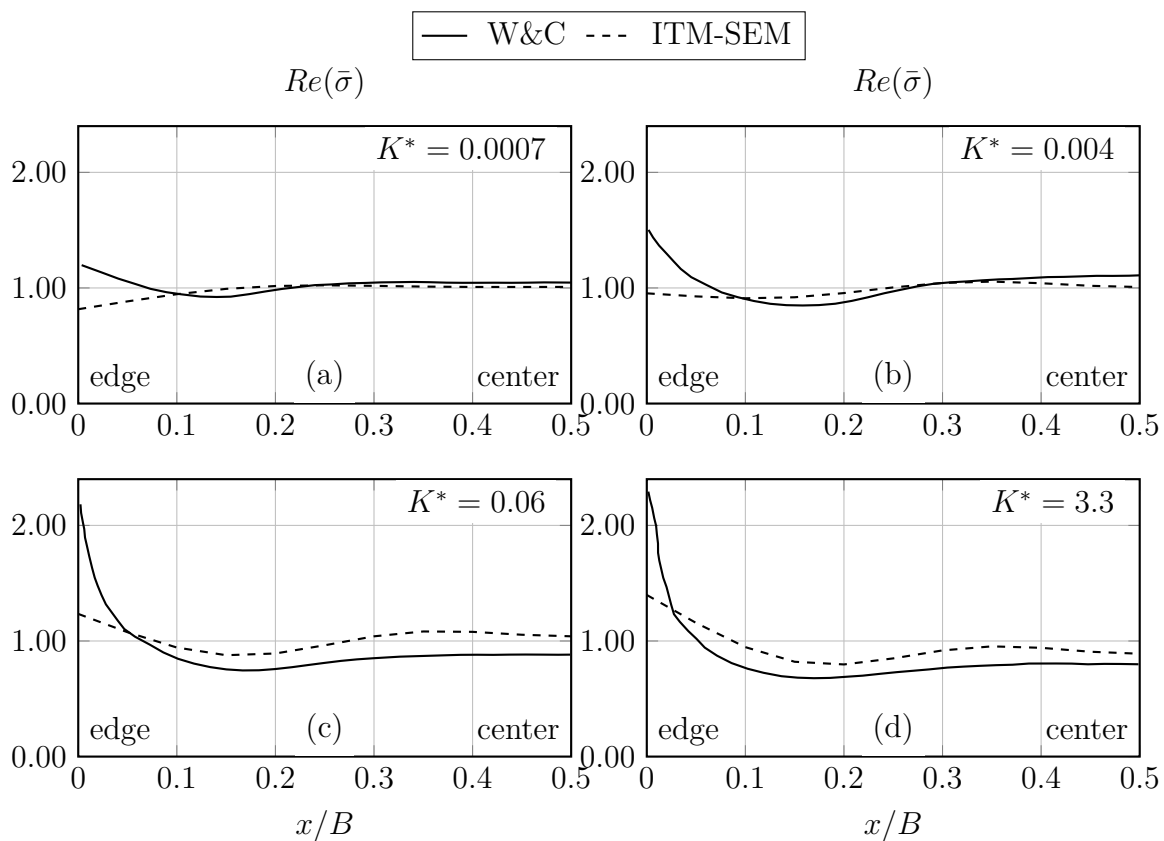


Figure 3.50: Contact stress, real part, $a_0 = 5$

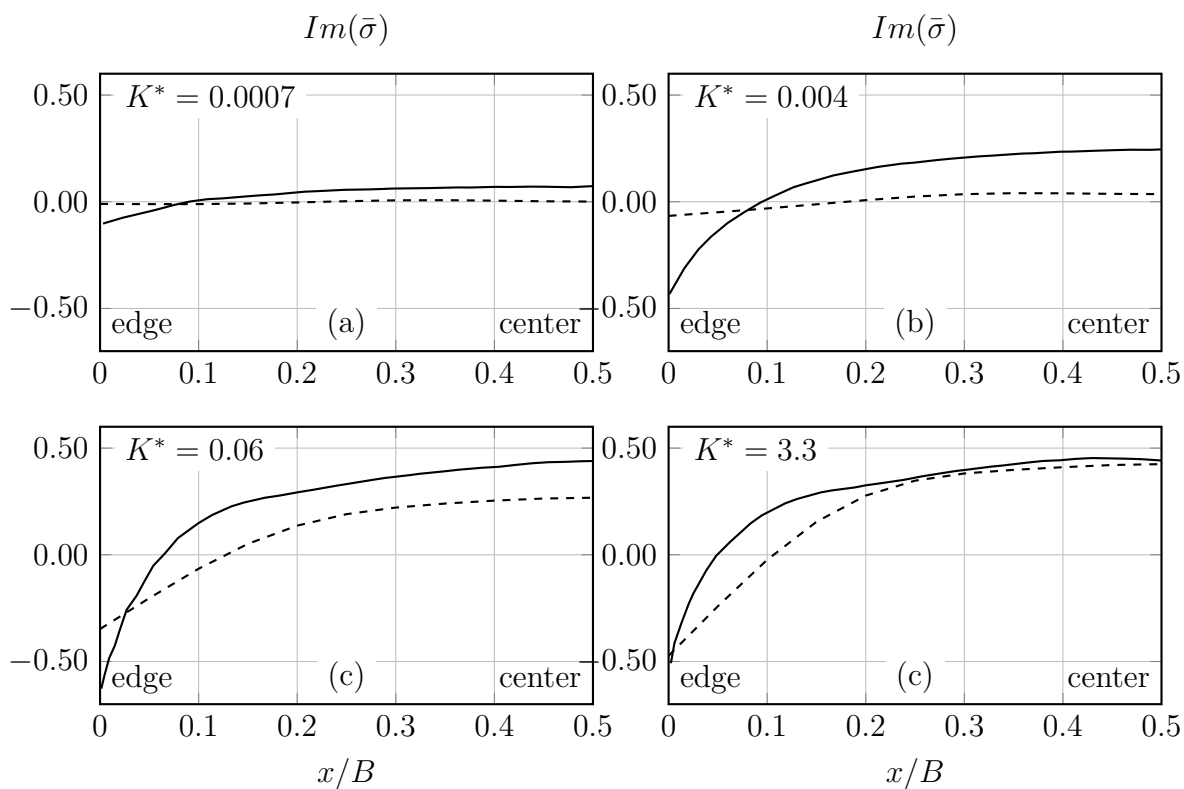


Figure 3.51: Contact stress, imaginary part, $a_0 = 5$

4 Summary

In this dissertation, the solution of Soil Foundation Interaction (SFI) problems is obtained using the substructuring approach. The modeling of the substructures is performed using transform methods. The governing system of equations of motion is transformed from the original space-time domain into the space-frequency or wavenumber-frequency domain, where the effects of the input parameters on the results are more visible.

The foundation is modeled using the Spectral Element Method (SEM). The method is based on the exact solution of the governing differential equations of motion in the space-frequency domain. This results in the exact frequency dependent shape functions of a dynamic stiffness element. The dynamic stiffness matrices of elements are also frequency dependent and developed explicitly for one-dimensional beam elements and Levy-type plates. Only one element is sufficient to represent the dynamic behavior at any frequency. In the case of plate with arbitrary boundary conditions, plate displacements are presented in infinite series form, and the boundary problem is solved using the Projection method.

The soil medium is modeled using the Integral Transform Method (ITM). The method is based on the analytical solution of Lamé's differential equations of motion in wavenumber-frequency domain. It is able to describe the dynamic behavior of the infinite medium completely, but under certain assumptions. The material has to be

4. Summary

homogeneous, linear and elastic within the layer, and the layers have to be parallel to the surface.

The differential equation of the soil-foundation system is solved in space-frequency domain using the modal superposition method.

Regarding the type of the analysis required for obtaining the response of the system, the foundations are divided in two groups: rigid and flexible.

Rigid foundations are considered massless. This analysis does not require the explicit modeling of the foundation. Hence, the system is consisted of the soil model only. The foundation is considered an area of the surface of the soil that is forced to act rigidly using kinematic transforms. The dynamic stiffness matrix of the foundation is obtained using the ITM. The soil is subjected to the dynamic unit force acting on the surface. This requires the discretization of the surface. In order to avoid ill conditioning of the flexibility matrix two different meshes are introduced: a fine one, for the calculation of the displacement field of the surface of the soil, and a coarse one, for the calculation of the displacement field of the foundation. The unit force is approximated with the distributed load in order to avoid numerical errors caused by the truncation of the spectrum of functions used for the calculation of the response. The functions must be sampled in a way that would ensure that the areas around the local minima and maxima are described well.

Two numerical examples regarding rigid foundations are presented:

- square rigid foundation on the halfspace and
- a group of two square rigid foundations on a layer over the bedrock.

The obtained vertical, horizontal and rocking compliances of a single square foundation are compared with results from literature, showing good matching. The values

4. Summary

of the compliances obtained by the proposed method are lower in general, since a small damping coefficient has been introduced in the ITM in order to avoid aliasing.

The foundation-soil-foundation interaction analysis is analyzed using a group of two square rigid foundations resting on a layer over the bedrock. The results obtained for various layer depth and various distance between the foundations are compared with results from literature. It is shown that the influence of the loaded foundation on the adjacent one is higher than the influence of the adjacent foundation on the loaded one. The interaction between the foundations decays with an increase of the distance between them. The adjacent foundation can reduce the amplification of the loaded foundation around the first resonant frequency of the layer, if it is positioned close enough to the loaded foundation. The translational compliances are more sensitive to the layer depth change than the rocking compliances. The ITM approach gives higher amplification of the response for the first natural frequency, but not for the other natural frequencies of the layer.

The problem of a flexible foundation resting on the halfspace is solved using the ITM-SEM coupling. The response of the flexible strip foundation loaded with a uniformly distributed load and resting on the surface of the halfspace is calculated. The analysis is performed as a steady state plane strain analysis taking into account only vertical vibrations. The foundation is treated as an Euler-Bernoulli spectral beam. The natural shapes of the beam are obtained using the SEM. The first three modes of the beam are used for the analysis. The results of the analysis are compared with the results obtained using a software package SASSI. The proposed approach results in higher displacements of the soil under the foundation and lower displacements of the soil outside the soil-foundation interface zone.

The analysis of the flexible square massless foundation is performed using the proposed method. Naturally, this analysis is more complex than the one concerning strip foundation. The most complex part is obtaining the mode shapes of the

4. Summary

foundation. The proposed algorithm for the mode shape calculation is used together with Wittrick-Williams algorithm in order to be sure that the obtained results are not misinterpreted. The obtained results in terms of compliance functions of the center, edge and corner point of the foundation, displacement field and contact stress field are compared with the results from the literature. The results are calculated for various foundation stiffness-soil stiffness ratio, K . It is shown that the response of the system is highly sensitive to the active load distribution. With an increase of the relative stiffness K the displacements of the foundation become less spatially dependent, regardless of the frequency. This dependence is also low in the case of low values of the stiffness ratio in the high frequency zone. Even a small plate stiffness leads to a concentration of the contact stress along the edges. The concentration zone is considerably narrow and it requires a very fine discretization in order to be presented properly. This operation is very costly and it is not optimal to use with uniform discretization.

The results presented in this dissertation shows that the proposed method built by coupling ITM and SEM has capabilities to deal with the problems of rectangular foundations resting on the elastic halfspace. The major advantage of the method is that it is based on the analytical solution of wave propagation in the plate so it gives a clear insight in the physics of the problem. However, the method relies on the Discrete Fourier Transform (DFT). It requires many input parameters that have to be in accordance with the rules of DFT in order to avoid numerical errors. It can be a very demanding method in terms of computational resources.

It can be concluded that the proposed method is very useful for understanding the problem of the dynamic Soil Structure Interaction (SSI). This dissertation shows one part of the field where the method could be used. The future research should involve

- a generalization of the method - considering all vibration directions,

4. Summary

- a more detailed parametric analysis investigating the effect of the material and geometry parameters on the response of the system,
- an analysis of flexible foundation on a layered halfspace,
- a Foundation Soil Foundation Interaction (FSFI) analysis concerning flexible foundations,
- a further improvement of the numerical techniques that would lower the computational efforts.

A Appendix

A.1 Tensor Notation

In tensor notation coordinate axes are denoted with x_j , and corresponding basis vectors with \mathbf{i}_j . The index j takes values 1, 2 and 3 since we are using a 3D Cartesian coordinate system.

If the components of the vector \mathbf{u} are denoted with u_j then

$$\mathbf{u} = u_1\mathbf{i}_1 + u_2\mathbf{i}_2 + u_3\mathbf{i}_3 \quad (\text{A.1})$$

According to summation convention, repeated index implies a summation. Therefore, equation (A.1) could be written as

$$\mathbf{u} = u_j\mathbf{i}_j \quad (\text{A.2})$$

An exemplar of summation convention is scalar product of two vectors:

$$\mathbf{u} \cdot \mathbf{v} = u_j v_j = u_1 v_1 + u_2 v_2 + u_3 v_3 \quad (\text{A.3})$$

Index j in equations (A.2) and (A.3) is called dummy index and it always takes all three values 1, 2 and 3.

Quantities containing two indices represents second order tensors. Kronecker delta symbol is a second order tensor which components have the following property

$$\delta_{ij} = \begin{cases} 1 & \text{if } i = j \\ 0 & \text{if } i \neq j \end{cases} \quad (\text{A.4})$$

Quantities containing three indices represents third order tensors. Permutation symbol, or Levi-Civita tensor, is a third order tensor defined as

$$e_{ijk} = \begin{cases} +1 & \text{if } (i, j, k) \text{ is an even permutation of } (1, 2, 3) \\ -1 & \text{if } (i, j, k) \text{ is an odd permutation of } (1, 2, 3) \\ 0 & \text{if any index is repeated} \end{cases} \quad (\text{A.5})$$

Using permutation symbol and summation convention, components of any cross product $\mathbf{h} = \mathbf{u} \times \mathbf{v}$ could be written as

$$h_i = e_{ijk} u_j v_k \quad (\text{A.6})$$

or in expanded form

$$\begin{aligned} h_1 &= u_2 v_3 - u_3 v_2 \\ h_2 &= u_3 v_1 - u_1 v_3 \\ h_3 &= u_1 v_2 - u_2 v_1 \end{aligned} \quad (\text{A.7})$$

Vector differential operator ∇ is defined as

$$\nabla = \mathbf{i}_1 \frac{\partial}{\partial x_1} + \mathbf{i}_2 \frac{\partial}{\partial x_2} + \mathbf{i}_3 \frac{\partial}{\partial x_3} \quad (\text{A.8})$$

If $f(x_1, x_2, x_3)$ is a scalar field, a vector field ∇f is gradient of scalar field f

$$\text{grad} f = \nabla f = \mathbf{i}_1 \frac{\partial f}{\partial x_1} + \mathbf{i}_2 \frac{\partial f}{\partial x_2} + \mathbf{i}_3 \frac{\partial f}{\partial x_3} \quad (\text{A.9})$$

Partial derivatives are denoted with comma symbol (,) in index. Equation (A.9) could be written using partial derivative symbol

$$\text{grad} f = \nabla f = \mathbf{i}_p f_{,p} \quad (\text{A.10})$$

Components of the vector field $\mathbf{u}(\mathbf{x})$ are functions of spatial coordinates $u_i(x_1, x_2, x_3)$. If we assume that the components of the vector field $\mathbf{u}(\mathbf{x})$ are differentiable, nine partial derivatives $\partial u_j(x_1, x_2, x_3)/\partial x_j$ could be written in tensor notation as $u_{i,j}$. These partial derivatives represent the components of a second order tensor.

If $\mathbf{u}(\mathbf{x})$ is a vector field, scalar field $\nabla \cdot \mathbf{u}$ is a divergence of a vector field $\mathbf{u}(\mathbf{x})$:

$$\text{div} \mathbf{u} = \nabla \cdot \mathbf{u} = u_{i,i} \quad (\text{A.11})$$

If $\mathbf{u}(\mathbf{x})$ is a vector field, vector field $\nabla \times \mathbf{u}$ is a curl of a vector field $\mathbf{u}(\mathbf{x})$:

$$q_i = e_{ijk} u_{k,j} \quad (\text{A.12})$$

Laplace operator or Laplacian ∇^2 represents a divergence of a gradient. Laplacian of a twice differentiable scalar field is a scalar field:

$$\operatorname{div} \operatorname{grad} f = \nabla \cdot \nabla f = f_{,ii} \quad (\text{A.13})$$

Laplacian of a vector field is a vector field:

$$\nabla^2 \mathbf{u} = \nabla \cdot \nabla \mathbf{u} = u_{p,jj} \mathbf{i}_p \quad (\text{A.14})$$

A.2 Fourier transformation

A.2.1 Continuous Fourier transformation

The Fourier transformation of the function $f(t)$ is defined as

$$\bar{f}(\omega) = \int_{-\infty}^{\infty} f(t) e^{-i\omega t} dt \quad (\text{A.15})$$

The inverse Fourier transform is defined as

$$f(t) = \frac{1}{2\pi} \int_{-\infty}^{\infty} \bar{f}(\omega) e^{i\omega t} d\omega \quad (\text{A.16})$$

In Section 2.1 a threefold Fourier transform is applied on the potentials Φ and Ψ_i .

The transform is carried out from spatial-time into wavenumber-frequency domain

$(x, y, z, t) \circ \bullet (k_x, k_y, z, \omega)$. It is defined as

$$\hat{f}(k_x, k_y, z, \omega) = \int_{x=-\infty}^{\infty} \int_{y=-\infty}^{\infty} \int_{t=-\infty}^{\infty} f(x, y, z, t) e^{-ik_x x} e^{-ik_y y} e^{-i\omega t} dx dy d\omega \quad (\text{A.17})$$

The inverse threefold Fourier transform is defined as

$$f(x, y, z, t) = \int_{k_x=-\infty}^{\infty} \int_{k_y=-\infty}^{\infty} \int_{\omega=-\infty}^{\infty} \hat{f}(k_x, k_y, z, \omega) e^{ik_x x} e^{ik_y y} e^{i\omega t} dx dy d\omega \quad (\text{A.18})$$

The properties and the application of the continuous Fourier transform is explained in details in the literature [54].

A.2.2 Discrete Fourier transformation

The discrete Fourier transform is developed from the continuous Fourier transform for the needs of machine computation. Let $g(t)$ be a function defined at N equally distributed samples of a period T . The Fourier transform of a function $g(t)$ is defined as

$$\bar{g}(\omega) = \sum_{k=0}^{N-1} g(kT) \exp\left(-i \frac{2\pi nk}{N}\right) \quad (\text{A.19})$$

The resulting function $\bar{g}(\omega)$ is defined at N equally distributed samples at intervals of $\omega = 1/(NT)$.

The inverse discrete Fourier transform is defined as

$$g(kT) = \frac{1}{N} \sum_{n=0}^{N-1} \bar{g}\left(\frac{n}{NT}\right) \exp\left(i \frac{2\pi nk}{N}\right) \quad (\text{A.20})$$

The properties and the application of the discrete Fourier transform is explained in details in the literature [54].

Bibliography

- [1] E. Kausel, “Early History of Soil–structure Interaction”, *Soil Dynamics and Earthquake Engineering*, Special Issue in honour of Prof. Anestis Veletsos 30.9 (Sept. 1, 2010), pp. 822–832, ISSN: 0267-7261, DOI: 10.1016/j.soildyn.2009.11.001.
- [2] H. Lamb, “I. On the Propagation of Tremors over the Surface of an Elastic Solid”, *Phil. Trans. R. Soc. Lond. A* 203.359-371 (Jan. 1, 1904), pp. 1–42, ISSN: 0264-3952, 2053-9258, DOI: 10.1098/rsta.1904.0013.
- [3] G. Gazetas, “Analysis of Machine Foundation Vibrations: State of the Art”, *Soil Dynamics and Earthquake Engineering* 2.1 (1983), pp. 2–42.
- [4] G. N. Bycroft, “Forced Vibrations of a Rigid Circular Plate on a Semi-Infinite Elastic Space and on an Elastic Stratum”, *Philosophical Transactions of the Royal Society of London. Series A, Mathematical and Physical Sciences* 248.948 (1956), pp. 327–368, ISSN: 0080-4614, JSTOR: 91621.
- [5] A. O. Awojobi, P. Grootenhuis, “Vibration of Rigid Bodies on Semi-Infinite Elastic Media”, *Proc. R. Soc. Lond. A* 287.1408 (Aug. 17, 1965), pp. 27–63, ISSN: 0080-4630, 2053-9169, DOI: 10.1098/rspa.1965.0168.
- [6] J. E. Luco, R. A. Westmann, “Dynamic Response of Circular Footings”, *Journal of the Engineering Mechanics Division* 97.5 (1971), pp. 1381–1395.

-
- [7] J. E. Luco, “Impedance Functions for a Rigid Foundation on a Layered Medium”, *Nuclear Engineering and Design* 31.2 (Jan. 1, 1974), pp. 204–217, ISSN: 0029-5493, DOI: 10.1016/0029-5493(75)90142-9.
- [8] J. Lysmer, R. L. Kuhlemeyer, “Finite Dynamic Model For Infinite Media”, *Journal of the Engineering Mechanics Division* 95.4 (1969), pp. 859–878.
- [9] G. Waas, *Linear Two-Dimensional Analysis of Soil Dynamics Problems in Semi-Infinite Layered Media*. OCLC: 920414808, 1972.
- [10] J Lysmer et al., *SASSI2000, User’s Manual*, 1999.
- [11] P. Bettess, J. A. Bettess, “Infinite Elements for Static Problems”, *Engineering Computations Engineering Computations* 1.1 (1984), OCLC: 4649012872, pp. 4–16, ISSN: 0264-4401.
- [12] P. Bettess, J. A. Bettess, “Infinite Elements for Dynamic Problems: Part 1”, *Engineering Computations Engineering Computations* 8.2 (1991), OCLC: 4649020144, pp. 125–151, ISSN: 0264-4401.
- [13] E. Mesquita, R. Pavanello, “Numerical Methods for the Dynamics of Unbounded Domains”, *Mat. apl. comput. Computational & Applied Mathematics* 24.1 (2005), OCLC: 4643610377.
- [14] S.-B Yang, S.-R Kuo, H.-H Hung, “Frequency-Independent Infinite Elements for Analysing Semi-Infinite Problems”, *International journal for numerical methods in engineering*. 39.20 (1996), OCLC: 104774548, p. 3553, ISSN: 0029-5981.
- [15] S.-S. Chen, J.-G. Hou, “Response of Circular Flexible Foundations Subjected to Horizontal and Rocking Motions”, *Soil Dynamics and Earthquake Engineering* 69 (Feb. 2015), pp. 182–195, DOI: 10.1016/j.soildyn.2014.10.022.
- [16] S. S. Chen, J. G. Hou, “Modal Analysis of Circular Flexible Foundations under Vertical Vibration”, *Soil Dynamics and Earthquake Engineering* 29.5 (2009), pp. 898–908, DOI: 10.1016/j.soildyn.2008.10.004.

-
- [17] W. L. Whittaker, P. Christiano, “Dynamic Response of Plate on Elastic Half-Space”, *Journal of the Engineering Mechanics Division* 108.1 (1982), pp. 133–154.
- [18] H. Wong, J. Luco, “Dynamic Interaction between Rigid Foundations in a Layered Half-Space”, *Soil Dynamics and Earthquake Engineering* 5.3 (1986), pp. 149–158.
- [19] D. L. Karabalis, M. Mohammadi, “3-D Dynamic Foundation-Soil-Foundation Interaction on Layered Soil”, *Soil Dynamics and Earthquake Engineering* 17.3 (Jan. 1998), pp. 139–152, DOI: 10.1016/S0267-7261(97)00047-X.
- [20] J. Qian, D. Beskos, “Harmonic Wave Response of Two 3-D Rigid Surface Foundations”, *Soil Dynamics and Earthquake Engineering* 15.2 (Feb. 1996), pp. 95–110, DOI: 10.1016/0267-7261(95)00026-7.
- [21] D. L. Karabalis, D. E. Beskos, “Dynamic Response of 3-D Flexible Foundations by Time Domain BEM and FEM”, *International Journal of Soil Dynamics and Earthquake Engineering* 4.2 (Apr. 1, 1985), pp. 91–101, ISSN: 0261-7277, DOI: 10.1016/0261-7277(85)90004-X.
- [22] C. Spyrakos, D. Beskos, “Dynamic Response of Flexible Strip-Foundations by Boundary and Finite Elements”, *Soil Dynamics and Earthquake Engineering* 5.2 (Apr. 1986), pp. 84–96, DOI: 10.1016/0267-7261(86)90002-3.
- [23] F. T. Kokkinos, C. C. Spyrakos, “Dynamic Analysis of Flexible Strip-Foundations in the Frequency Domain”, *Computers & Structures* 39.5 (1991), pp. 473–482.
- [24] L. Auersch, “Dynamic Plate-Soil Interaction — Finite and Infinite, Flexible and Rigid Plates on Homogeneous, Layered or Winkler Soil”, *Soil Dynamics and Earthquake Engineering* 15.1 (Jan. 1996), pp. 51–59, DOI: 10.1016/0267-7261(95)00021-6.
- [25] J. P. Wolf, *Dynamic Soil-Structure Interaction*, Prentice-Hall, 1985, 488 pp., ISBN: 978-0-13-221565-7.

- [26] M. Hackenberg, “A Coupled Integral Transform Method - Finite Element Method Approach to Model the Soil-Structure-Interaction”, PhD thesis, Munich, Germany: Technischen Universität München, 2016.
- [27] G. Frühe, “Superposition of Fundamental Solutions in Elastodynamics to Discuss the Dynamic Tunnel-Soil-Structure-Interaction”, PhD thesis, Technischen Universität München, 2011.
- [28] G. Müller, *Ein Verfahren zur Erfassung der Fundament-Boden Wechselwirkung unter Einwirkung periodischer Lasten*, vol. 25, Mitteilungen aus dem Institut für Bauingenieurwesen I, Technische Universität München, 1989.
- [29] A. Konrad, “Der Zylinder, der zylindrische Hohlraum und die dickwandige Kreiszyinderschale unter beliebigen, ruhenden oder bewegten Lasten”, PhD thesis, Technischen Universität München, 1985, 144 pp.
- [30] M. Lieb, “Adaptive Numerische Fouriertransformation in Der Bodendynamik Unter Verwendung Einer Waveletzerlegung”, PhD thesis, Technischen Universität München, 1997.
- [31] S. Lenz, “Nichtlineare Interaktion Zwischen Fahrzeug Und Untergrund Unter Zuhilfenahme von Integraltransformationen”, PhD thesis, Technischen Universität München, 2003.
- [32] G. Müller, “Ein Verfahren Zur Kopplung Der Randelementmethode Mit Analytischen Lösungsansätzen”, PhD thesis, Technischen Universität München, 1993.
- [33] G. F. A. Zirwas, “Ein Hybrides Verfahren Zur Behandlung Der Bauwerk-Bodenwechselwirkung Mit Analytischen Integraltransformationen Und Numerischen Ansätzen”, PhD thesis, Technischen Universität München, 1996.
- [34] M. Buchschmid, “ITM-Based FSI-Models for Rooms with Absorptive Boundaries”, PhD thesis, Technischen Universität München, 2011.

-
- [35] G. Müller, “Ein Verfahren Zur Erfassung Der Fundament-Boden Wechselwirkung Unter Einwirkung Periodischer Lasten”, PhD thesis, Technischen Universität München, 1989.
- [36] J. Rastandi, “Modelization of Dynamic Soil-Structure Interaction Using Integral Transform-Finite Element Coupling”, Munich: Technical University Munich, 2003, 100 pp.
- [37] M. Radišić, G. Müller, M. Petronijević, “Impedance Matrix for Four Adjacent Rigid Surface Foundations”, *IX International Conference on Structural Dynamics - EURODYN 2014*, EURODYN, M33, Porto, Portugal, July 2, 2014, pp. 653–660, ISBN: 978-972-752-165-4.
- [38] H Grundmann, “Nonlinear Interaction between a Moving SDOF System and a Timoshenko Beam/Halfspace Support”, *Archive of Applied Mechanics* 72 (2003), pp. 830–842, DOI: 10.1007/s00419-002-0260-7.
- [39] M. Radišić, M. Nefovska-Danilović, M. Petronijević, “Vertical Vibrations of 3D Structure Caused by Moving Load”, *First International Conference for PhD Students in Civil Engineering, CE-PhD 2012*, International Conference for PhD Students in Civil Engineering, CE-PhD, M33, Cluj-Napoca, Romania, Nov. 4, 2012, pp. 177–183, ISBN: 978-973-757-710-8.
- [40] U. Lee, *Spectral Element Method in Structural Dynamics*, John Wiley & Sons, July 31, 2009, 471 pp., ISBN: 978-0-470-82375-0.
- [41] J. F. Doyle, *Wave Propagation in Structures: Spectral Analysis Using Fast Discrete Fourier Transforms*, 2nd edition, New York: Springer, June 20, 1997, 321 pp., ISBN: 978-0-387-94940-6.
- [42] J. R. Banerjee, F. W. Williams, “Coupled Bending-Torsional Dynamic Stiffness Matrix of an Axially Loaded Timoshenko Beam Element”, *International Journal of Solids and Structures* 31.6 (Mar. 1, 1994), pp. 749–762, ISSN: 0020-7683, DOI: 10.1016/0020-7683(94)90075-2.

-
- [43] P. H. Kulla, “High Precision Finite Elements”, *Finite Elements in Analysis and Design* 26.2 (June 1, 1997), pp. 97–114, ISSN: 0168-874X, DOI: 10.1016/S0168-874X(96)00073-X.
- [44] J. B. Casimir, S. Kevorkian, T. Vinh, “The Dynamic Stiffness Matrix of Two-Dimensional Elements: Application to Kirchhoff’s Plate Continuous Elements”, *Journal of Sound and Vibration* 287.3 (Oct. 22, 2005), pp. 571–589, ISSN: 0022-460X, DOI: 10.1016/j.jsv.2004.11.013.
- [45] M. Boscolo, J. R. Banerjee, “Dynamic Stiffness Elements and Their Applications for Plates Using First Order Shear Deformation Theory”, *Computers & Structures* 89.3 (Feb. 1, 2011), pp. 395–410, ISSN: 0045-7949, DOI: 10.1016/j.compstruc.2010.11.005.
- [46] M. Boscolo, J. R. Banerjee, “Dynamic Stiffness Formulation for Composite Mindlin Plates for Exact Modal Analysis of Structures. Part II: Results and Applications”, *Computers & Structures* 96–97 (Apr. 2012), pp. 74–83, ISSN: 0045-7949, DOI: 10.1016/j.compstruc.2012.01.003.
- [47] M. Boscolo, J. R. Banerjee, “Dynamic Stiffness Formulation for Composite Mindlin Plates for Exact Modal Analysis of Structures. Part I: Theory”, *Computers & Structures* 96–97 (Apr. 2012), pp. 61–73, ISSN: 0045-7949, DOI: 10.1016/j.compstruc.2012.01.002.
- [48] M. Nefovska-Danilović, “Dynamic Analysis of Soil-Structure System Using Spectral Element Method”, PhD thesis, Belgrade, Serbia: University of Belgrade, 2012, 132 pp.
- [49] M. Petronijević, M. Nefovska-Danilović, M. Radišić, “Analysis of Frame Structure Vibrations Induced by Traffic”, *Građevinar - Journal of the Croatian Association of Civil Engineers* 65 (2013), M23, pp. 811–824, ISSN: 0350-2465.

-
- [50] C. F. Long, “On the Completeness of the Lamé Potentials”, *Acta Mechanica* 3.4 (Dec. 1, 1967), pp. 371–375, ISSN: 0001-5970, 1619-6937, DOI: 10.1007/BF01181496.
- [51] A. Sommerfeld, *Partial Differential Equations in Physics*, New York: Academic Press, Feb. 11, 1949, 335 pp., ISBN: 978-0-12-654656-9.
- [52] S. L. Kramer, *Geotechnical Earthquake Engineering*, 1 edition, Upper Saddle River, N.J: Pearson, Jan. 7, 1996, 653 pp., ISBN: 978-0-13-374943-4.
- [53] MathWorks, *MATLAB 2013a*, version 2013a, 2013.
- [54] E. Brigham, *Fast Fourier Transform and Its Applications*, 1st, Prentice Hall, Apr. 8, 1988, 448 pp., ISBN: 0-13-307505-2.
- [55] H Grundmann, M Lieb, E Trommer, “The Response of a Layered Half-Space to Traffic Loads Moving along Its Surface”, *Archive of Applied Mechanics* 69.1 (Feb. 1999), pp. 55–67, DOI: 10.1007/s004190050204.
- [56] K Müller, H Grundmann, S Lenz, “Nonlinear Interaction between a Moving Vehicle and a Plate Elastically Mounted on a Tunnel”, *Journal of Sound and Vibration* 310.3 (Feb. 2008), pp. 558–586, DOI: 10.1016/j.jsv.2007.10.042.
- [57] L Auersch, “The Effect of Critically Moving Loads on the Vibrations of Soft Soils and Isolated Railway Tracks”, *Journal of Sound and Vibration* 310.3 (Feb. 2008), pp. 587–607, DOI: 10.1016/j.jsv.2007.10.013.
- [58] Y. B. Yang, H. H. Hung, *Wave Propagation for Train-Induced Vibrations: A Finite/Infinite Element Approach*, World Scientific Publishing Company, June 22, 2009, 492 pp., ISBN: 978-981-283-582-6.
- [59] N. Chouw, G. Schmid, *Wave 2000: Wave Propagation, Moving Load, Vibration Reduction*, Rotterdam Netherlands: A.A. Balkema, 2000, ISBN: 90-5809-173-2.
- [60] J.-G. Sieffert, F. Cevaer, *Handbook of Impedance Functions (French Edition)*, Editions Ouest-France, 1995, 176 pp., ISBN: 2-908261-32-4.

- [61] A. Maravas, G. Mylonakis, D. L. Karabalis, “Discrete Impedance Matrix for Flexible Surface Foundations”, *COMPADYN 2013*, 4th ECCOMAS Thematic Conference on Computational Methods in Structural Dynamics and Earthquake Engineering, Kos Island, Greece, June 12–14, 2013, pp. 12–14.
- [62] A. Maravas, G. Mylonakis, D. L. Karabalis, “Dynamic Analysis of Flexible Foundations Based on a Discrete Impedance Matrix Approach”, *IX International Conference on Structural Dynamics - EURODYN 2014*, EURODYN, Porto, Portugal, 2014, pp. 675–680, ISBN: 978-972-752-165-4.
- [63] J.-g. Sieffert, G. Schmid, “Soil-Structure Interaction Foundations Vibrations” (2005).
- [64] M. Mohammadi, D. L. Karabalis, “3-D Soil-Structure Interaction Analysis by BEM: Comparison Studies and Computational Aspects”, *Soil Dynamics and Earthquake Engineering* 9.2 (1990), pp. 96–108.
- [65] S. Kevorkian, M. Pascal, “AN ACCURATE METHOD FOR FREE VIBRATION ANALYSIS OF STRUCTURES WITH APPLICATION TO PLATES”, *Journal of Sound and Vibration* 246.5 (Oct. 4, 2001), pp. 795–814, ISSN: 0022-460X, DOI: 10.1006/jsvi.2001.3709.
- [66] H. R. Riggs, G. Waas, “Influence of Foundation Flexibility on Soil-Structure Interaction”, *Earthquake Engineering & Structural Dynamics* 13.5 (1985), pp. 597–615.

Biography

Marko Radišić was born on April 14, 1986 in Banja Luka. He finished elementary school and gymnasium in Podgorica as a holder of the diploma 'Luča'. He has also finished an elementary music school.

In the period between 2005 and 2010 he enrolled the BSc and MSc studies at the Faculty of Civil Engineering University of Belgrade. He graduated with the average grade of 8.83/10 and 9.14/10 respectively, on the topics related to his current research field: "Calculation of Impedance Functions of Rectangular Foundation Using FEM" and "Calculation of Soil Displacements and Stresses Under Harmonic Load Using ITM". He enrolled the PhD studies at the same faculty in 2010/2011. He has passed all the exams from the curriculum with the average grade of 10/10.

Marko has been working at the Faculty of Civil Engineering in Belgrade as a Teaching Assistant - PhD Student, since 2011. He has also been a Scholarship Holder of the international PhD program SEEFORM financed by DAAD. He went on three three-months-long research stays at TU Munich during 2012, 2013 and 2015. In 2012, he was elected as the speaker of SEEFORM PhD candidates.

As an author or coauthor, Marko has published 19 scientific papers, one of which is published in the international journal. He was awarded Best Paper Award by the First International Conference for PhD Students in Civil Engineering, Ce-PhD, held in Cluj-Napoca, Romania 2012. He is engaged as a researcher on the Project financed by the Ministry of Science and Technological Development of Serbia TR36046.

Изјава о ауторству

Име и презиме аутора Марко Радишић

Број индекса 906/10

Изјављујем

да је докторска дисертација под насловом

ITM-Based Dynamic Analysis of Foundations Resting on a Layered Halfspace

(Динамичка анализа темеља на слојевитом полупростору примјеном Методе интегралне трансформације)

- резултат сопственог истраживачког рада;
- да дисертација у целини ни у деловима није била предложена за стицање друге дипломе према студијским програмима других високошколских установа;
- да су резултати коректно наведени и
- да нисам кршио/ла ауторска права и користио/ла интелектуалну својину других лица.

Потпис аутора

У Београду, Мај 2018.

Марко Радишић

Изјава о истоветности штампане и електронске верзије докторског рада

Име и презиме аутора	Марко Радишић
Број индекса	906/10
Студијски програм	Грађевинарство
Наслов рада	ITM-Based Dynamic Analysis of Foundations Resting on a Layered Halfspace
Ментор	Проф. Др. Мира Петронијевић Универзитет у Београду, Грађевински факултет Univ.-Prof. Dr.-Ing. Gerhard Müller Technical University of Munich, Dpt. of Civil, Geo and Environmental Engineering

Изјављујем да је штампана верзија мог докторског рада истоветна електронској верзији коју сам предао/ла ради похрањена у **Дигиталном репозиторијуму Универзитета у Београду**.

Дозвољавам да се објаве моји лични подаци везани за добијање академског назива доктора наука, као што су име и презиме, година и место рођења и датум одбране рада.

Ови лични подаци могу се објавити на мрежним страницама дигиталне библиотеке, у електронском каталогу и у публикацијама Универзитета у Београду.

Потпис аутора

У Београду, Мај 2018.

Марко Радишић

Изјава о коришћењу

Овлашћујем Универзитетску библиотеку „Светозар Марковић“ да у Дигитални репозиторијум Универзитета у Београду унесе моју докторску дисертацију под насловом:

ITM-Based Dynamic Analysis of Foundations Resting on a Layered Halfspace

(Динамичка анализа темеља на слојевитом полупростору примјеном Методе интегралне трансформације)

која је моје ауторско дело.

Дисертацију са свим прилозима предао/ла сам у електронском формату погодном за трајно архивирање.

Моју докторску дисертацију похрањену у Дигиталном репозиторијуму Универзитета у Београду и доступну у отвореном приступу могу да користе сви који поштују одредбе садржане у одабраном типу лиценце Креативне заједнице (Creative Commons) за коју сам се одлучио/ла.

1. Ауторство (CC BY)
2. Ауторство – некомерцијално (CC BY-NC)
3. Ауторство – некомерцијално – без прерада (CC BY-NC-ND)
4. Ауторство – некомерцијално – делити под истим условима (CC BY-NC-SA)
5. Ауторство – без прерада (CC BY-ND)
6. Ауторство – делити под истим условима (CC BY-SA)

(Молимо да заокружите само једну од шест понуђених лиценци.
Кратак опис лиценци је саставни део ове изјаве).

Потпис аутора

У Београду, Мај 2018.

Марко Рагумит

1. **Ауторство.** Дозвољаваате умножавање, дистрибуцију и јавно саопштавање дела, и прераде, ако се наведе име аутора на начин одређен од стране аутора или даваоца лиценце, чак и у комерцијалне сврхе. Ово је најслободнија од свих лиценци.

2. **Ауторство – некомерцијално.** Дозвољаваате умножавање, дистрибуцију и јавно саопштавање дела, и прераде, ако се наведе име аутора на начин одређен од стране аутора или даваоца лиценце. Ова лиценца не дозвољава комерцијалну употребу дела.

3. **Ауторство – некомерцијално – без прерада.** Дозвољаваате умножавање, дистрибуцију и јавно саопштавање дела, без промена, преобликовања или употребе дела у свом делу, ако се наведе име аутора на начин одређен од стране аутора или даваоца лиценце. Ова лиценца не дозвољава комерцијалну употребу дела. У односу на све остале лиценце, овом лиценцом се ограничава највећи обим права коришћења дела.

4. **Ауторство – некомерцијално – делити под истим условима.** Дозвољаваате умножавање, дистрибуцију и јавно саопштавање дела, и прераде, ако се наведе име аутора на начин одређен од стране аутора или даваоца лиценце и ако се прерада дистрибуира под истом или сличном лиценцом. Ова лиценца не дозвољава комерцијалну употребу дела и прерада.

5. **Ауторство – без прерада.** Дозвољаваате умножавање, дистрибуцију и јавно саопштавање дела, без промена, преобликовања или употребе дела у свом делу, ако се наведе име аутора на начин одређен од стране аутора или даваоца лиценце. Ова лиценца дозвољава комерцијалну употребу дела.

6. **Ауторство – делити под истим условима.** Дозвољаваате умножавање, дистрибуцију и јавно саопштавање дела, и прераде, ако се наведе име аутора на начин одређен од стране аутора или даваоца лиценце и ако се прерада дистрибуира под истом или сличном лиценцом. Ова лиценца дозвољава комерцијалну употребу дела и прерада. Слична је софтверским лиценцама, односно лиценцама отвореног кода.